June 2020

Comprehensive Optimization Models for Voltage Regulation in PV-rich Multi-phase Distribution Systems

Ibrahim Alsaleh
University of South Florida

Comprehensive Optimization Models for Voltage Regulation in PV-rich Multi-phase Distribution Systems

by

Ibrahim Alsaleh

A dissertation submitted in partial fulfillment
of the requirements for the degree of
Doctor of Philosophy in Electrical Engineering
Department of Electrical Engineering
College of Engineering
University of South Florida

Major Professor: Lingling Fan, Ph.D.
Zhixin Miao, Ph.D.
Nasir Ghani, Ph.D.
Qiong Zhang, Ph.D.
Sumit Paudyal, Ph.D.

Date of Approval:
June 8, 2020

Keywords: Photovoltaic, volt var optimization, unbalanced distribution systems, convex programming, mixed-Integer programming

Dedication

To my beloved parents, Nowayer and Hamoud.

To my cherished wife and daughter, Nuha and Sadeem.

To the soul of my everlasting friend, Ayman.

Acknowledgments

I am profoundly beholden to Allah, The Knowing, The Bountiful, who lavishly blessed my life with gifts and favors that I can never articulate nor compute.

First, I would like to express my sincerest gratitude to my supervisor Dr. Lingling Fan without whom this dissertation would not have been possible. Dr. Fan has influenced me through her enthusiasm and perseverance for excellence, and instilled in me the research skills since the formative years of my grad school. I am in great debt for her immense endorsement and guidance throughout my time at USF.

I would like to thank my Ph.D. committee, Dr. Zhixin Miao, Dr. Nasir Ghani, Dr. Qiong Zhang, and Dr. Sumit Paudyal for their insightful comments and suggestions.

I would also like to thank Dr. Hossein Aghamolk, Minyue Ma, and Dr. Mohammadhafez Bazrafshan for the invaluable discussions that led to fruitful collaborations. I am also grateful to all my intelligent colleagues at the the smart grid power system laboratory.

Special thanks go to my friends Abdullah Alassaf, Dr. Anas Almunif, Saleh Alhomaid and Mahdi Sarsour who inspired me in many ways and made this journey fun and interesting.

Last, *but not least*, I would like to express my heartiest appreciation for my mother Nowayer Alrashid and my father Hamoud Alsaleh, whose prayers, altruistic support, and motivation have been continuously conferred upon my life. Enormous gratitude must go to my wife Nuha Alshaer, who not only journeyed with me, but looked after me, boosted my morale, and heartened me every day. It is through her care and patience that I was able to finish this dissertation duly. I would also like to extend my gratitude to my brothers and sisters for the unwavering support that they have always shown for their youngest brother. Finally, I am thankful to my daughter Sadeem for being a constant source of joy and distraction over the past year and a half.

Table of Contents

List of Tables

List of Figures

Abstract

The distribution systems are increasingly challenged by the continued prevalence of distributed energy resources (DERs), signaling the need for new computational tools to systemize their involvement, coordinate their operation with existing control devices, and mitigate undesired actuation of expensive equipment. Co-optimized operation of the various control devices becomes possible with the advancement in the power system optimization algorithms and the increased deployment of advanced metering infrastructure, offering system awareness and two-way communication. The steady-state alternating-current optimal power flow (ACOPF) problem, being the most descriptive form of OPF, lies at the root of power system optimization, aiming to minimize an operating point subject to the system's physical and security constraints. The last fifteen years have witnessed some seminal convexifications of the ACOPF problem, offering more computational tractability when compared to the original non-convex ACOPF model and a more accurate representation of the physical model when compared to the linear OPF models. The existing literature has addressed a breadth of obstacles with particular relevance to the voltage/voltage ampere reactive power flow continuous and discrete models.

This research aims to build comprehensive computational methodologies that promote the accuracy of the convex distribution ACOPF (D-ACOPF) problem. Specifically, we propose to mitigate the trade-off between model precision and computational efficiency by encoding the precise mathematical models of the physical system and control devices, taking into account their limits and maintaining moderate actuation.

The first chapter serves as an introduction to the volt var control, the main components used in current distribution systems as well as the emergent challenges that face the conventional volt var control. The second chapter surveys and reviews the literature on the various modeling aspects of the model-based volt/var optimization (VVO). It begins by identifying the essential components of the optimization problem, namely, the objectives and constraints, and then compares and contrasts the current state-of-the-art while highlighting the need for new methodologies to overcome the modeling and computational bottlenecks to the existing volt/var scheduling problem.

The third chapter of this dissertation models a general off-line VVO problem for balanced distribution systems, relying on predicted load and generation profiles. We extend our research in the fourth chapter to consider the unbalances in the distribution system, which is of practical concern to the validity of the VVO dispatch. A methodology based on the generalized Benders decomposition (GBD) is proposed to incorporate the discrete devices into the D-ACOPF. Relying on predicted load and generation profiles, we explore the possibility of preventing excessive mechanical adjustments of tap changers to reduce higher maintenance costs.

It is a fact that only exact relaxations to the convex D-ACOPF problem are deemed feasible to the original non-convex problem. The exactitude of the solution is of paramount importance because it not only reflects the minimum operational objective that can be translated into financial savings, but provides the most realistic dispatch of control variables. Hence, inexact solutions are deemed less realistic. Although inevitably compromising the exactness, internalizing the distribution system's fundamental components into the D-ACOPF problem is of the essence for the solution quality and control dispatch viability. In the third part of this research, we propose to incorporate two improperly-constrained applications and a special objective function that initially render the problem inexact. Our contribution is to circumvent this conundrum and retrieve the exactness (AC feasibility) by

utilizing the concept of convex iteration, in which the relaxation is strengthened iteratively. The simulations on various distribution feeders and comparative case studies with the literature evince the success of the proposed method for recovering exact solutions. Moreover, comparisons with existing methods demonstrate the global optimality of the solution with lower penalty weights.

The dissertation has resulted in two published conference papers, and two journal papers (one accepted and one under revision).

Chapter 1: Introduction

1.1 Background

The distribution systems are the downstream part of the electric grid operating at medium and low voltage levels. Consumers connected to the distribution systems comprise residential houses (operating at 120 V or 240 V) and commercial buildings (operating at 480 V or 690 V) [1]. The majority of distribution systems in the US have a radial structure, where a single source (substation) feeds the rest of the feeder. The radiality causes power quality issues due to the energy wasted along the lines in the form of heat, which is neither used by consumers nor reflected on the utility revenue. In response, volt/volt-ampere control (VVC) devices dispersed along the feeder come into play to increase the efficiency of the system. VVC refers to the process of managing the distribution system's control assets with voltage regulation and reactive power (supply and absorption) abilities to improve the power quality while maintaining voltage levels within the required limits specified by ANSI standard C84.1. The controllable devices are owned by the utility and mainly comprise on-load tap changers (OLTC), step-voltage regulators (VSRs), and switched capacitor banks (CBs).

1.1.1 On-load Tap Changers

The distinctive feature of changing voltages in alternating current (AC) circuits using transformers is exploited to follow the load changes. An OLTC is a transformer with the ability to step up or step down the output (*secondary*-side) voltage. There are commonly 33 levels (including the neutral position) that tap positions of OLTCs can take. Further,

OLTCs can be installed as one three-phase unit or as multiple units. However, OLTCs typically operate on a three-phase basis, where phase taps switch uniformly.

1.1.2 Step-Voltage Regulators

In principle, SVRs have the same functionality as OLTCs. Physically, SVRs are single-winded transformers (autotransformers). In this research, we use the terms VRs and SVRs interchangably. SVRs are more flexible than OLTC since they can be located either at the substation or along the feeder, thus enabling the regulation of voltages at remote buses. Also, SVRs have the flexibility to be installed at individual phases and can operate nonuniformly.

SVRs can be of type-A or type-B, depending on where the series impedance is located. In this section, we derive the equation for Type-A and B connections for the single-phase SVR.

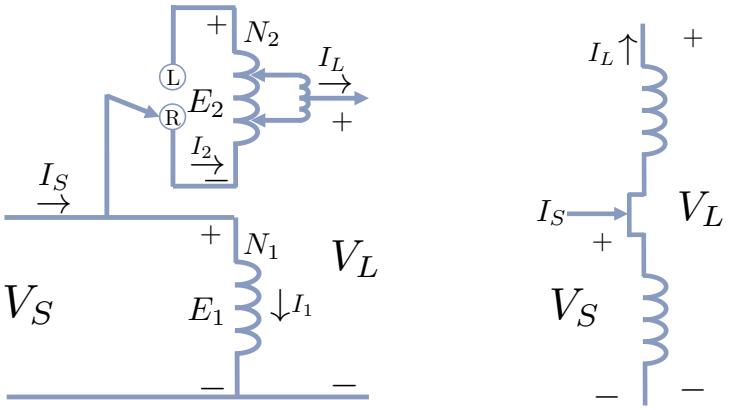

Figure 1.1: Single-phase type-A SVR.

1.1.2.1 Type-A

Fig. 1.1 shows the single-phase connection for type-A SVRs on the raise position (higher voltage is desired at the secondary side), where the primary bus is directly connected to the shunt winding.

For the ratio r, the voltage on both sides are derived as follows:

$$\frac{E_1}{N_1} = \frac{E_2}{N_2} \tag{1.1}$$

$$V_S = E_1 \tag{1.2}$$

$$V_L = E_1 + E_2 \tag{1.3}$$

$$\rightarrow V_L = (1 + \frac{N_2}{N_1})E_1 = rV_S \tag{1.4}$$

Similarly, the currents into and out of the SVR are affected by the turns ratios.

$$2N_1I_1 = N_2 \tag{1.5}$$

$$I_S = I_1 + I_2 \tag{1.6}$$

$$I_L = I_2 \tag{1.7}$$

$$\rightarrow I_S = (1 + \frac{N_2}{N_1})I_2 = rI_L \tag{1.8}$$

When a lower voltage is desired at the secondary side, the effective ratio becomes:

$$r = 1 - \frac{N_2}{N_1}$$

1.1.2.2 Type B

Fig. 1.2 shows the single-phase connection for type-B SVRs on the raise position (higher voltage is desired at the secondary side), where the secondary bus is directly connected to the shunt winding.

The voltage on both sides are derived as follows:

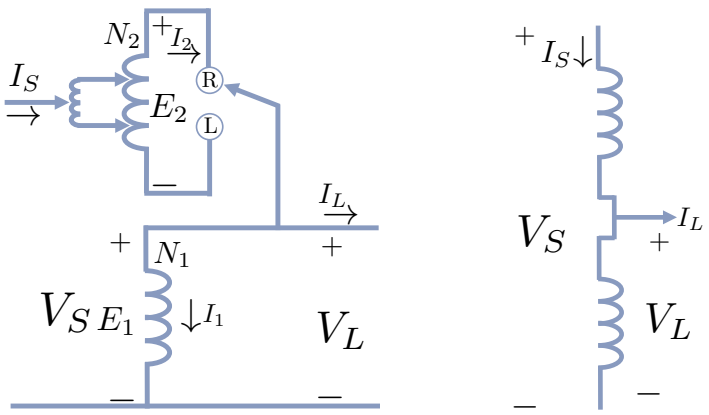

Figure 1.2: Single-phase type-B SVR.

$$\frac{E_1}{N_1} = \frac{E_2}{N_2} \tag{1.9}$$

$$V_S = E_1 - E_2 \tag{1.10}$$

$$V_L = E_1 \tag{1.11}$$

$$\rightarrow V_S = (1 - \frac{N_2}{N_1})E_1 = rV_L \tag{1.12}$$

Similarly, the currents into and out of the SVR are affected by the turns ratios.

$$N_1 I_1 = N_2 I_2 \tag{1.13}$$

$$I_S = I_2 \tag{1.14}$$

$$I_L = I_S - I_1 \tag{1.15}$$

$$\rightarrow I_L = (1 - \frac{N_2}{N_1})I_2 = rI_S \tag{1.16}$$

When a lower voltage is desired at the secondary side, the effective ratio becomes:

$$r = 1 + \frac{N_2}{N_1}$$

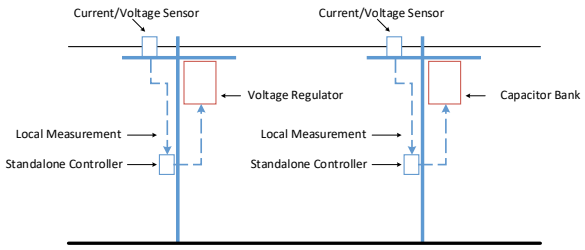

Figure 1.3: Local control of volt/var devices.

1.1.2.3 Capacitor Banks

CBs provide reactive power support to reduce or nullify the effect of large inductive loads and inductances on the system voltages, thereby yielding lower losses. CBs can be equipped with a switching functionality, which turns the unit on only when the voltage falls below a predetermined threshold. However, CB units installed at each phase can only be switched (either on or off) as a group.

1.2 Some Emerging Challenges in VVC

The following subsections briefly describe the issues associated with the management of current and future distribution systems, which serve as the main motivations for this work.

1.2.1 Incompetency of Local VVC Methods

Traditionally, the VVC devices operate in standalone mode. That is, the mechanical settings are automated to act to local measurements of voltage/current. Fig. 1.3 illustrates the measurement and action mechanism. For voltage regulators, as an example, demand current (or power flow) measurements at nearby the device are used to determine whether they should step up or down the voltage. A predetermined logical rule triggers the action. Hence, the VRs step up when the current flows increase (load increases) to reduce voltage drop and vice versa. While the local-feedback control can maintain voltages within acceptable limits, it could be only optimal to the vicinity of the control device, providing a lower

efficiency on the broad scale. Besides the lack of coordination among the devices, locally-triggered actions do not take actions of other local controls into account, and so devices may counteract one another.

1.2.2 Increased Integration of Distributed Energy Resources (DERs)

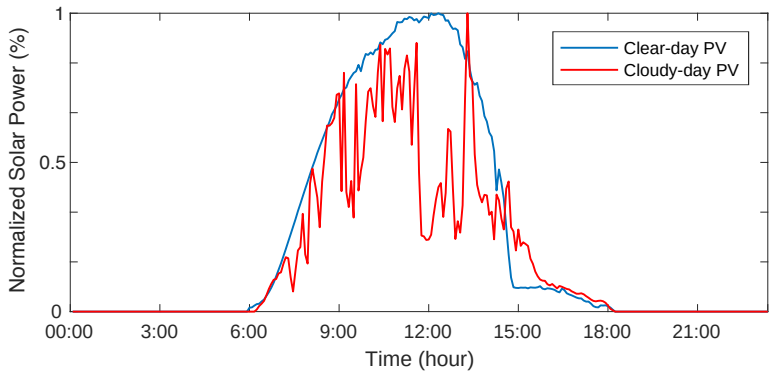

Figure 1.4: Examples of clear-day and cloudy-day solar profiles recorded on May 15, 2013 and August 15, 2013 at USF.

The distribution system continues to undergo a proliferation of distributed energy resources (DERs), especially those powered by solar photovoltaic panels (PVs) and wind turbines, a.k.a distributed generators (DGs). Because of the decline of PV prices and the Solar Investment Tax Credit (ITC), the annual PV installations have been experiencing an average growth rate of 50% from 2010 to 2018, and expected to follow the same trend [2]. The local supply of renewables plays a crucial role in reducing the net demand seen by the utility, and so the overall diurnal energy demand is reduced. In turn, the reduction in the demand current flowing through the transmission cables contributes to the reduction of line losses. However, the increased adoption of these renewables poses a few operational challenges. The fact that distribution systems are characterized with high R/X ratios increases the susceptibility of nodal voltages to real-power injections. Also, ramping and fluctuating voltage issues have mainly been attributable to the immoderate and intermittent renewable power levels.

Fig. 1.4 shows normalized profiles depicting the variability of solar energy during clear and cloudy weather conditions.

With the local control mechanisms of the VVC device, the high penetrations of DGs could lead to increased mechanical adjustments, which is adversely impactful on the maintenance costs and the lifespan of these devices.

1.3 Centralized Volt/Var Optimization (VVO)

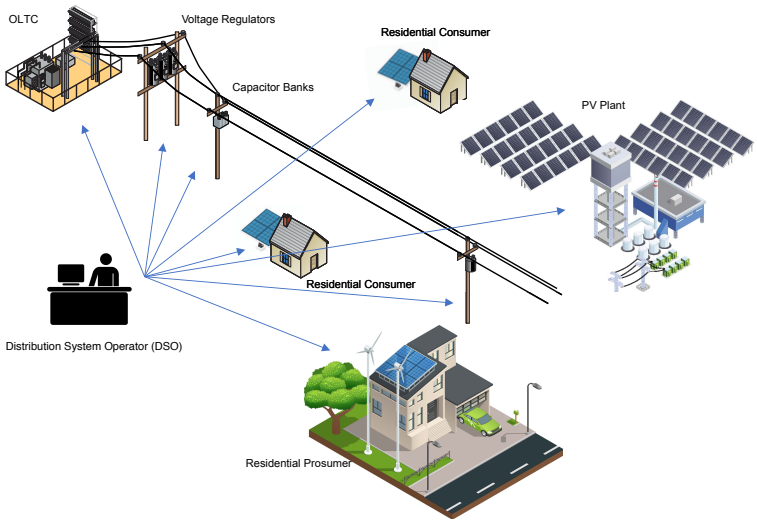

Figure 1.5: Visual interpretation of VVC control by DSO.

Intuitively, the aforementioned issues concerning the local control of VVC devices and the high penetration of DGs can be circumvented by collectively optimizing the control setting of all devices based on the topological and load/supply information, which is referred to as centralized volt/var optimization. According to [1], [3], [4], there are two types of centralized VVO: i) rule-based VVO and ii) model-based VVO. The first one relies on predetermined logical rules, which is similar to the standalone (local) operation, except that communication is utilized, and the automation is determined by the DSO. This type, however, provides sub-optimal solutions [4]. The second type is based on the optimal settings generated by optimal

power flow engines, utilizing the computational capabilities of optimization solvers. For both types, communication facilities are essential for acquiring the system's information and sending command signals. Due to the advances of optimization solvers, the model-based type provides optimal solutions to the VVO. The advantage of the model-based approach over the rule-based approach has also been demonstrated in [5]. The simulation results have shown that the model-based can accommodate larger penetrations of solar energy.

The deployment of smart advanced metering infrastructure (AMI) is envisioned to improve how utilities cope with the ever-changing patterns in the net demand. In 2017, the installations of advanced metering infrastructure (AMI), also known as smart meters, rose to 78 million, 88% of which were for residential consumers [6]. AMI provides full monitoring of hourly and near-real-time (averaged 5 and 15 minutes) electricity usage. Also, AMI has built-in two-way communication channels, which enable controllable assets and prosumers (consumers with demand response or DGs) to receive dispatch signals, i.e. ON/OFF status or amount of power supply/absorption [7]. Fig. 1.5 depicts how the DSO receives information on energy usage and sends direct command signals to VVC devices.

To this end, the distribution system operators (DSOs) utilized this technology to manage dispatchable devices and DGs' inverters jointly. This operation is referred to as centralized volt/var optimization (VVO). The centralized VVO is based on the solution of an AC optimal power flow (ACOPF) model of the system where controllable devices' settings are among the decision variables to achieve circuit-wide objectives while abiding by ANSI voltage limits.

1.4 Preliminaries to Convex and Integer Programming

This section serves as a prelude to the mathematical concepts of *convex* and integer programming. For a broader coverage, the reader is referred to the textbooks [8] and [9], from which the following summary is extracted.

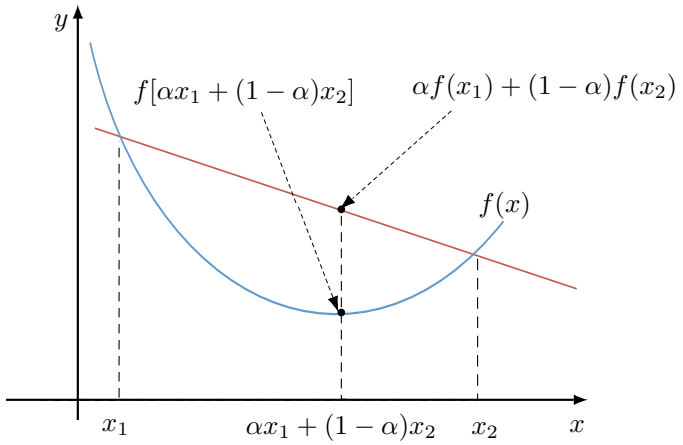

Figure 1.6: A conceptualization of a convex function.

1.4.1 Convex programming

Before we delve into the classes of *convex* problems, we begin by defining the basic concept of convexity. Assume a point x^* existing in a set X, and a function $f(x)$ over the same set. It is said that x^* is the global minimum of the function $f(x^*)$ if and only if $f(x^*) \leq f(x)$ for all $x \in X$. That said, a local minimum exists when there is $\epsilon > 0$ such that $||x - x^*|| \leq \epsilon$. Functions can generally have multiple local and global minima, but minima of a *convex* function yield the same value, which is the global minimum. In optimization, this characteristic lends a computational advantage of the *convex* problems, as developed algorithms can solve a problem to the global minimum much faster than that of non-convex problems (speed is dependent on the problem size, i.e. number of variables and constraints). A *convex* function is *convex* when any point on a straight line of its domain, say $(x_1, f(x_1))$ and $(x_2, f(x_2))$, is greater than or equal to the function value. For first-order *convex* functions, (1.17) should be met.

$$\begin{aligned} &f(\alpha x_1 + (1-\alpha)x_2) \geq \alpha f(x_1) + (1-\alpha)f(x_2) \\ &0 \leq \alpha \leq 1 \end{aligned} \tag{1.17}$$

Among the *convex* classes, the linear programming is deemed the simplest, and solved with simplex algorithm. In what follows we present the summarize the forms of the other two classes of *convex* programming (cone programming), which will mostly be used in our modeling.

1.4.1.1 Second Order Conic Programming (SOCP)

It refers to a class of problems that involve a second-order conic constraint of the form:

$$||Ax + b|| \leq c^T x + d \tag{1.18}$$

The constraint satisfies the convexity check in (1.17). Therefore, the standard form of this class of optimization is

$$\begin{aligned} \underset{x}{\text{minimize}} \quad & f(x) \\ \text{subject to} \quad & ||Ax + b|| \leq c^T x + d \end{aligned} \tag{1.19}$$

1.4.1.2 Semidefinite Programming (SDP)

Positive semidefiniteness (PSD) of a $n \times n$ matrix, say X, has the following equivalent properties:

- $a^H X a \geq 0 \quad \forall a \in \mathbb{C}^n$.
- All eigenvalues of X are non-negative.
- All principal minors (the determinants of all submatrices of X whose diagonal elements are of the full matrix diagonal X) are non-negative.

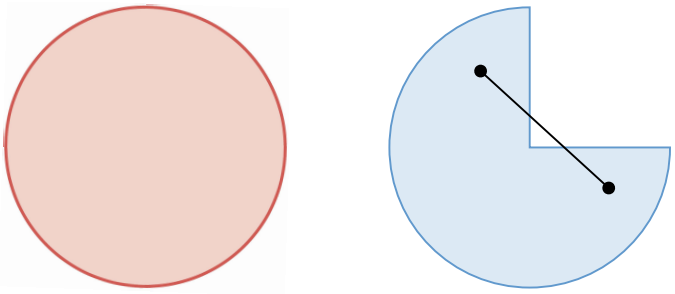

(a) convex set (b) non-convex set

Figure 1.7: Graphical interpretations of convex and non-convex sets.

The standard form of an SDP problem is expresses as follows:

$$\begin{aligned} \underset{x}{\text{minimize}} \quad & C \bullet X \\ \text{subject to} \quad & A \bullet X \leq b, \qquad X \succeq 0 \end{aligned} \tag{1.20}$$

where $\succeq$ denotes that X is psd matrix.

1.4.2 Mixed-integer programming (MIP)

Mixed-integer programming refers to a class of of optimization problems that have a combination of continuous and discrete variables. The discrete variables are used to replicate the necessary condition of constraint. For example, the tap positions of SVRs are of discrete nature, and so the model should be designed such that one tap position is switched at a time (rest of discrete values are zero). Another example is the on/off status of a capacitor, where the discrete variable represents its commitment to operate. In this report, we use the discrete variables in combination with the *convex* continuous variables.

1.5 Outline of the Dissertation

The dissertation is organized as follows: Chapter 2 introduces the fundamental components of the centralized ACOPF-based volt/var optimization. Specifically, it summarizes

the most common objective functions, controllable devices and topological considerations incorporated into the D-ACOPF problem. Moreover, it sheds light on the theoretical gaps in the current state-of-the-art ACOPF problem, upon which the research is based. Chapter 3 formulates an offline volt/var optimization problem based on mixed-integer second order programming that coordinates the VVC devices in distribution systems with high solar penetration levels. The problem holistically encompasses the most commonly-used objective functions and models, and is solved with two timescales. A methodology based on generalized Benders decomposition (GBD) is proposed in chapter 4 to co-optimize discrete-based SVRs with photovoltaics into the semidefinite programming branch flow model (SDP BFM). Acceleration techniques are proposed to enable a multi-time operation and reduce unnecessary mechanical actuation. Further, comparison with available MISDP solvers substantiate the merits of the GBD-based method. Chapter 5 designs a comprehensive distribution power network comprised of the practical connections of loads, distributed energy resources and SVRs. The models are integrated into the SDP BFM with necessary relaxations. Consequently, the overall problem with the objective of minimizing voltage deviations from nominal values loses its AC feasibility due to the introduced models and the strict non-monotonicity of the objective function. A framework based on the convex iteration is proposed to recover AC feasibility, providing a solution to otherwise a complex non-convex problem.

Chapter 2: Literature Review, Research Gaps and Challenges

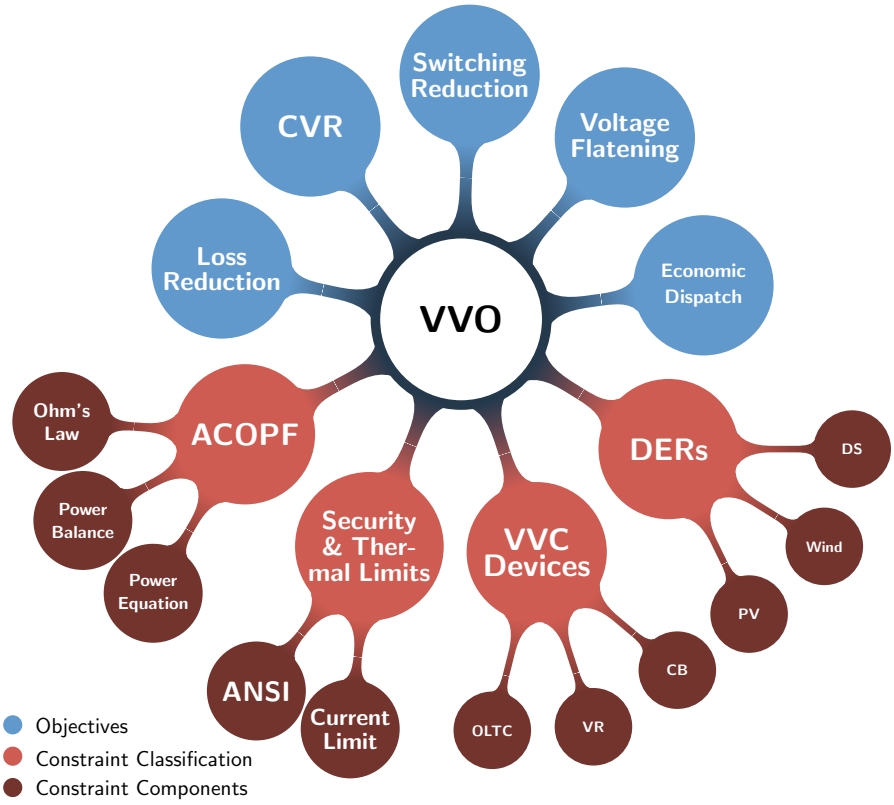

Figure 2.1: Essential Objectives and constraints of the volt/var optimization.

2.1 Overview

Given that the model-based VVO depends on the optimal power flow of the distribution networks, the following overviews the main objectives and constraints typically used to model the OPF. Fig. 2.1 depicts the VVO components.

2.1.1 Objectives

The objectives include, but are not limited to, the following:

2.1.1.1 Loss Reduction (LR)

About 6% of the electricity produced is lost in transmission and distribution systems. Because distribution feeders operate at lower voltage levels (tens of kV) and have high resistive lines, the majority of losses are consumed by their lines [10]. Since the power losses are inversely proportional to voltage levels, the VVC devices have the capacity to reduce the line losses by increasing the nodal voltages.

2.1.1.2 Conservation of Voltage Reduction (CVR)

The CVR originates from the fact that voltage-dependent loads, i.e. constant-impedance loads (CILs) and constant-current loads (CCL), consume more energy when the voltage is above nominal, increasing annual energy costs. CILs are proportional to the voltage and the voltage squared, respectively. Therefore, CVR practices aim at reducing voltage magnitudes to the lower half of the ANSI limit (from 0.95 to 1 p.u.), particularly at buses to which voltage-dependent loads are connected. On the other hand, constant power loads (CPLs) are not affected by the increase/decrease of voltage. Switching Reduction (SR) The life expectancy and maintenance costs of utility-owned voltage regulation equipment is dependent on the number of operations. Therefore, reducing mechanical switching is of economic importance. This can be achieved via i) scheduling the operations on an hourly basis and ii) reducing the intra-day adjustments as an operational objective.

2.1.1.3 Voltage Flattening (VF)

The DSO may wish to keep the nodal voltages around the nominal value so as to mitigate the voltage fluctuations caused by the DER's intermittent supply. Increasing the voltage from the lower half of the allowable limit comes in the interest of preventing excessive voltage drop at the point of interconnection, which may be further away from the regulated bus.

2.1.1.4 Economic Dispatch (ED)

This comes in the interest of financially incentivizing private owners to engage in regulating the voltage and reducing system losses. This is achieved by minimizing the day-ahead energy from the substation and DERs. The substation energy is minimized with respect to the locational marginal pricing at the substation, while energy from DERs is minimized based on fixed prices determined by long-term power purchase agreements (PPA) with the utility.

2.1.1.5 Other Objectives (O)

Different strategies can also be considered and formulated as objective functions. For example, utilizing the demand response models, adjusted directly by the DSO or load aggregators through contracts or incentivized through consumption prices, one can achieve peak shaving or valley filling of the daily load profile. Another example is to maximize the capacity hosting of distributed generators.

2.1.2 Constraints

The constraints comprise the modeling of the electrical concept of power flows along the topological graph representing the transmission lines and node connections. It also includes the modeling of flexibilities (voltage adjustment and power injection/absorption) of volt/var

Table 2.1: Objectives, VVC devices and DERs in the relevant literature

Ref.	Objective						Phase	Controllable Assets	
	LR	CVR	SR	VF	ED	O		VVC	DER
[11]			✓				S	OLTC,VR	PV
[12]	✓	✓	✓				M	OLTC,VR,CB	
[13]	✓		✓				M	OLTC,VR,CB	PV
[14]	✓		✓				M	OLTC,VR,SVC	PV
[15]	✓		✓				S	OLTC,VR,CB	DG
[16]	✓			✓			S	OLTC,VR,CB	DG
[17]	✓						S	OLTC,VR,CB	PV,DS
[18][1]						✓	M	OLTC,VR,CB	PV
[19]	✓	✓					M	OLTC,VR,CB	PV
[20]	✓			✓			M	VR	
[21]					✓		M	VR	DG
[22]					✓		M	VR	DG
[23]					✓		M	VR	DG

[1] The objective is to maximize the hosting capacity of DGs

devices and DERs, whose main components are summarized in Fig. 2.1. In this report, we focus on a combination of these devices.

Table 5.3 compares the objectives used by the literature along with the considerations of system connection (S for single-phase and M for multi-phase) and controllable assets. Take note that we only focused on references where at least a single VVC device is modeled. DG is used when DER type is not specified.

2.2 Current State-of-the-art OPF Models and Challenges

The VVO constraints should be explicitly modeled with a high degree of accuracy in order for the dispatch solutions to be viable for the physical system. There are some tech-

nical challenges facing the VVO as an OPF-based problem, revolving around the solution optimality, computational efficiency, and scalability.

2.2.1 The Distribution System OPF Models

The fact that OPF model is *nonconvex* and NP-hard, which is short for non-deterministic polynomial-time hardness, by structure is the main obstacle of the VVO. This comes as a consequence of multiple nonlinearities in the constraints, i.e. quadratic power and voltage-current multiplication. References [12]- [14] explore to solve the problem in its original form with local nonlinear programming (NLP) algorithms. Besides being a hard-to-tackle task, reaching a *global optimum* is not guaranteed theoretically with *nonconvex* problems.

Towards this end, the literature has endeavored various models that approximate the complicating variables. The following two assumptions have been abused by [18], [19], [24] and [25] to solve the multiphase distribution systems using linear programming (LP). This is merely achieved by 1) removing or approximating the quadratic loss terms, and 2) ignoring the mutual impedances to remove the phase dependency which is another source of nonconvexity. While the resultant models are computationally-friendly, compromising some of the main components making up the D-ACOPF, such as line losses, may compromise the practicality of the dispatch solutions.

Another approach that has been widely used by the literature is to assume a per-phase representation of the system. To our knowledge, the *convex* relaxation was first introduced to the raidal power feeders in [26], where the nonlinear equality constraint is relaxed as a second-order conic program (SOCP). The SOC relaxation has also been captured by [27] for the radial branch flow model (BFM), first proposed by [28] as an NLP-based problem. In [29], the conditions under which the SOCP-based BFM relaxation is tight are identified. The tight relaxation guarantees a *global optimum*. The SOCP-based BFM has been proven to be applicable for balanced and single-phase feeders as applied in [15]- [17].

The fact that LV feeders are commonly composed of inherently-unbalanced loads and untransposed lines is yet of major significance and substantive to the mathematical replication to provide useful insights into the VVO dispatch. The multi-phase D-ACOPF has been first convexified by (a) [30] (extended from the SDP-based single-phase D-ACOPF [31]) and subsequently by (b) [24] (extended from the SOCP-based single-phase D-ACOPF [27]) via the rank relaxation of a semidefinite program (SDP). In [32], it has been demonstrated that the rank relaxation in [30] does not always yield tight solutions, and rank-one recovery is proposed via *convex* iteration and chordal conversion algorithm where rectangular variables are used. Recently, reference [22] has also proposed to replace the large PSD matrix in [30] with chordal relaxation, thereby improving the solution quality and the computational performance. In contrast, the SDP-based D-ACOPF in [24], referred to as SDP-based BFM, consists of *complex-valued* matrix variables and a $|6 \times 6|$ per-branch positive semidefinite (PSD) matrix. It has been shown to yield tight solutions for most IEEE feeders with superior computational tractability.

The linear approximation is the least descriptive model. On the other hand, The SDP and SOCP *convex* relaxations generally enlarge the feasible set, promising a *global optimality* only when the relaxation is exact, and providing lower bounds to the original *nonconvex* problem when the relaxation is not exact. Therefore, the following inclusions of the feasible region, F, are valid:

$$F_{\text{NLP}} \subseteq F_{\text{SDP}} \subseteq F_{\text{SOCP}} \subseteq F_{\text{LP}}$$

2.2.2 Discrete-based Model Integration into VVO

It is recognized that mixed integer programming (MIP) is essential for encoding the physical realization of discrete-based devices such as VRs, yet cumbersome to incorporate into the some of the OPF models causing an additional computational burden. For NLP-based VVO, [12] proposes to relax the integer variables with a rounding scheme to speed

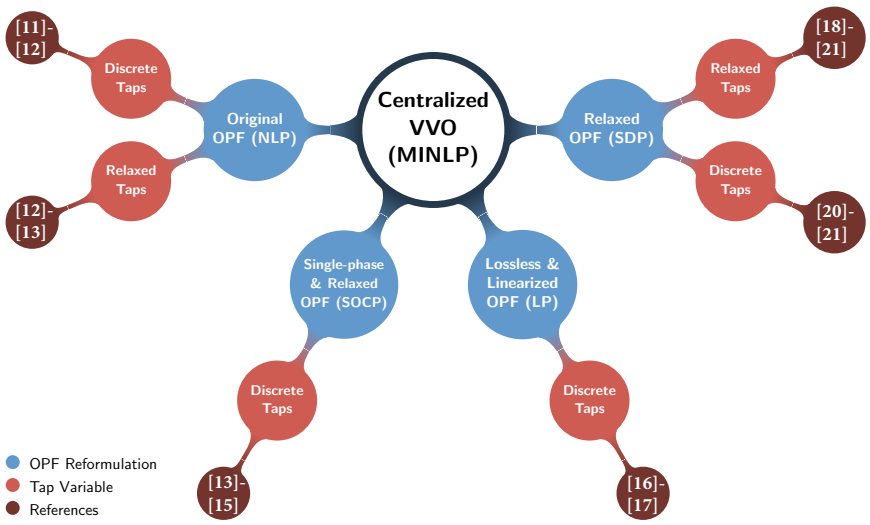

Figure 2.2: Centralized VVO implementations and VR considerations in the literature. None of the SDP-based papers consider multi horizons.

up the computation. In [14], a two-stage problem is proposed in which binary variables are relaxed for the multi-time operation, and re-considered for the single-horizon operation. Recently, reference [13] solves the MINLP-based problem via the application of predictor-corrector primal-dual interior point method (PCPDIPM). Integrating the discrete variables is not an issue with LP-based VVO, as indicated by [18]- [19].

Because of the advent in standardized MISOCP algorithms, i.e. branch-and-bound (B&B), the literature [15]- [17] has prevalently accounted for various discrete-based devices into the SOCP-based VVO, as mentioned in Table 5.3. Incorporating the discrete variables into the SDP-based VVO models is a challenging task due to the immaturity of current solvers. As a result, the assumption that VRs possess highly-granular tap ratios is abused by [20]- [23] in order to replace the discrete positions with continuous ones. This is realized in [20] merely by confining the diagonal of the *secondary*-side voltage within the tap ratio range. However, the arbitrariness of *secondary*-side phase angles, that stems from this relaxation may cause solutions to deflect from rank-one. The proposed solution to tighten the relaxation involves the placement of a tunable resistance between the primary and secondary

sides of the VR. However, it is reported that solution quality depends on carefully tuning the resistance value, which is case-specific. In [21], McCormick envelopes are employed to linearize the ratio-voltage relationship, while tap ratios with an SDP constraint. This relaxation is possible with a predetermined phase-angle differences between each pair of phases. Unfortunately, the relaxation is not tight for all case studies, and therefore requires power flow methods, such as the Z-bus method, to retrieve feasible voltages.

References [22] and [23] investigated both continuous and discrete tap models. The tap positions over the multiphase lines are assumed to operate uniformly. For the discrete tap model, a total of 8 taps are assumed for each three-phase VR. Past research [14] has found that uniform phase tap operation leads to more losses compared to the nonuniform operation. Fig. 2.2 provides the categorization of the reference papers.

2.2.3 The Multi-Time Co-optimization

The multi-time is usually a requirement to minimize the operational cost over look-ahead forecasts of load and supply. Although the primary power flow constraints are independent of time, decoupling the problem by time horizons is not readily achievable for the switching reduction objective and energy constraints of the distributed storage. Decoupling the switching reduction objective is possible by using the optimal solution of previous horizons, as in [15], but it yields sub-optimal solutions. This interdependence among time intervals poses a computational challenge due to the limit of the number of variables in a single problem.

The fact that multi-time optimization problem relies on the predicted data of load and generation may create two challenges.

- Contrary to the load prediction models, the generation prediction models may be associated with higher error margins.

- The control devices have different response capabilities. The discrete-based models that entail larger mechanical actions are generally slower than the power-electronic inverters.

In this research, we explore the multi-time scheduling problem from the computational perspective. In order to obtain the advantage of the multi-time operation global optimality and, at the same time, avoid the computational burden of incorporating stochastic variations, we assume that the generation predication models have as high an accuracy as the load predication models. Also, we solve the multi-time scheduling problem with a larger timescale to ensure that all control devices' actions can coincide. By committing the dispatch of the slow devices, another problem can be performed over a smaller timescale with the reactive power of the inverters as the only control variables. The latter is not included in this research as it is generally less challenging.

In the third chapter, we perform the VVO problem for balanced systems for the next day on 15-minute and hourly basis. For unbalanced systems, we perform the problem for the next day on hourly-basis. Fig. 2.2 indicates that the literature adopting the SDP-based VVO has not considered the multi-time operation.

2.2.4 Incorporation of Broader Applications into the D-ACOPF

Internalizing the distribution system's fundamental components into the D-ACOPF problem is of the essence for the solution quality and control dispatch viability. Our initial work and the majority of the literature are based on the assumption that all loads, DERs and SVRs are wye-connected. Moreover, the current convex Multi-phase D-ACOPF cannot solve for voltage-related objective functions

In this this research, we develop a problem to minimize the voltage deviations from desired thresholds subject to the physical constraints of a comprehensive distribution ACOPF model. We elevate the model to encompass all connections of loads, distributed energy re-

sources (DERs), and step-voltage regulators (SVRs). We capitalize on extending the branch flow model (EBFM) with non-convex primary-to-secondary voltage constraint, and rank-one constraints belonging to the power flow and delta-connected net injections. Relaxing the constraints renders a semidefinite programming (SDP), whose AC feasibility depends on the solution exactness (proximity of all positive semidefinite (PSD) matrices to being rank 1). For the underlying model, three sources of inexactness (higher rank) are identified: (i) the voltage-related objective function, (ii) the delta-connected load and DER constraints, and (iii) the relaxed constraints for voltage regulators (SVRs) with continuous and non-uniformly-operated tap positions. We propose to ultimately circumvent this rank conundrum via the application of convex iteration, whereby the inexact solution initializes a sequence of rank-constrained problems. The correlation among the previous components allows the convergence to coincide. The merits of the proposed problem are evinced by case studies on IEEE distribution feeders with retrieved rank-1.

Chapter 3: VVO for Balanced Distribution Systems

3.1 Introduction

In this chapter, we conduct a multi-objective multi-time VVO on distribution systems with the assumption that loads and line impedances are balanced [1]. In which case, the per-phase representation is valid since VVO dispatch is unified among phases. This assumption significantly reduces the problem size, and hence increases the efficiency of the problem. Moreover, it enables us to make use of the SOCP-based BFM to represent the D-ACOPF problem.

The formulated VVO aims at the following:

1. Formulating a comprehensive objective function that comprises LR, CVR, SR, and VL.

2. Leveraging the standardized MISOCP solvers to model and optimally set discrete devices, namely VRs and CBs in the presence of high PV penetration.

3. Exploring the coordination between off-unity PV and discrete devices towards attaining the operational objectives with lower switching counts of VRs and CBs.

[1] This chapter was published in North American Power Symposium [33], 2018. Permission is included in Appendix A.

3.2 Problem Formulation

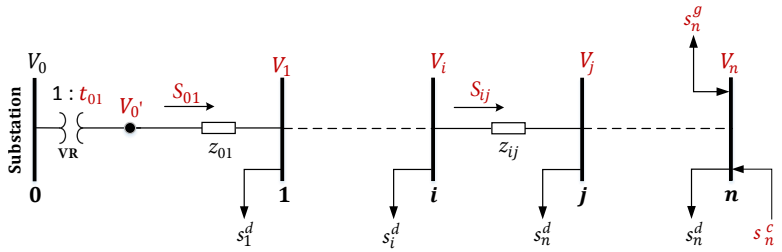

Figure 3.1: One-line diagram of a balanced radial distribution feeder and system variables.

3.2.1 Branch Flow Model Based on Second-order Conic Programming

3.2.1.1 Notation

Consider a radial distribution system, where each bus has a distinct parent, represented by the graph $\mathcal{G}(\mathcal{B}, \mathcal{L})$, where $\mathcal{B}$ and $\mathcal{L}$ denote the sets of buses and line segments. Generally, buses are indexed by $i \in \mathcal{B}$, thus $\mathcal{B} = \{i : i = 0, 1, 2, \ldots, n\}$, whereas lines are indexed by $(i, j) \in \mathcal{L}$. Another set is used, $\mathcal{B}^+ = \mathcal{B} - \{0\}$, to denote descent buses from the substation whose voltage magnitude is fixed, $V_0 = V_{\text{nom}}$.

3.2.1.2 Ohm's Law

The voltage drop on (i, j) is

$$V_j = V_i - z_{ij} I_{ij} \qquad \forall (i, j) \in \mathcal{L} \tag{3.1}$$

where V_i, V_j I_{ij}, and $z_{ij} = r_{ij} + j x_{ij} \in \mathbb{C}$ are either *complex-valued* or *phasors* (phase and angle). Since voltage magnitudes are more indicatory of the system's security. The equation in (3.1) can be re-written to consist of *real-valued* variables. Note that this is a practical assumption given that angle instability is rare in distribution systems [34]. Thence, the angle is removed by multiplying both sides by their conjugates, and substituting the variables with

$v_i = V_i V_i^*$, $v_j = V_j V_j^*$, $\ell_i = I_{ij} I_{ij}^*$ and $S_{ij} = V_i I_{ij}^*$.

$$v_j = v_i - 2z_{ij}^* S_{ij} + |z_{ij}|^2 \ell_{ij} \qquad \forall (i,j) \in \mathcal{L} \tag{3.2}$$

3.2.1.3 Power Balance

For each $i \to j \to k$, to interpret the power balance at j, (3.1) is multiplied by I_{ij}^*

$$V_j I_{ij}^* = V_i I_{ij}^* - z_{ij} I_{ij} I_{ij}^* \tag{3.3}$$

$$V_j \Big(\sum_{(j,k) \in \mathcal{L}} I_{jk}^* + I_j^* \Big) = S_{ij} - z_{ij} \ell_{ij} \qquad \forall (i,j) \in \mathcal{L} \tag{3.4}$$

where I_j is the net current at bus j. The net load power at bus j is s_j, and thus the power balance becomes

$$\sum_{(j,k) \in \mathcal{L}} S_{jk} + s_j = S_{ij} - z_{ij} \ell_{ij} \qquad \forall (i,j) \in \mathcal{L} \tag{3.5}$$

3.2.1.4 Power, Current and Voltage Constraint

To set the relationship among the surrogate variables, the power equation is constrained as

$$\ell_{ij} v_i = |S_{ij}|^2 \qquad \forall (i,j) \in \mathcal{L} \tag{3.6}$$

3.2.1.5 Convexification

The constraint in (3.6) is *nonconvex* due to the multiplication of variables and squared apparent power. However, it can be relaxed into a second-order conic program, as first proposed by [27]. The relaxation is achieved by transforming (3.6) into an inequality constraint

as in (3.7)

$$\ell_{ij} v_i \geq |S_{ij}|^2 \qquad \forall (i,j) \in \mathcal{L} \tag{3.7}$$

which can be translated into a linear inequality constraint as follows

$$\ell_{ij} v_i \geq |S_{ij}|^2 \tag{3.8}$$

$$\ell_{ij}^2 - \ell_{ij}^2 + v_i^2 - v_i^2 + 4\ell_{ij} v_i \geq 4|S_{ij}|^2 \tag{3.9}$$

$$(\ell_{ij} + v_i)^2 - (\ell_{ij} - v_i)^2 \geq (2\mathrm{Re}(S_{ij}))^2 + (2\mathrm{Im}(S_{ij}))^2 \tag{3.10}$$

$$\ell_{ij} + v_i \geq \left\| \begin{matrix} 2\mathrm{Re}(S_{ij}) \\ 2\mathrm{Im}(S_{ij}) \\ \ell_{ij} - v_i \end{matrix} \right\| \tag{3.11}$$

In [29], [35], sufficient conditions under which the SOC constraint is guaranteed to be exact are provided, and summarized as follows:

1. the objective function is strictly increasing in active power injection.

2. the upper bounds on voltage magnitudes are not binding.

3.2.2 Discrete-based Device Models

3.2.2.1 Voltage Regulator Model

A fictitious node, i', is assumed at the transformer primary to describe the power flow into the branch (i,j), and set relations among variables. Here, an ideal VR is assumed (the leakage impedance is negligible), and the primary is connected to substation bus 0. Subsequently, a virtual bus is introduced to the system, $0' \in \mathcal{B}^+$, to represent the secondary side. Fig. 3.1 shows a per-phase VR installed on $(0,1)$. The tap ratios $r_{i'}$ are modeled

as decision variables so as to adjust the *secondary*-side and descent voltage levels. Let K be the number of positions the tap can take, i.e. typically ± 16 and a neutral position, $K = \{k|k = 0, 1, 2, \ldots, 32\}$. Then, the per-phase discrete adjustment process is reflected by the following

$$r_{i'} = \sum_{k=0}^{K} (r_{\min} + \Delta r_{i'} \times k) u_{i',k}, \qquad \sum_{k=0}^{K} u_{i',k} = 1 \tag{3.12}$$

$$\Delta r_{i'} = (r_{\max} - r_{\min})/|K| \tag{3.13}$$

where $r_{\min}$ and $r_{\max}$ are the minimum and maximum turns ratios, and $\Delta r_{i'}$ is the ratio change per tap. To enforce the ratio selection, a binary variable, $u_{i',k}$, is multiplied by each ratio, and the sum to 1 results in a single ratio. The formulation in (4.8) requires $3|K|$ of binary variables for each VR. The *secondary*-side voltage is then expressed in terms of the variable tap ratio as follows.

$$v_{i'} = r_{i'} v_i \tag{3.14}$$

Note that (3.14) is only linear if the *primary*-side voltage is known, as in our case. If not, further linearization are required [15]- [18], [36].

3.2.2.2 Capacitor Bank Model

A set of switchable capacitors can be installed at the jth node, where each capacitor is switched on to increase the voltage at the node of installation and adjacent nodes. Assuming a CB is connected to bus $n \in \mathcal{B}_{\text{cap}} \subset \mathcal{B}^+$, an integer variable, c_n, is defined to enforce the switching operation.

$$0 \leq c_n \leq N_c, \qquad \text{Im}(s_n^c) = Q_c \frac{c_n}{N_c}, \qquad \text{Re}(s_n^c) = 0 \tag{3.15}$$

where $\text{Im}(s_n^c)$ is the CB' variable included in (1b), and Q_c and N_c are the rating and number of the total SCB units; respectively.

3.2.3 Continuous-based PV Inverter Model

In order to represent the operating points shown in Fig. 3.2, the reactive-power constraint is expressed as

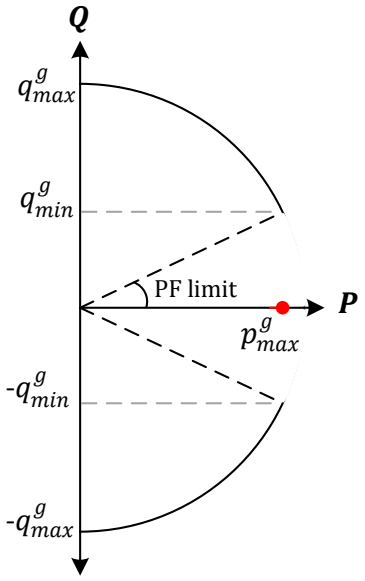

Figure 3.2: Operating region of a variable power-factor photovoltaic inverter.

$$|\text{Im}(s_n^g)| \leq \sqrt{(s_n^{\max})^2 - (\text{Re}(s_n^g))^2} \tag{3.16}$$

Overcapacity of the inverter and thus reactive power generation/absorption during peak PV generation are ensured if the nameplate MVA, namely $s_n^{\max}$, is larger than peak PV active power.

3.2.4 VVO Problem

3.2.4.1 CVR and VF Limits

The purpose of conservation voltage reduction (CVR) and voltage flattening (VF) was introduced in the previous chapter. CVR (VF) aim at regulating the nodal voltages at the lower half of ANSI limits (around the reference voltage). The constraints in (3.17) are used to keep the voltage of the ith node between minimum and maximum thresholds.

$$y_i \geq 0, \qquad y_i \geq v_i - (V_{i\,\min}^{thr})^2, \qquad y_i \geq -v_i + (V_{i\,\max}^{thr})^2 \tag{3.17}$$

Tighter threshold, i.e. $V_{i\,\max}^{thr} = 1$, can be assigned for nodes at which voltage-dependent loads are installed, $i \in \mathcal{B}_{\text{cvr}} \subset \mathcal{B}^+$, and y_i is minimized with large cost coefficients to create a trade-off with the loss-minimization objective. Moreover, this objective can be generalized for all nodes with lower costs and wider limits, say $\pm 3\%$, to flatten the voltage. The desired lower threshold is -3% so as to avoid excessive voltage drop at the point of interconnection and maintain the safety of the equipment behind the meter.

3.2.4.2 Overall Problem

$$\begin{aligned}
\textbf{VVO} := \min_{v,\ell,S,s^c,s^g,r,u} \quad & \sum_t^T \Bigg(\alpha_{\text{loss}} \sum_{(i,j)\in\mathcal{L}} r_{ij}\ell_{t,ij} + \alpha_{\text{cvr}} \sum_{i\in\mathcal{B}_{\text{cvr}}} z_{t,i} \\
& + \alpha_{\text{flat}} \sum_{i\in\mathcal{B}^+-\mathcal{B}_{\text{cvr}}} z_{t,i} + \alpha_{\text{cap}} \sum_{i\in\mathcal{B}_{\text{cap}}} |c_{t,i} - c_{t-1,i}| \\
& + \alpha_{\text{vr}} \sum_{(i')\in\mathcal{B}^+} |r_{t,i'} - r_{t-1,i'}| \Bigg) \\
\text{s.t.} \quad & 0.95^2 \leq v_{i,t} \leq 1.05^2 \quad \forall i \in \mathcal{B}^+ \\
& (3.2), (3.5), (3.11), (4.8), (3.14) - (3.17)
\end{aligned} \tag{3.18}$$

3.3 Numerical Example

The case study highlights the following:

1. the impacts of cloudy day and clear day forecasted with 15 minutes slots ($T = 96$) on the frequency of an VR and CB operations.

2. the effectiveness of the centralized VVO to mitigate the equipment operations and adhere to the other objectives leveraging of the inverter's inherent Var capability.

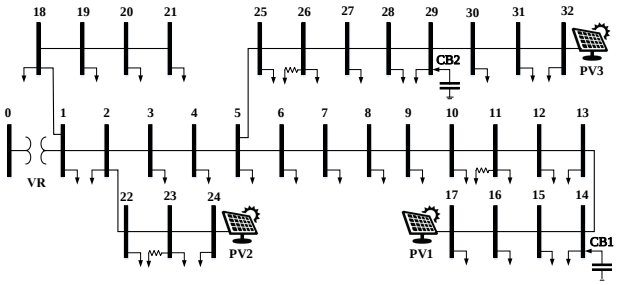

Figure 3.3: Modified IEEE 33-node feeder.

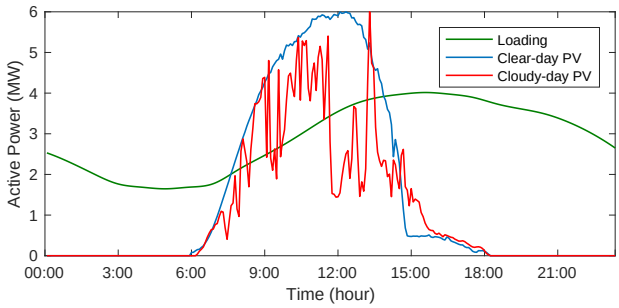

Figure 3.4: Loading, clear-day PV and cloudy-day PV profiles.

Fig. 3.3 illustrates the IEEE 33-node feeder, which was modified to include a VR, CBs and voltage-dependent loads. The original peak load is 4.55 MVA with power factor of 0.82. Loads at each node and line parameters are obtained from [28]. Three resistive loads are modeled, each with 100 kW, at nodes 11, 23 and 26. The VR is installed on the substation branch, with a turns ratio varying from 0.95 to 1.05. The tap position is constrained by

$r_{\max} = 32$, which is a typical limit of a practical tap changer's winding. Also, two CBs, each with a total of 360 kVAR and three switchable units ($N_c = 3$), are installed at the remote node 14, and the heavy reactive power loaded bus 29, whose adjacent buses consume 30% of the load.

Fig. 3.4 shows a typical loading curve depicted by the total active power load. Also, three 2-MW PV plants are installed at nodes 17, 24 and 32. Each PV inverter has 110% apparent-power capacity of the peak active power. Fig. 3.4 shows two PV power profiles by the total MW at 5-minute resolution. The profiles mimic a real solar panel's data collected at the University of South Florida on May 15, and August 15 of 2013.

3.3.1 Case Studies

Two timescales are used to solve (3.18): every 15 minutes ($T = 96$), and every hour ($T = 24$). Multiple scenarios are carried out interchangeably, with more emphasis on the tap and CB operations. The figures showcasing the tap changes are only limited to the 15-minute timescale. Equipment-operation penalties are fine-tuned starting with small values to achieve the best coordination with PV VARs [11]. For simplicity, loss reduction and CVR objectives are set with unity penalties, while flatness is found to take effect with 0.3.

Table 3.1: Objectives and cost coefficients

Objective	Symbol	Range	Cost ($)
Loss Reduction (LR)	λ_{loss}	-	1
Conservation of Voltage Reduction (CVR)	α_{cvr}	0.97-1.00 pu	1
Voltage Flattening (VF)	α_{flat}	0.97-1.03 pu	0.3
Switching	α_{vr}	0-32 taps	3
Reduction (SR)	α_{cap}	0-3 units each	0.1

3.3.1.1 Case I: VVO without SR Objective and PV Vars

At unity power factor of the PV inverters, the three scenarios are compared in terms of equipment operations. Since the inverter's VAR is absent for this case, the tap-cap costs in the VVO are zeroed out ($\alpha_{\text{vr}} = \alpha_{\text{cap}} = 0$) so as to let the VR and CBs satisfy the operation constraints.

At no PV, the tap actions are moderate and following the load, while CBs kept supplying full VARs. However, during both clear-day and cloudy-day PV penetrations, the VR and CB actions dramatically increased in frequency to cope with the dynamic net load for the 15-minute timescale. PV power at a cloudy-day in particular results in significant increase of switching actions, and is consequently deemed the worst-case scenario.

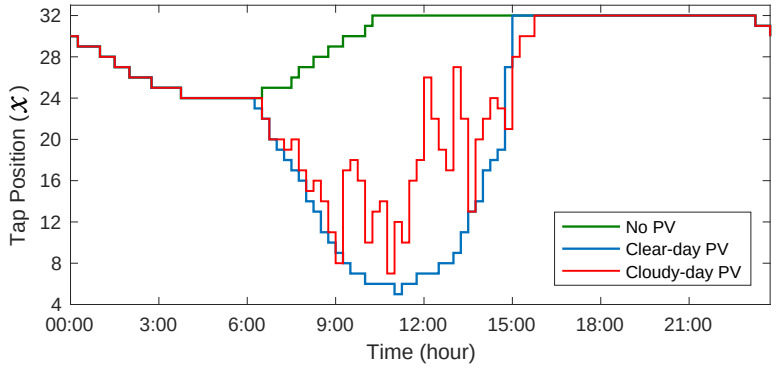

(a)

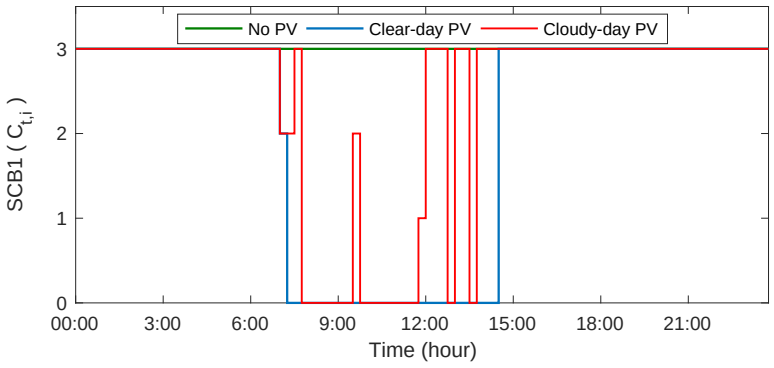

(b)

Figure 3.5: 15-minute scheduling: (a) Tap positions. (b) Number of switched CBs.

Table 3.2: Operation counts at unity PF of PVs for case I

Equipment	No PV	Clear-day PV	Cloud-day PV
15-minute Timescale			
VR	16	36	43
CB1	-	3	11
CB2	-	5	8
Hourly Timescale			
VR	9	14	14
CB1	-	4	5
CB2	-	3	2

3.3.1.2 Case II: VVO without CVR and VF Objectives

Keeping SR zeroed out, the scenario with cloudy-day and unity-PF PVs is solved with and without costs that penalize CVR and VF ($\alpha_{\text{cvr}} = \alpha_{\text{flat}} = 0$) objectives to highlight the significance of these objectives and explore the capability of traditional equipment to abide by their voltage thresholds. The main feeder is selected to examine voltage profiles, which has the VR, a resistive load at node 11, switched CBs at node 14, and a PV at node 17. Fig. 3.6a shows that without the penalties, the LR objective operates taps and CB units mostly at their maximum bound, thus increasing voltage variations at the downstream nodes and violating CVR. The taps and CB1 are suddenly reduced when the voltage at node 17 tends to exceed 1.05 pu. This is because minimum losses are obtained with maximum allowed voltages. On the other hand, with the penalties, Fig. 3.6b shows that voltages are regulated closely within the desired limits specified in Table 3.1, and with tap-cap actions shown in Table 3.2. During evening hours 16:00-21:00, the flatness penalty, α_{flat}, takes less effect on the VR secondary voltage as more taps are switched to counteract the heavy loading. It can be concluded that traditional equipment can effectively regulate voltages within the specified thresholds. This however comes at the cost of increased equipment operations.

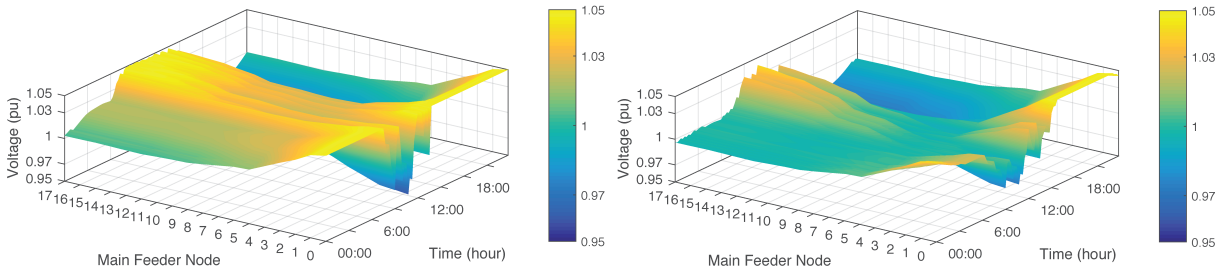

Figure 3.6: 15-minute scheduling: Main feeder voltages (a) without and (b) with CVR and flat-profile penalties.

3.3.1.3 Case III: VVO with Comprehensive Objectives

With off-unity power factor PV inverters, the possibility of coordination between traditional equipment and inverters towards reducing tap-cap operations and improving voltage profiles is explored utilizing the multi-objective function in (3.18) and considering all costs in Table 3.1.

Being the worst-case scenario in terms of equipment operation and voltage variation, the VVO is solved for the cloudy-day PV. The results in Fig. 3.7-3.8 focuses on the period when PV power is most variable.

Table 3.3: Cloudy-day operations at off-unity PF of PVs for case III

Equipment	With PV VARs	With PV VARs & switching penalties
15-minute Timescale		
VR	47	20
CB1	12	-
CB2	-	-
Hourly Timescale		
VR	16	6
CB1	2	-
CB2	-	-

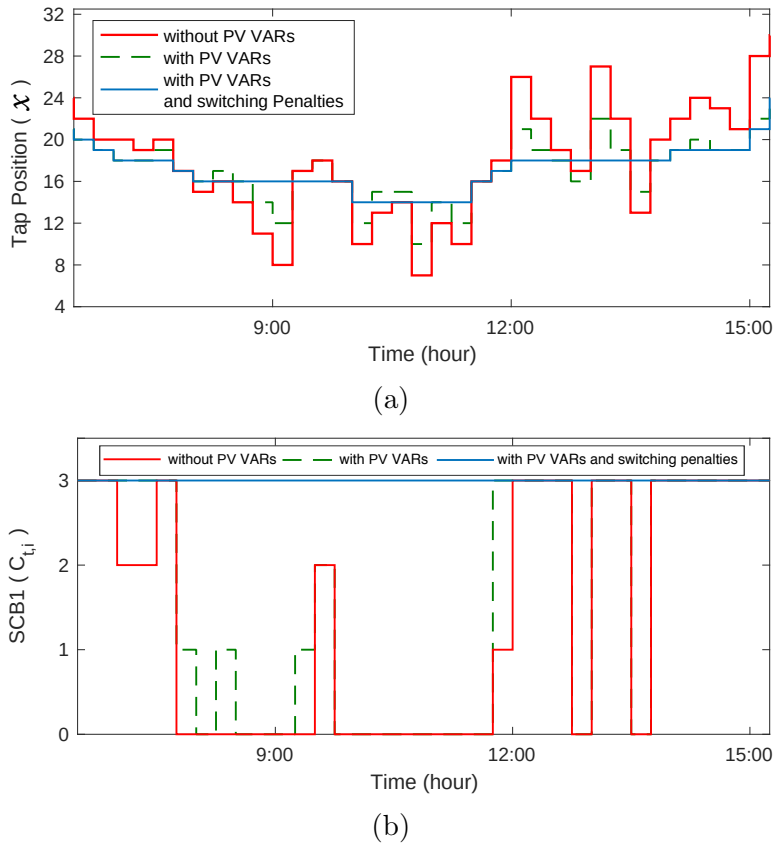

Figure 3.7: 15-minute scheduling: (a) Tap positions. (b) Number of switched CBs.

Fig. 3.7-3.8 shows that when the VVO is solved without the switching penalties, the inverters are not urged to generate/absorb enough VARs so as to reduce the tap-cap actions, since voltages are within the limits as in Fig. 3.8a. As a result, the switching not only maintains a similar behavior, but also increased for the VR and CB1 as in Table 3.3. Exceptionally, CB2 remains unswitched without the switching penalty. In contrast, with the switching penalties in Table 3.1, the PV VARs coordinates well with the VR taps, while keeping CB1 unswitched as in the baseline case. The coordination can be observed at instances when PV VARs approach zero, VR taps switch with smaller steps than those simulated without switching penalties and/or VARs.. Also, the reactive/capacitive PV VARs boost

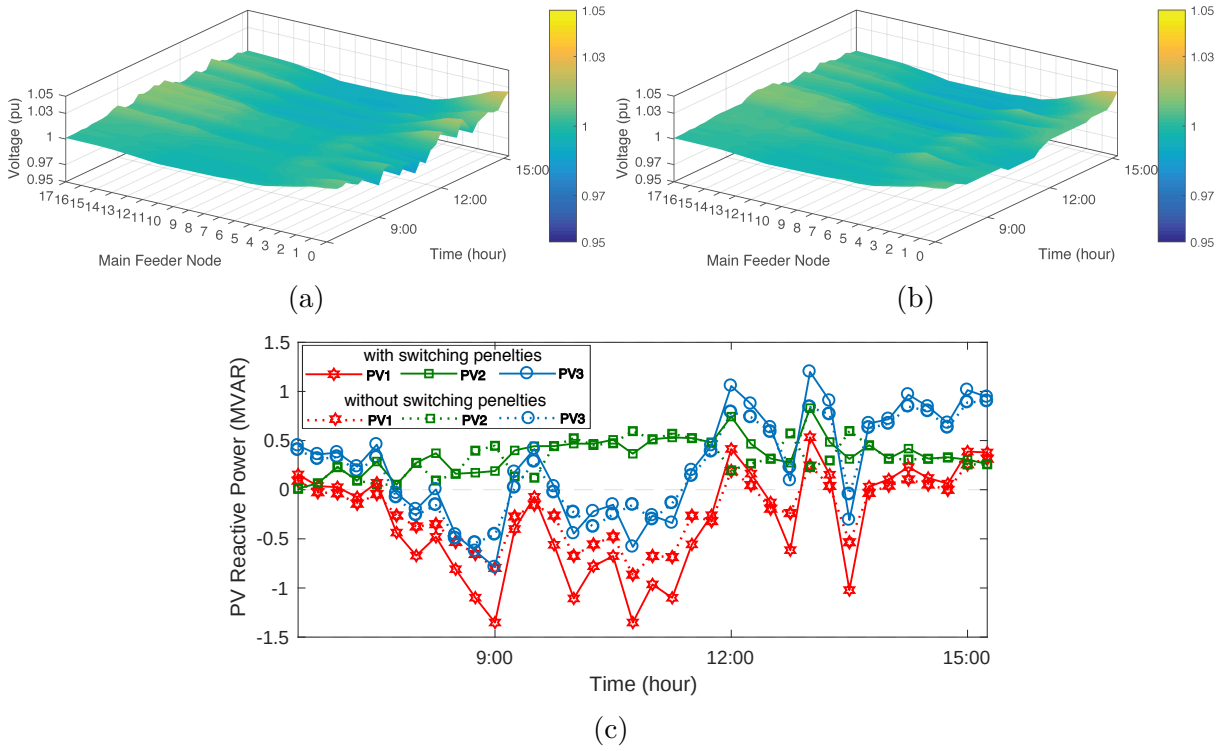

Figure 3.8: 15-minute scheduling: (a) VAR-compensated main feeder voltages without switching penalties, and (b) with switching penalties. (c) VARs from each inverter with and without switching penalties.

to counteract the peaks and valleys of PV active power. The resulting voltage profiles are further improved as in Fig. 3.8b. Table 3.3 lists the switching counts for each device.

3.3.2 Performance of the MISOCP VVO

3.3.2.1 Computation

The optimization problem is implemented CVX [37,38] solved by GUROBI optimizer [39]. The number of variables and solve times for each timescale are given in Table 3.4. The solve times are retrieved from the fifth time argument reported by CVX, which can be obtained by enforcing `cvx_tic` and `cvx_toc`. Due to the high computational burden imposed by

Table 3.4: Computational performance

Timescale	Number of Variables	Solve Time (s)
15-minute	46728	-
Hourly	11682	47.75

the number of discrete variables (binary and integer), we conclude that the hourly timescale is more amenable to be used for day-ahead volt var scheduling.

3.3.2.2 SOCP Exactness

The implementability of the presented centralized VVO is verified via examining the exactness of the SOCP relaxation. The SOCP relaxation is said to be exact if the solution admits the power flow characteristics. That is, the SOC inequality constraint of the squared current in (3.7) satisfies a sufficiently small error. Therefore, the exactness for the solution of all currents and over all time horizons is examined by computing the error in (3.19). The results are shown in Fig. 3.9.

$$\text{Exactness} = \sum_{t\in T}\sum_{(i,j)\in\mathcal{E}} |\ell_{t,ij} - (P_{t,ij}^2 + Q_{t,ij}^2)/v_{t,i}| \tag{3.19}$$

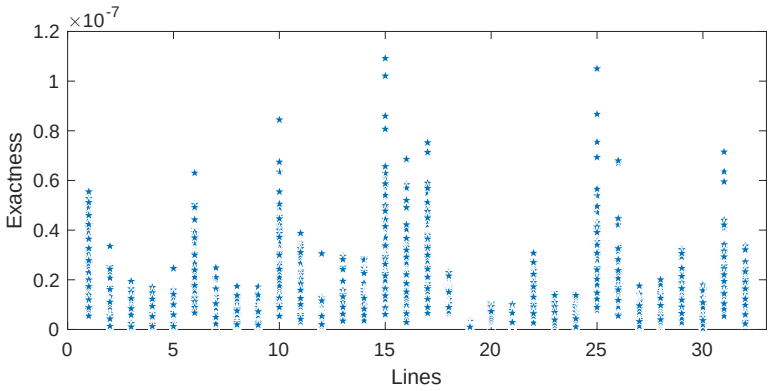

Figure 3.9: Exactness of the centralized VVO solution for the 15-minute scheduling.

Since the overall errors are in the vicinity of 1×10^{-7}, the solution is exact and the presented VVO is implementable. The maximum error for the 15-minute and hourly timescales are 1×10^{-7} and 8×10^{-8}, respectively.

3.3.2.3 Comments on the Integration of More DERs

In this chapter, we only focused on the co-optimization of discrete-based devices, i.e. SVRs and CBs, with PVs. The PV is assumed to have known real power supply (solar power), where curtailment is not accessible to the DSO. Further, there exists more continuous models such as energy storage units, whose DC/AC inverters can also produce and absorb reactive powers.

Increasing the pentration level to higher percentages and incorporating more models into the single-phase BFM may weaken the SOCP relaxation, thereby producing infeasible solutions to the ACOPF problem. Such inexactness can be caused by the excess of the power dispatch which may cause the binding the voltage to the upper allowable limit as demonstrated in [29], [35]. The existing literature presented some techniques to strengthen the SOCP relaxation of the single-phase BFM in particular [34, 40], and the SDP relaxation of the multi-phase BFM [32]. The latter can be used by retrieving the SDP relaxation of the single-phase BFM.

3.4 Conclusion

This chapter formulates a centralized VVO that aims at reducing equipment operations and keeping overall voltage profiles within the satisfactory limit at high penetration of PV. CVR practices are also taken into account. Case studies of three scenarios were conducted to demonstrate the effectiveness of the VVO. At unity power factor of the PV inverters , the results have shown that the traditional equipment approximately fulfilled the specified limits for voltage. This was at the expense of increased and repetitive operations of VR

taps and CBs. By minimizing the switching cost of VR taps and switched CBs, off-unity inverters operate as the fundamental voltage regulators mainly via boosting reactive-power supply/absorption throughout the variable PV penetration. Therefore, coordination between the traditional equipment and PV inverters can effectively reduce equipment operations, make optimal utilization of PV powers, and flatten voltage profiles even at mid-way nodes.

Chapter 4: VVO for Unbalanced Distribution Systems

4.1 Introduction

In this chapter, we extend the VVO problem to consider the distribution system's unbalances[1]. An offline volt/var framework is proposed that optimally coordinates the day-ahead scheduling of voltage regulators with off-unity inverters of photovoltaics (PVs) subject to physical and security constraints of unbalanced distribution systems. Similar to [11], the proposed problem makes use of predicted load and generation profiles to return a globally optimal operating point for the next day with minimized voltage regulator actions (VRAs). The operational objectives comprise minimizing the energy import from the substation (maximize solar utility), the line losses, and the inter-temporal actions of voltage regulators (VRs) to reduce their maintenance costs and better coordinate with the PV Var compensation. To account for the multi-phase and unbalanced nature of distribution systems, we build upon the rank-relaxed semidefinite programming branch flow model (SDP BFM), whose tight solutions ensure global optimality. Also, exact discrete-based VRs exhibiting the mechanical adjustments of tap positions are used. The resultant day-ahead volt/var optimization (VVO) is a mixed-integer semidefinite program (MISDP).

From the existing methods presented by the relevant literature and summarized in Chapter 2, we observe the following limitations:

[1]This chapter was accepted for publication in IEEE Transactions on Sustainable Energy [41], 2020. Permission is included in Appendix B.

- The detailed model of discrete-based VRs with nonuniform dispatch of phase taps has not been incorporated into *convex* multi-phase OPF models.
- The capability of current MISDP solvers is limited to smaller instances of binary variables. Besides, solving the multi-time problem may not be possible. The two aspects are shown in the section of computational performance.
- The multi-time consideration to minimize the VR's cycling over predicted load and supply has not been explored using *convex* multi-phase OPF models.

What follows are the challenges identified to address the limitations using SDP-based BFM [24]:

- The presence of trilinear terms emanating from ratio-voltage relationship.
- The difficulty of incorporating binary variables into the SDP-based problems due to the immaturity of current MISDP solvers.
- The difficulty to account for the multi-time operation in a single closed-form problem since it increases the cardinality.

4.2 Contributions

Motivated by the former limitations, this paper proposes a customized GBD-based algorithm that provides a global optimal multi-time scheduling of VRs and PVs over an hourly horizon window, accurately internalizes the discrete nature of three-phase VR model with independently-controlled tap positions (33 tap ratio per phase), and reduces the inter-temporal VRAs, which can ultimately be achieved via re-adjustments of continuous PV Var compensation throughout the scheduling horizon.

1. A multi-time co-optimization of VRs and PVs is formulated which integrates detailed discrete tap positions into the state-of-the-art SDP-BFM model to minimize VRAs.

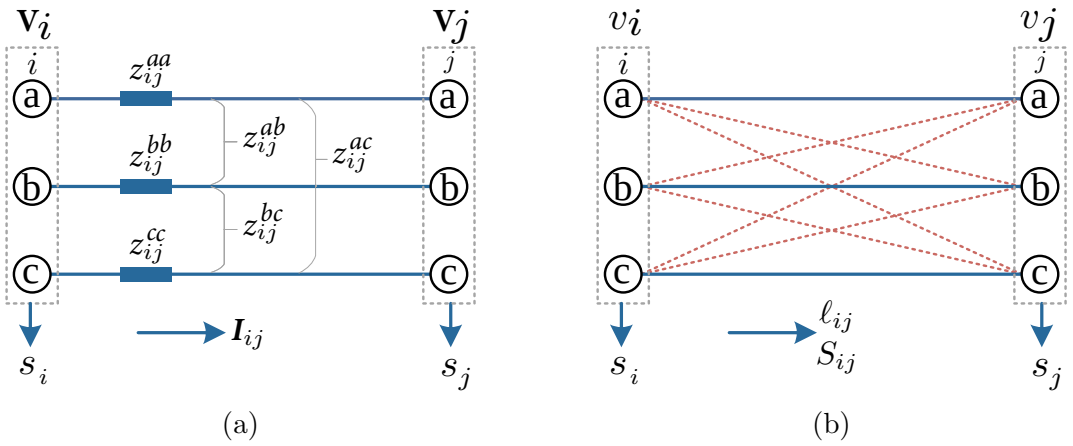

Figure 4.1: (a) Original distribution line. (b) Matrix-based representation with angle relaxation.

The binary expansion technique, presented in [36] for single-phase tap changers, is extended to the multiphase BFM. To the best of our knowledge, accounting for the multi-time coordinated operation with VRA reduction on the SDP-based multiphase D-ACOPF have not been accomplished by the literature.

2. An efficient solving algorithm based on GBD is designed. The subproblem (SP) is decoupled by the prediction horizons and computed sequentially, and the multi-cut master problem (MP) solves the tap ratio variables and inter-temporal VRA objective. The problem separation not only provides an alternative to integrate the binary variables, but also sidesteps the non-convexities and the rank conundrum originating from the VR incorporation.

3. Enhancement of GBD convergence is designed for the specific structure of the problem. The convergence is improved by adding constraints to the master problem that bind the tap ratios by the voltage limits.

4.3 Problem Formulation

In this section, we review the multiphase BFM, introduce the VR and PV models, and set the objectives for the proposed multi-time scheduling problem. For brevity, the time index, t, is removed from modeling subsections.

4.3.1 Branch Flow Model Based on Semidefinite Programming

Consider a radial distribution system (each bus has a distinct parent) represented by the graph $\mathcal{G}(\mathcal{B}, \mathcal{L})$. The root bus, whose voltage is set to V_{nom}, is denoted as 0, thus $\mathcal{B}^+ = \mathcal{B} - \{0\}$. In what follows, we use the Ohm's law to derive the matrix-based SDP BFM constraints [24].

4.3.1.1 Ohm's Law

The voltage drop on (i, j) is

$$V_j = V_i - z_{ij} I_{ij} \tag{4.1}$$

where V_i, V_j, and $I_{ij} \in \mathbb{C}^{|\Phi_j|}$, while $z_{ij} \in \mathbb{C}^{|\Phi_j| \times |\Phi_j|}$. When both sides are multiplied by their Hermitian transposes, and $v_i = V_i V_i^{\text{H}}$, $v_j = V_j V_j^{\text{H}}$, $S_{ij} = V_i I_{ij}^{\text{H}}$ and $\ell_i = I_{ij} I_{ij}^{\text{H}}$ are defined, (5.1) can be re-expressed as

$$v_j = v_i - (S_{ij} z_{ij}^{\text{H}} + z_{ij} S_{ij}^{\text{H}}) + z_{ij} \ell_{ij} z_{ij}^{\text{H}}, \quad \forall \ (i, j) \in \mathcal{L}. \tag{4.2}$$

In this form, actual phase angles are implicit in the nondiagonal complex entries of the surrogate variables, whereas diagonal entries represent the squared voltage magnitudes (real values).

4.3.1.2 Power Balance

For each $i \to j \to k$, to interpret the power balance at j, (5.1) is multiplied by I_{ij}^{H}:

$$V_j I_{ij}^{\mathrm{H}} = V_i I_{ij}^{\mathrm{H}} - z_{ij} I_{ij} I_{ij}^{\mathrm{H}}, \tag{4.3}$$

$$V_j \Big(\sum_{(j,k)\in\mathcal{L}} I_{jk}^{\mathrm{H}} + I_j^{\mathrm{H}} \Big) = S_{ij} - z_{ij} \ell_{ij}, \tag{4.4}$$

where I_j is the net current at bus j. The net load power at bus j is $s_j \in \mathbb{C}^{|\Phi_j|}$, and thus the power balance is expressed as the diagonal of (4.4):

$$\sum_{(j,k)\in\mathcal{L}} \mathrm{diag}(S_{jk}) + s_j = \mathrm{diag}(S_{ij} - z_{ij}\ell_{ij}), \quad \forall (i,j) \in \mathcal{L}. \tag{4.5}$$

4.3.1.3 PSD and Rank-1 Matrix

The following positive and rank-1 $2|\Phi| \times 2|\Phi|$ matrix, written in a 2×2 block, are essential for the power flow constraint ($v_i \odot \ell_{ij} = S_{ij} \odot S_{ij}^{\mathrm{H}}$, where $\odot$ is an element-wise multiplication operator).

$$F_{ij} = \begin{bmatrix} v_i & S_{ij} \\ S_{ij}^{\mathrm{H}} & \ell_{ij} \end{bmatrix} \succeq 0 \qquad \forall \ (i,j) \in \mathcal{L} \tag{4.6}$$

$$\mathrm{rank}(F_{ij}) = 1 \qquad \forall \ (i,j) \in \mathcal{L} \tag{4.7}$$

where $\succeq$ enforces the positive semidefiniteness (all matrix eigenvalues are nonnegative).

4.3.1.4 Convexification

The rank-1 constraint (4.7) is removed from the set of constraints to arrive at a convex problem. The solution of each F_{ij} should however promise a close proximity to rank1, for

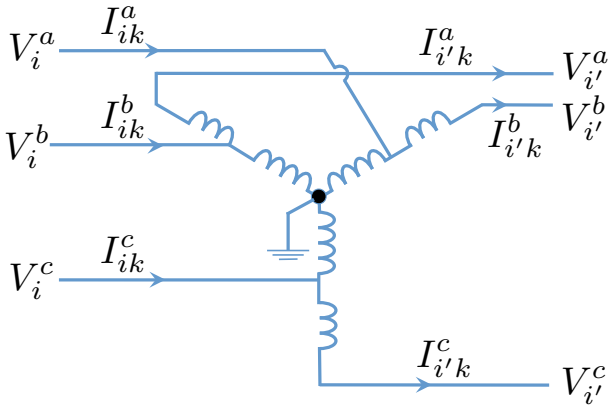

(a)

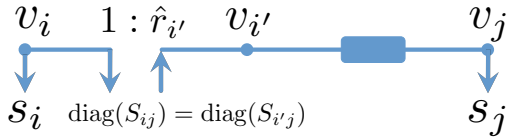

(b)

Figure 4.2: (a) Three-phase VR. (b) Simplified representation of the VR line in SDP-based BFM.

which an exactness check will be conducted on the results in the section of computational performance.

4.3.2 Three-phase Voltage Regulator Model

A three-phase VR consists of three single-phase autotransformers, each equipped with an independent tap changer to regulate the system unbalances. In this chapter, we consider a wye-connected type-A VR, in which the primary-side bus i is connected to the shunt directly. A virtual bus is introduced to the system, $i' \in \mathcal{B}^{\mathrm{s}}$, to represent the secondary side, which is connected to the series impedance via taps. Fig. 5.2 shows the connection of the three-phase VR. The tap ratios $r_{i'} \in \mathbb{R}^{|\Phi_j|}$ are modeled as decision variables so as to adjust the secondary-side and descent voltage levels. For simplicity and given that the VR series impedance is too small [42], an ideal VR is assumed and the series impedance is neglected.

4.3.2.1 Per-phase VR Model

Let $|\mathcal{K}|$ be the number of positions the tap can take, i.e. typically ± 16 and a neutral position, $\mathcal{K} = \{k|k = 0, 1, 2, \ldots, 32\}$. Then, the per-phase discrete adjustment process is reflected by the following:

$$V_{i'}^{\phi} = r_{i'}^{\phi} V_i^{\phi} \forall i' \in \mathcal{B}^{\mathrm{s}} \tag{4.8a}$$

$$r_{i'}^{\phi} = \sum_{k=0}^{\mathcal{K}} (r^{\min} + \Delta^r \times k) u_{i',k}^{\phi} \qquad \forall i' \in \mathcal{B}^{\mathrm{s}} \tag{4.8b}$$

$$\sum_{k=0}^{\mathcal{K}} u_{i',k}^{\phi} = 1 \qquad \forall i' \in \mathcal{B}^{\mathrm{s}} \tag{4.8c}$$

where $\Delta^r = (r^{\max} - r^{\min})/|\mathcal{K}|$. To enforce the ratio selection, a vector of 33 binary variables, $u_{i'}$, is multiplied by all possible each ratio, and the sum to 1 results in a single ratio. The formulation in (4.8) requires 99 of binary variables for each three-phase VR [43]. For fewer variables, the binary expansion technique [36] is adopted, and (4.8b)-(4.8c) is reformulated as:

$$r_{i'}^{\phi} = r^{\min} + \Delta^r \sum_{e=0}^{\mathcal{E}} 2^e u_{i',e}^{\phi} \qquad \forall \ i' \in \mathcal{B}^{+} \tag{4.9}$$

where $\mathcal{E} = \{e|e = 0, 1, \ldots, 5\}$. In this form, only $|\mathcal{E}| = 6$ binary variables are needed to construct 33 possible tap ratios, and a total of 18 binary variables for each three-phase VR.

4.3.2.2 Secondary-Side Voltage Constraint in the BFM Problem

To integrate the tap ratio model into the SDP BFM, the secondary-side voltage constraint (4.8a) is transformed into:

$$v_{i'} = \left(r_{i'} r_{i'}^{\mathrm{T}}\right) \odot v_i = \hat{r}_{i'} \odot v_i \qquad \forall \ i' \in \mathcal{B}^{\mathrm{s}} \tag{4.10}$$

It is easily observed that the newly-defined ratio variable, $\hat{r}_{i'} \in \mathbb{R}^{|\Phi_j|\times|\Phi_j|}$, is a symmetric matrix with each of the diagonal elements as the square of (4.9), and mutual elements as the products of composite tap ratios, e.g. $\hat{r}_{i'}^{ab} = r_{i'}^{a} r_{i'}^{b}$. In addition to (4.9), we define $\xi_{i',e}^{\phi} = u_{i',e}^{\phi} r_{i'}^{\phi}$ to linearize each of the diagonal elements using the big-M method as follows

$$\forall \phi \in \Phi, i' \in \mathcal{B}^{\mathrm{s}}:$$

$$\hat{r}_{i'}^{\phi\phi} = (r^{\min} \times r_{i'}^{\phi}) + \Delta^{r} \sum_{e=0}^{\mathcal{E}} 2^{e} \xi_{i',e}^{\phi} \tag{4.11a}$$

$$0 \leq \xi_{i',e}^{\phi} - r_{i'}^{\phi} \leq (1 - u_{i',e}^{\phi}) M \tag{4.11b}$$

$$0 \leq \xi_{i',e}^{\phi} \leq u_{i',e}^{\phi} M \tag{4.11c}$$

M can be replaced with $r^{\max}$ to avoid ill-conditioning. The nondiagonal elements can be treated similarly, each with two sets of binary variables, but are simplified with tap ratio products leveraging the problem decomposition as clarified in the following sections.

Remark 1 *For exposition, the uniform tap operation can be resembled by reformulating* (4.10) *to have a single tap ratio represented by one set of binary variables.*

The separation of the two circuits is disambiguated by conserving power flows through bus i'.

4.3.3 Three-phase PV Inverter with Variable Power Factor

Off-unity PV inverters can be governed to supply or absorb reactive power. Fundamentally, power-electronic inverters can function with a variable power factor (PF) which has a continuous reactive power capability during on- and off-peak (STATCOM mode) periods. It is assumed that the DSO has a direct dispatch control over PVs. For a PV at $i \in \mathcal{B}^{\mathrm{g}}$, the operating region based on solar power and bounded by the inverter's capacity is shown in Fig. 4.3. This is translated into the following set of an SDP constraint and inequality

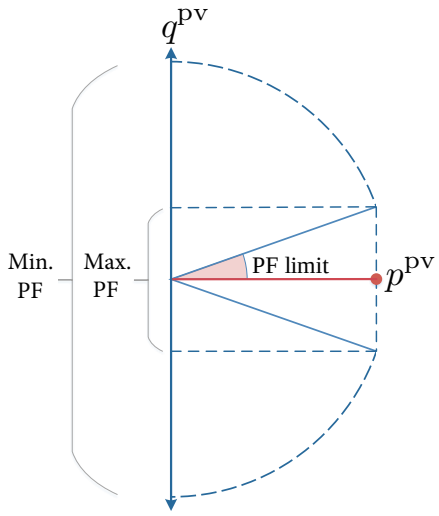

Figure 4.3: Var capability of a variable-PF PV inverter

constraints:

$$G_i = \begin{bmatrix} s^{\max} & s_i^{\text{g},\phi} \\ (s_i^{\text{g},\phi})^{\text{C}} & s^{\max} \end{bmatrix}$$

$$G_i \succeq 0 \qquad \forall \phi \in \Phi, i \in \mathcal{B}^{\text{g}} \tag{4.12a}$$

$$0 \leq \text{Re}(s_i^{\text{g},\phi}) \leq p^{\text{for}} \qquad \forall \phi \in \Phi, i \in \mathcal{B}^{\text{g}} \tag{4.12b}$$

where $(^{\text{C}})$ denotes the conjugate. Note that an oversized inverter is assumed, thereby ensuring Var injection/absorption during peak solar generation.

Remark 2 *The inverter's capacity limit constraint in* (4.12a) *is in Schur complement form [9], which is a generalization of the SOCP constraint,* $(s_i^{\max})^2 \geq |s_i^{\text{g},\phi}|^2$.

Considering the PV model in (4.12) and the constant-power demand s^{d}, the net load at bus $i \in \mathcal{B}^{\text{g}}$ then becomes

$$s_i = s_i^{\text{d}} - s_i^{\text{g}}. \tag{4.13}$$

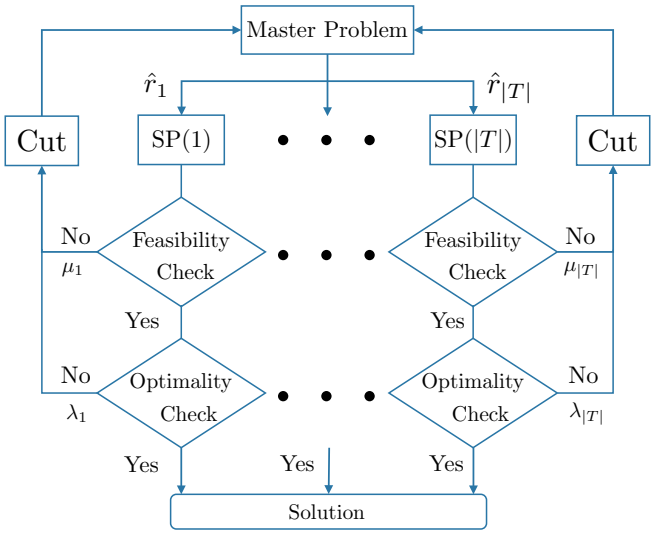

Figure 4.4: GBD structure with temporally-decomposed subproblems

4.3.4 The Multi-time Scheduling Problem

The problem is formulated with two sets of variables defined as follows:

$$\mathcal{X} := \{x | x = v, \ell, S, s^{\mathrm{g}}\}, \quad \mathcal{Y} := \{y | y = r, \hat{r}, \xi, u\}$$

4.3.4.1 Objectives

4.3.4.1.1 Substation Energy and Loss Reduction

Minimizing the energy purchase from the substation comes in the interest of reducing energy consumption and prioritizing the solar utility (minimizing curtailment). Reducing the real line losses incites control variables (tap positions and PV Var) to increase the voltage.

$$f_t(x) = c_{\mathrm{pri}} \left(\mathrm{Tr}\left(\mathrm{Re}\left(S_{01,\mathrm{t}}\right)\right) + \sum_{(j,k)\in\mathcal{L}} \mathrm{Tr}\left(\mathrm{Re}\left(z_{ij}\ell_{ij,t}\right)\right) \right) \tag{4.14}$$

4.3.4.1.2 VRA Reduction

The change among intra-day ratio variables is minimized without imposing an initial state, so as to reduce the VR's mechanical switching, and thus maintenance costs.

$$f_t(y) = \sum_{i' \in \mathcal{B}^+} \sum_{\phi \in \Phi} c_{\mathrm{vr}} |\hat{r}^{\phi\phi}_{i',t} - \hat{r}^{\phi\phi}_{i',t-1}| \tag{4.15}$$

4.3.4.2 Overall Multi-Time Scheduling Problem

$$\mathbf{VVO} := \min_{x,y} \quad \sum_{t=1}^{\mathcal{T}} f_t(x) + \sum_{t>1}^{\mathcal{T}} f_t(y) \tag{4.16a}$$

$$\text{s. t.} \quad v_{0,t} = V_{\mathrm{nom}} V_{\mathrm{nom}}^{\mathrm{H}} \tag{4.16b}$$

$$\underline{V}^2 \leq \mathrm{diag}(v_{i,t}) \leq \overline{V}^2 \ \ \forall i \in \mathcal{B}^+ \tag{4.16c}$$

$$(4.2), (5.3), (4.6), (4.9)\text{-}(4.13), \quad x \in \mathcal{X}, \quad y \in \mathcal{Y} \tag{4.16d}$$

The ratio-voltage multiplication in (4.10) renders (4.16) nonconvex. In the next section, this nonconvexity is overcome by applying the GBD, which solves variables of $\mathcal{X}$ and $\mathcal{Y}$ in separate problems.

4.4 Generalized Benders Decomposition

In this section, we apply the GBD [44], which was extended from [45], to decouple and solve the problem iteratively, thereby avoiding the aforementioned nonlinearity, and providing an effective approach to solve the MISDP problem. In each iteration, the solution to the master problem over $\mathcal{Y}$ is passed to the subproblems. In turn, the subproblems will be solved over $\mathcal{X}$ and optimality cuts will be created for the master problem. Conventionally,

if the master renders one subproblem infeasible, the subproblem will be reformulated and a feasibility cut will be created.

Remark 3 *Because of the wide range of tap ratios that VRs can take, the MP could pass a tap ratio to a single SP that results in the secondary-side voltage exceeding the upper bound or falling below the lower one, thus making the respective SP infeasible. In which case, a feasibility-check problem (FCP) should be formulated to create a feasibility cut whenever a single-time SP is infeasible, and ensure the MP avoids this particular combination of ratios. This prolongs the convergence, as the FCP is computed each time the MP oversteps or understeps a tap position at a certain phase and a certain time. Motivated by the work in [46], additional constraints are enforced on the tap ratios to respect the secondary-side voltage limits relying on primary-side voltage parameters acquired from cumulated iterations.*

4.4.1 Subproblem (SP)

The SP corresponding to the SDP-based BFM in the x-space only can succinctly be written as following.

$$\mathbf{SP} := \min_{x} \quad f_t^n(x) \tag{4.17a}$$

$$\text{s. t.} \quad v_{i',t}^n = \hat{r}_{i',t}^{*n} \odot v_{i,t}^n \tag{4.17b}$$

$$(4.2), (5.3), (4.6), (4.12), (4.13), (4.16\text{b}), (4.16\text{c}), \quad x \in \mathcal{X} \tag{4.17c}$$

where superscript $(^*)$ distinguishes quantities obtained from the MP, and n denotes the iteration. The solutions to the SPs provide optimal Lagrangian multipliers $\lambda \in \mathbb{R}^{|\Phi_{i'}|\times|\mathcal{T}|}$ associated with the real diagonal of the secondary-side voltage.

Note for each VR, based on (11), there are 9 equality constraints. To streamline the cut-creating process, only three constraints related to the diagonal components are considered:

$$v_{i',t}^{\phi\phi^n} = \hat{r}_{i',t}^{\phi\phi,*^n} \odot v_{i,t}^{\phi\phi^n} \quad : \text{dual variable } \lambda_{i',t}^{\phi^n} \tag{4.18}$$

The tap ratios in (4.9) are then utilized to realize the nondiagonal elements, and thereby the matrix $\hat{r}_{i'}$, to preserve voltage phase angles.

The upper bound of the original problem in (4.16) is composed of the aggregated solutions to the SPs and the fixed objective pertaining to the switching reduction.

$$\theta_{\text{ub}}^n = \sum_{t=1}^{\mathcal{T}} f_t^n(x) + \sum_{t>1}^{\mathcal{T}} f_t^n(y^*) \tag{4.19}$$

4.4.2 Feasibility-Check Problem (FCP)

The FCP is formed by re-formulating the original problem such that a feasible solution is guaranteed for any given tap ratio. The objective function is to minimize the diagonal of the nonnegative auxiliary variable relaxing the ratio-voltage equality constraint, $f_t(w) = \text{diag}(w_t)$.

$$\textbf{FCP} := \min_{x,w} \quad f_t^n(w) \tag{4.20a}$$

$$\text{s. t.} \quad v_{i',t}^n = \hat{r}_{i',t}^{*^n} \odot v_{i,t}^n + w_{i'}^n \tag{4.20b}$$

$$w_{i'}^n \succeq 0 \tag{4.20c}$$

$$(4.2), (5.3), (4.6), (4.12), (4.13), (4.16\text{b}), (4.16\text{c}), \quad x \in \mathcal{X} \tag{4.20d}$$

The dual variables, $\mu \in \mathbb{R}^{|\Phi_{i'}| \times |\mathcal{T}|}$, associated with the diagonal of the constraint (4.20b) are used to generate the feasibility cut.

Algorithm GBD for Multi-time Scheduling

Step 1 → set $n = 1$ and $\theta^1_{\text{lb}} = -\infty$, and pick any $y^1_t \in \mathcal{Y}$
Step 2
for $t = 1{:}T$ **do**
  solve SP
  if solution is feasible **then**
    update θ^n_{ub} and λ^n_t, and set $f^n_t(w) = \mu^n_t = 0$
  else
    solve FCP
    update μ^n_t, and set $f^n_t(x) = \lambda^n_t = 0$
  end if
end for
Step 3 → check convergence:
if $|\theta^n_{\text{ub}} - \theta^n_{\text{lb}}| \leq \epsilon$ **then**
  break
  disclose optimal results
else
  continue
end if
Step 4 → increase n by 1
  → solve MP, and update θ^n_{lb} and y^n_t
  → return to **Step 2** =0

4.4.3 Master Problem (MP)

With solutions to (4.17) and (4.20), the MP is formulated in y-space with constraints on the VRs.

$$\mathbf{MP} := \min_{y,\eta} \quad \sum_{t=1}^{\mathcal{T}} \eta^n_t + \sum_{t>1}^{\mathcal{T}} f^n_t(y) \tag{4.21a}$$

$$\text{s. t.} \quad \eta^n_t \geq f^N_t(x^*) + \sum_{i' \in \mathcal{B}^+} \sum_{\phi \in \Phi} v^{\phi\phi,*^N}_{i,t} \lambda^{\phi^N}_{i',t} (\hat{r}^{\phi\phi^n}_{i',t} - \hat{r}^{\phi\phi,*^N}_{i',t})$$

$$N = 1, 2, \ldots, n-1, \qquad t = 1, 2, \ldots, |\mathcal{T}| \tag{4.21b}$$

$$0 \geq f^N_t(w^*) + \sum_{i' \in \mathcal{B}^+} \sum_{\phi \in \Phi} v^{\phi\phi,*^N}_{i,t} \mu^{\phi^N}_{i',t} (\hat{r}^{\phi\phi^n}_{i',t} - \hat{r}^{\phi\phi,*^N}_{i',t})$$

$$N = 1, 2, \ldots, n-1, \qquad t = 1, 2, \ldots, |\mathcal{T}| \tag{4.21c}$$

$$\max(\mathbf{v}_{i,t}^{\phi\phi})\hat{r}_{i',t}^{\phi\phi^n} \leq \overline{V}^2 \quad t = 1, 2, \ldots, |\mathcal{T}| \tag{4.21d}$$

$$\min(\mathbf{v}_{i,t}^{\phi\phi})\hat{r}_{i',t}^{\phi\phi^n} \geq \underline{V}^2 \quad t = 1, 2, \ldots, |\mathcal{T}| \tag{4.21e}$$

$$(4.9), (4.11), \quad y \in \mathcal{Y} \tag{4.21f}$$

Constraints (4.21b)-(4.21c) are respectively the optimality and feasibility cuts. The multi-cut GBD yields the same result as the uni-cut GBD (a single cut over the entire time horizon), but with faster convergence [47]. $\mathbf{v}_{i,t}^{\phi\phi} \in \mathbb{R}^{|N|}$ in (4.21d)-(4.21e) denotes a vector of primary-side voltage quantities obtained from accumulated iterations, $[v_{i,t}^{\phi\phi,*^1}, \ldots, v_{i,t}^{\phi\phi,*^{n-1}}]^{\mathrm{T}}$, where max/min yields one quantity. Though not strictly removing infeasible tap selection, these two constraints reduce the search space and substantially improve the convergence process, and so removing them returns the classic GBD problem. The optimal solution to (4.21), θ_{lb}^n, is the lower bound of the original problem.

4.5 Numerical Case Studies

In this section, the efficacy of the proposed scheduling problem is evaluated using multiple case studies on the radial structures of modified 37-bus and 123-bus feeders. The hourly normalized profiles shown in Fig. 4.5 are uniformly applied to real and reactive power demand and PV real power. Per-phase VRs are assumed to operate with 33 levels and a turns ratio varying from 0.9 to 1.1. The primary cost is assumed to be ($c_{\mathrm{pri}} = 100$\$/MWh). Due to the uncertainty of the VR's life expectancy [48], their tap adjustment cost, c_{vr}, is unified for all VRs and varied to yield a targeted adjustment reduction, i.e. close to 50% reduction. Peak PV real power will capacitate oversized inverters to generate/absorb 46% of $|s^{\max}|$ as a reactive power.

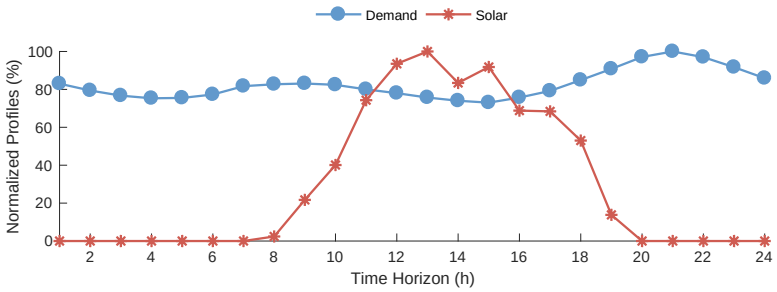

Figure 4.5: Hourly demand and solar profiles.

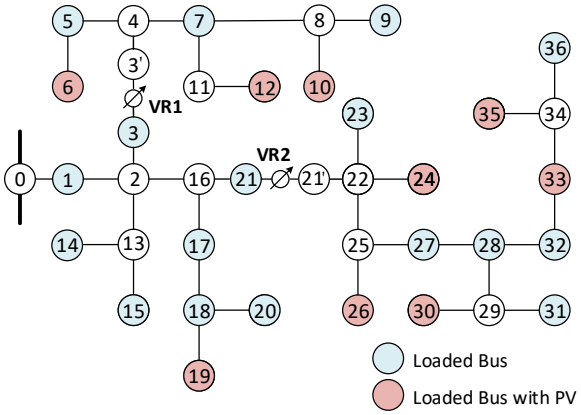

Figure 4.6: Modified IEEE 37-bus feeder.

4.5.1 Modified 37-bus Feeder

Fig. 4.6 depicts the modified IEEE 37-bus feeder with peak demand 2.7348 MVA and 0.9 PF. All lines are three-phase configured. Two VRs are placed as in Fig. 4.6 to compensate for voltages at remote buses. Nine three-phase PV are considered. Each PV inverter has a capacity of 250 kVA, and their combined penetration is 74% of the MW load.

4.5.1.1 Case I: Considering Primary Objective

The algorithm is computed with different scenarios to show the capability of VRs and PVs to attain minimum substation intake and line losses, and demonstrate the need for an extended objective. The switching penalty is set to zero ($c_{\text{vr}} = 0$). From Fig. 4.7a-6.3c and Table 5.3, it can be seen that the baseline case with no PVs has the highest energy import and losses, but least tap switching. When unity-PF PVs are added, the VRs together with

Table 4.1: Results for case I

Scenario	Sub. (MWh)	Loss (MWh)	Average Volt. (pu)	VRA Count
Baseline	49.8493	1.1982	1.0220	20
Unity-PF PVs	35.3499	0.9051	1.0246	60
0.9-PF PVs	35.1483	0.6929	1.0253	58

PV generation contribute to 29.1% and 24.5% of substation energy and loss reductions, albeit at the expense of excessive VRAs. PVs with off-unity PF, though contribute to a larger loss reduction during off-peak hours, do not seem to coordinate well with VRs or reduce the tap switching despite their reactive power capability. This signifies extending the objective to limit the VRAs.

The temporal variations of the average and range of the three-phase voltages are shown in Fig. 4.8a. Also, voltage magnitudes at phase C, whose MVA load accounts for 44.35% of the total load, are plotted in Fig. 4.8b-4.8c. It is noted that while voltages are regulated within the ±5% limit, the VRs tap high increasing the secondary-side voltage near the upper bound.

Table 4.2: Results for case II

VRA Cost c_{vr}	Sub. (MWh)	Loss (MWh)	Average Volt. (pu)	VRA Count	VRA Reduction
60	35.1518	0.7073	1.0254	37	36.2%
70	35.1521	0.7077	1.0247	34	41.4%
80 and 90	35.1513	0.7068	1.0238	30	48.3%

4.5.1.2 Case II: Considering Extended Objective

In light of the results in Case I, we solve the scheduling problem with the extended objective to explore the possibility of urging PVs to collectively produce/absorb enough

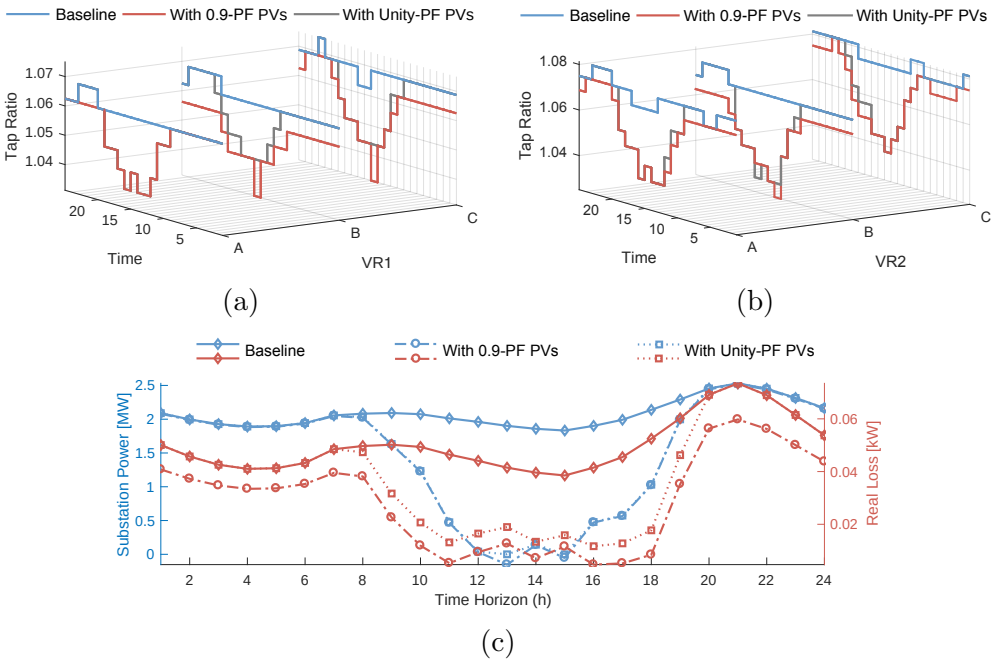

Figure 4.7: Case I: The tap ratio dispatch curves of (a) VR1 and (b) VR2 show that major VR switching occur during peak hours of PV generation. (c) Profiles of substation MW import/export, and line losses. 0.9-PF PVs further reduce the losses during off-peak hours.

reactive power so as to reduce VR mechanical switching. Table 4.2 lists the results with three incremental switching costs, all of which are less than the primary objective cost ($c_{\text{vr}} < c_{\text{pri}}$). With $c_{\text{vr}} = 90$, Fig. 4.9a-4.9b shows that VR1 spares 62.5% and VR2 spares 38.24% of their actions, bringing the total VRAs down to 30. In addition to the longevity advantage, the percentage VRA reduction is proportional to the maintenance interval schedules [11], [49].

Being close to the VRs, the dispatch curves of PV6 and PV24 are also plotted in Fig. 4.9c-4.9d. It is evident that major alterations of reactive power dispatch occur at times when a steep tap action is spared. Also, VR taps are kept at lower positions during peak-loading hours with almost insignificant PV reactive power changes. In general, the VRA penalization heightened the PV reactive energy absorption by 105% compared to the unpenalized case, whereas the total reactive energy supply only decreased by 18.3%.

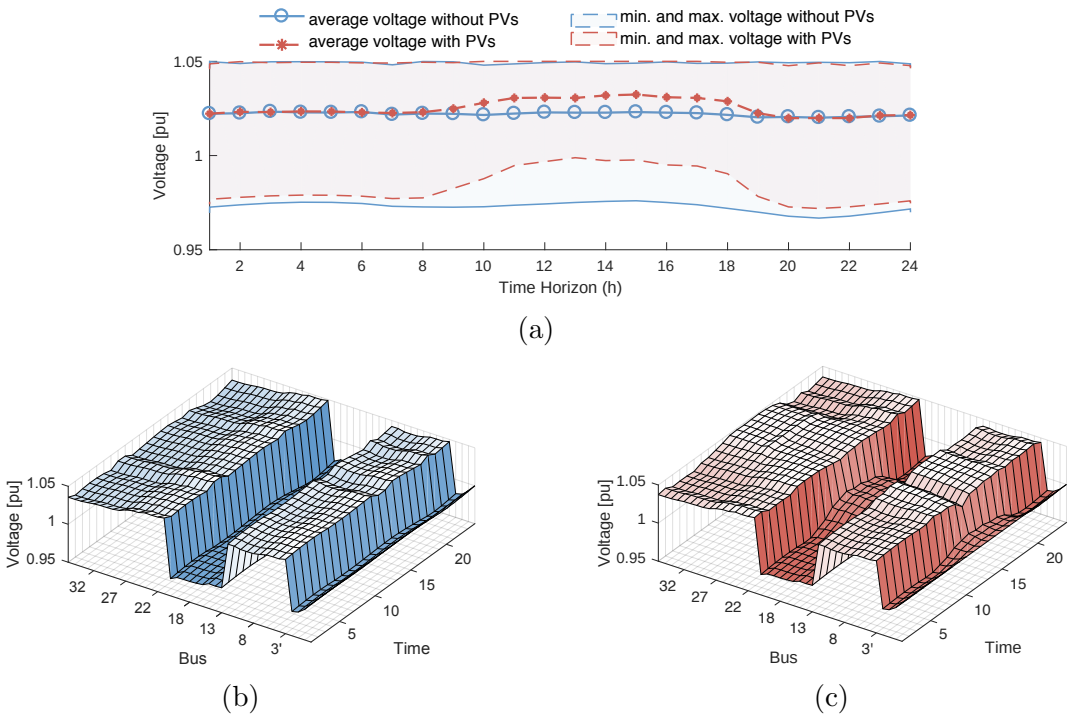

Figure 4.8: Case I: (a) Maximum, minimum and average voltage variations throughout the day. Nodal voltage variations of phase C (highest-loaded phase) voltages (b) without and (c) with PVs.

4.5.1.3 Case III: Comparison with Uniform Tap Operation

The results of nonuniform tap dispatch presented in Cases I and II are compared with the uniform tap operation, where phase tap positions of each VR switch uniformly. For this, the tap ratio is re-formulated to have one set of binary variables. Without the VRA penalization, the VRs with 0.9-PF PVs are scheduled with 54 VRAs in total, only 6% lower than the results in Case I. Enforcing the penalization with $c_{\text{vr}} = 90$ reduces VRAs to 51, which is 70% more than the results in Case II. This shows that the nonuniform ratio modeling is more economic and amenable to the VRA reduction, even with lower values of c_{vr} as demonstrated in Case II.

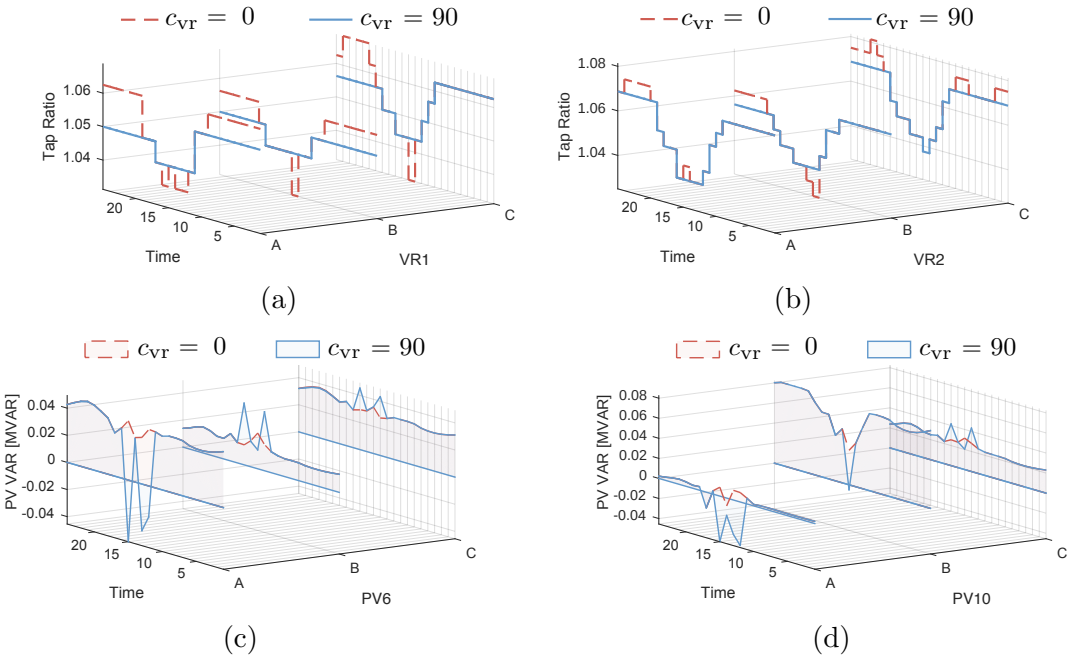

Figure 4.9: Case II: With $c_{vr} = 90$, the tap ratio dispatch curves of (a) VR1 and (b) VR2 evidently decreased by 48.3%, and dispatch curves of (c) PV6 and (d) PV24 are repositioned to absorb reactive powers during excessive PV generation.

Table 4.3: Results for case III

VRA Cost c_{vr}	Sub. (MWh)	Loss (MWh)	Average Volt. (pu)	VRA Count
0	35.1499	0.6943	1.0238	54
90	35.15	0.6945	1.0236	51

4.5.2 Modified 123-bus Feeder

The proposed algorithm is also solved for the IEEE 123-bus feeder, which has multiple line configurations and a peak demand of 3.9833 MVA and 0.88 PF. The modified system shown in Fig. 4.10 involves five VRs and three PV plants. We introduce VR5 to test the scalability to a higher number of VRs, and to regulate voltages of its downstream lateral. VR2 and VR3 are installed on single- and two-phase lines, respectively. The capacitor banks

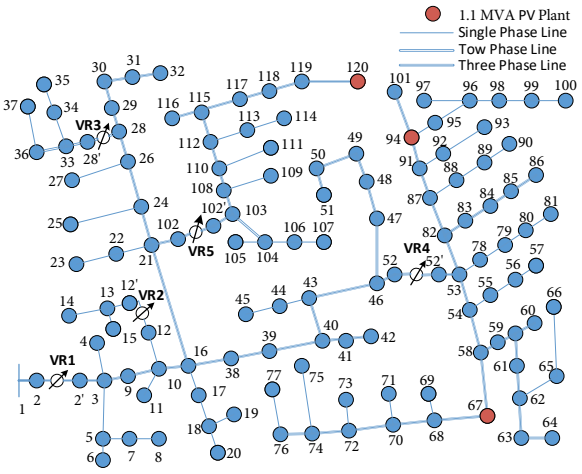

Figure 4.10: Modified IEEE 123-bus feeder.

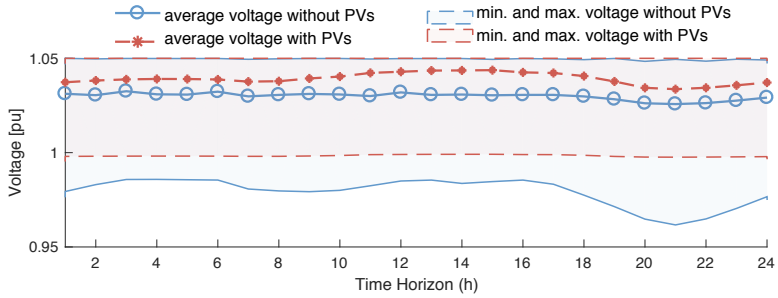

Figure 4.11: 123-bus feeder maximum, minimum and average voltage levels of the baseline case and the 0.9-PF PV case with the penalized VRA.

are assumed inactive. The capacity of each PV plant is 1.1 MVA, and their total penetration compounds to 86% of the MW load.

Table 4.4 lists the results with and without 0.9-PF PVs along with the penalized-adjustment case. For this feeder, the baseline has the highest number of tap switching in which all VRs are engaged in the regulation. With PVs and unpenalized switching, the total VR adjustments reduced by 24.7%. The tap ratios of VR1 remained unaltered at 1.05. VR4 and VR5 constitute 70.3% of the total adjustments since the MVA loads, downstream their secondary sides, are 63% of the system's total load in addition to all PVs. When a VRA cost of 60 was invoked, VR2 and VR3 did not switch. Moreover, the total adjustments of VR4 and VR5 reduced by 64.7% from the baseline (53.12% from the unpenalized VRA

Table 4.4: Results for modified 123-bus feeder

Scenario	Sub. (MWh)	Loss (MWh)	Average Volt. (pu)	VRA c_{vr}	VRA Count	VRA Reduction
Baseline	71.4343	2.3637	1.0299	0	85	-
0.9-PF PVs	49.6419	1.2954	1.0399	0	64	24.7%
	49.6419	1.2954	1.0392	60	30	64.7%

Table 4.5: Number of variables

Modified 37-bus Feeder		Modified 123-bus Feeder	
SPs	MP	SPs	MP
25320	4824	45840	12450

case), and without inciting added energy import or losses. The temporal voltage variations (average and range) for the baseline and penalized switching cases are plotted in Fig. 4.11.

The VRAs of a single VR depend on the system topology, VR location, and the net demand change downstream from the VR. These factors not only differ from one feeder to another, but also from one VR to another [5]. From the previous case studies, we can deduce that larger values of c_{vr} are required for the 37-bus feeder, where VRs are not cascaded, to spare 50% of VRAs. For the 123-bus feeder, where VR2-5 are cascaded by VR1, a smaller unified value of c_{vr} is sufficient to obtain a considerable VRA reduction.

4.5.3 Performance of the GBD-based Multi-time Scheduling

4.5.3.1 Computation

The problems are implemented in MATLAB 2016b with CVX [37, 38], where the SDP-based SPs are solved by Mosek solver [50], and the MILP-based MP is solved by Gurobi solver [39]. All simulations are performed on a laptop with Intel Core i7 at 2.7 GHz, 16 GB memory, and MAC OS 10.14. Table 4.5 lists the size of each problem for both feeders.

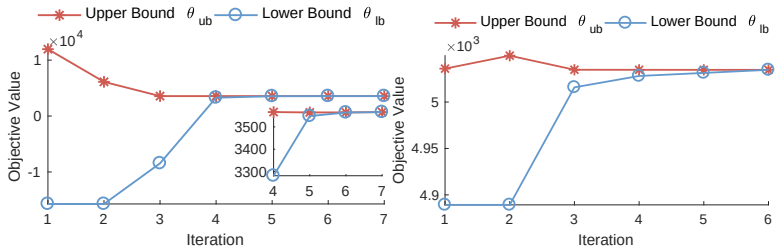

(a) (b)

Figure 4.12: GBD convergence of (a) the 37-bus feeder case with $c_{\text{vr}} = 90$, and (b) the 123-bus feeder case with $c_{\text{vr}} = 60$.

Table 4.6 lists the average number of iterations, the average convergence values, and solving time costs averaged over all cases on each feeder for both single- and multi-time horizon scheduling. The tolerance, ϵ, is chosen to be 1e$-$3. However, the problems converged to even lower error values shown in column 3. Though solved sequentially, parallel optimization computing of SPs is also possible [51].

4.5.3.2 SDP Exactness

For the rank-relaxed SDP problem, the exactness is customarily checked upon solving the problem by computing the eigenvalue ratio of each PSD matrix. If the ratio is small, it indicates that the PSD matrix has one dominant eigenvalue, which suffices to conclude that the solution is exact. The ratio is computed as in (4.22), where $|\text{eig}_1| > |\text{eig}_2|$, for all PSD matrices over the time horizon. The last column of Table 4.6 lists the ratio averaged over all cases.

$$\text{Ratios} = \sum_{t \in T} \sum_{\text{eig} \in F_{i,j}^t} |\text{eig}_2/\text{eig}_1| \tag{4.22}$$

The small ratio indicates that the relaxation is tight. Hence, the recovered optimal solutions are deemed AC feasible.

Table 4.6: Performance of the GBD

Scheduling	Average Iterations	Ave. Conv. $\lvert\theta_{\text{ub}} - \theta_{\text{lb}}\rvert$	Ave. Time (s)	Ave. Ratio
Modified IEEE 37-bus Feeder				
Single-time	4.95	6.91e-09	4.46	6.28e-09
Multi-time	9	1.04e-07	187.78	6.87e-09
Modified IEEE 123-bus Feeder				
Single-time	10.27	6.24e-09	10.41	7.48e-08
Multi-time	10	2.59e-08	266.54	1.45e-07

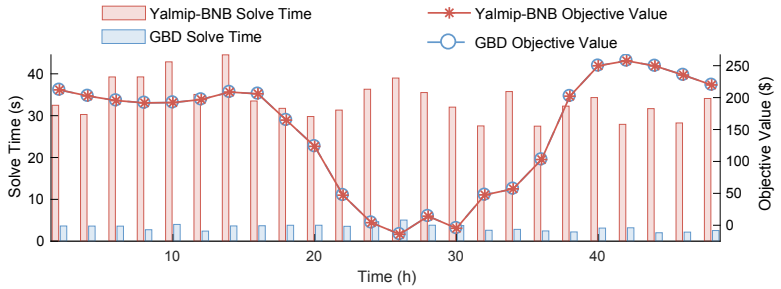

Figure 4.13: Comparing the solve time and objective values of Yalmip-BNB and GBD method solutions for the modified 37-bus feeder. Evidently, the proposed problem outperforms that of the Yalmip-BNB.

4.5.3.3 Comparison with Branch-and-Bound Method

To compare the proposed method with available solvers such as branch-and-bound method, we use Yalmip's built-in BNB solver [52] along with Mosek to solve the MISDP problem. First, the element-wise nonlinear constraints in (4.10) are linearized using additional sets of big-M inequality constraints in the flavor of (4.11). We attempt to solve the problem for a single-time dispatch, and a multi-time dispatch with reduced VRAs on the modified 37-bus feeder. For the nonuniform tap control, where three sets of binary variables are required, the problem did not converge for both time operations.

On the other hand, using the uniform tap control with one set of binary variables, the problem converges only for the single-time operation as in [22, 23] with average solve time of 33.85 s. The solve times and objective values are compared with the proposed GBD method in Fig. 4.13. It should be noted that the convergence is sensitive to the choice of big-M values. Randomly large or small values could also cause the problem to be non-convergent. In our experiments, we found that setting $M = 1000$ provides the fastest convergence. For the smallest consideration of multi-time operation (two time steps), the Yalmip-BNB problem is incapable of convergence even with maximizing BNB iterations to 50000. This also corroborates the capability of the proposed method to solve for multi-time operation with nonuniformly-operated taps.

4.6 Conclusion

This paper proposes a multi-time scheduling framework based on the SDP-based branch flow model to optimally dispatch discrete-based voltage regulators with nonuniform phase operation and off-unity inverters of photovoltaics, while considering the VRA costs. We circumvent the numerical complexities intrinsic to the MISDP problem and the nonlinear voltage-ratio relationship by the application of GBD with decoupled subproblems and a multi-cut master problem. We also propound additional constraints to accelerate the GBD convergence by narrowing the tap ratios with respect to secondary-side voltage limits. The case studies on the modified IEEE 37-bus and 123-bus test feeders evince the effectiveness of the proposed algorithm with a coordinated operation of VRs and PVs.

Chapter 5: Comprehensive and Exact D-ACOPF Model

5.1 Introduction

The distribution systems are increasingly challenged by the continuing emergence of distributed energy resources (DERs), signaling the need for optimized computational tools to systemize their involvement and coordinate their operation with existing control devices.

The alternating-current optimal power flow (ACOPF) problem lies at the root of power system optimization. It aims to minimize operating costs subject to system's physical and security constraints. Unfortunately, its non-convexity makes it difficult to solve. To break away from unrealistic dispatch solutions produced by the OPF problem [53], recent research has focused on convex relaxations. The breakthrough occurred when Jabr [26] and later Bai *et al.* [54] led the first convex relaxations of the ACOPF, respectively using second-order conic programming (SOCP) and semidefinite programming (SDP). This paved the way for assessing the optimality [31], exploiting sparsity [55–57] or cutting planes [58] to enhance the computational performance, and developing other relaxations such as SOCP BFM [27], moment relaxation [59], QC relaxation [60], and new SDP relaxation (nSDR) [61]. The previous models have exclusively targeted single-phase (radial and meshed) systems.

The multi-phase consideration in distribution ACOPF (D-ACOPF) is of practical importance for unbalanced distribution systems. Dall'Anese *et al.* [30] were the first to develop a multi-phase SDP D-ACOPF. Another seminal, and more stable, SDP model was proposed by Gan and Low [24] based on the BFM. Over time, a plethora of applications has been layered on top of these convex models. Some of these applications are bound to affect the

exactness of the relaxation. Generally, the rank-relaxed SDP problem is said to be exact, and thus AC-feasible, if the rank-1 condition is fulfilled. Fig. 5.1 virtually illustrates the difference between an exact and inexact solution. The exactness is customarily assessed upon obtaining the solution using the eigenvalue-ratio metric, where smaller ratios indicate the solution's proximity to a rank-1 PSD matrix. In what follows, we cast light on some applications in the literature that are known to trigger inexactness.

5.1.1 Applications with Relevance to Distribution Systems

5.1.1.1 Application I: Voltage Positioning Objective

The inexactness of D-ACOPF convex relaxations has been attributable to the choice of objective functions. The SOCP BFM is provably exact for radial graphs if the objective function is convex and strictly increasing in active power injection among other variable conditions [27], [29]. References [34, 40, 62] attempted to optimize the voltage profile as a secondary objective. To strengthen the relaxation, [34] proposes an approach based on the difference of convex programming (DCP), where the linear approximation of a concave inequality constraint is tightened sequentially. In [40], a non-iterative approach is explored to strengthen the relaxation using multiple SDP and linear equality constraints. Most recently, [62] employs an inner approximation while iteratively recovering solution feasibility via bound tightening. The aforesaid techniques have solely focused on single-phase D-ACOPF models.

5.1.1.2 Application II: Step-Voltage Regulators

The SVRs are essentially autotransformers equipped with a tap-changing mechanism to cope with net load changes. Leveraging the advances in multi-phase SDP D-ACOPF models [24, 30], system-wide voltage regulation is achieved through optimal SVR setting, conventionally formulated as trilinear equality constraint. The convex relaxations of the

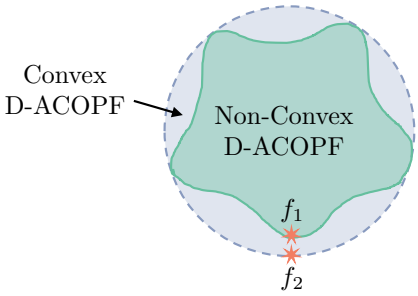

Figure 5.1: Conceptual illustration of the convex relaxation (dashed blue) of the non-convex sets (solid green). f_1 is the relaxed true minimum and thus feasible to the non-convex problem, whereas f_2 is a lower bound and infeasible to the non-convex problem.

trilinear constraint has attracted considerable interest [20–23, 63], generally assuming continuous tap positions to bypass the computational difficulty of solving a mixed-integer SDP problem. The diagonal of the secondary-side voltage can be implicitly confined within the tap ratio limit. However, leaving the non-diagonal elements unconstrained triggers inexactness, for which a non-ideal SVR with tunable resistance is proposed in [20]. References [22, 23] propound an SDP constraint that outputs a unified tap selection among phases. Most of the studies focused on the wye-connected SVRs. Recently, references [21, 63] developed the theoretical basis for relaxing delta-connected SVR constraints. The inequality constraints, proposed by [63], render inexact solutions. In response, reference [21] improved the relaxation to some extent by employing McCormick envelopes to relax the trilinearity with explicit ratio variables. The lower-bound solutions are then used to retrieve feasible voltages using Z-bus method [64]. In this paper, we compare our method to those proposed by [21–23]

5.1.1.3 Application III: Delta-connected Loads and DERs

Prior studies are limited to wye-connected distribution systems. The notion of extending the multiphase convex D-ACOPF to account for delta-connected power injections was first introduced by [65], where an additional PSD constraint describing the power injections across each pair of phases are enforced into the BFM, referred to as extended BFM (EBFM).

Unfortunately, the experiments reveal that the relaxation yields inexact solutions with respect to the delta-connected injections, and is therefore replaced by a linear approximation. Newly-developed techniques have been proposed by [66] to overcome the inexactness. The first technique relies on post-processing, in which delta-connection currents can be recovered if the line-to-line voltages are of rank-1. The other relaxation is inspired by [67, 68], in which the trace of delta-connection currents is suppressed in the objective function. The latter produces exact and rank-1 solutions with respect to the delta-connected power PSD matrices of the BFM formulation. In this paper, we compare the proposed method with the penalization technique [66, Algorithm 2].

Table 5.1: Comparison with the literature

Ref	System Unbalances	Voltage Positioning	Delta Connection	SVR			Exactness
				Y	△	⏊	
[34]		✓					✓
[40]		✓					
[62]		✓		✓			✓
[20]	✓			✓			
[22, 23]	✓			✓			✓
[21, 63]	✓			✓	✓	✓	
[65]	✓		✓				
[66]	✓		✓				✓
Proposed	✓	✓	✓	✓	✓	✓	✓

5.1.2 Contribution

Spurred by the preceding limitations, we propose a convex iterative problem that enhances the quality of the D-ACOPF solution while comprehending the voltage-positioning objective function and constraints, SVRs, and delta-connected injections. On top of rank relaxations, internal models of SVRs and delta-connected injections include relaxed equality constraints.

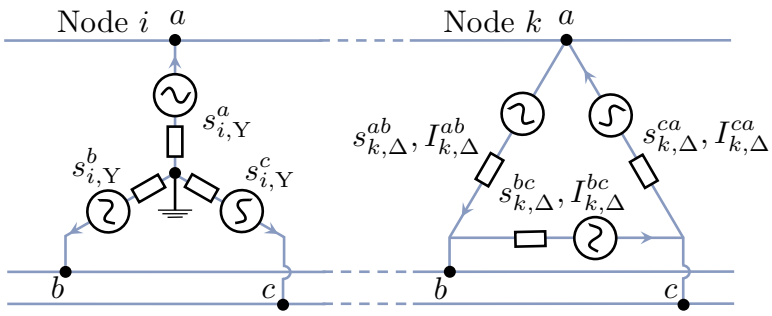

Figure 5.2: Illustration of the wye- and delta-connected DERs and loads.

The strength of our research lies in the capability to retrieve exact and AC-feasible solutions. More specifically, we circumvent the rank conundrum associated with the consideration of i) voltage-related objectives, ii) delta-connected loads and DERs, and iii) SVRs that are capable of a non-uniform tap operation. To the authors' knowledge, no prior studies have collectively subsumed the previous components into the SDP D-ACOPF. Table 5.1 compares the literature in terms of the previous applications. It should be noted that the comparison is focused on the literature that addresses the AC feasiblity as a concern for the solution quality. We compare the model with single-phase ACOPF models proposed [34, 40, 62] since they are the only known references to attempt to solve the exactness when a voltage-related objective is considered. Interestingly, the proposed problem has a fast convergence rate with rank-1 solutions for most connections of IEEE 13, 37, 123 bus feeders, demonstrating applicability for shorter-timescale applications. Besides, comparative case studies highlight differences between the proposed model and other methods used by the literature.

The rest of this manuscript is organized as follows. Section II presents the generic power distribution system model, describes the various connections of SVRs, and formulates the overall non-convex EBFM. Section III presents various techniques to convexify the EBFM with an iterative methodology to drive PSD matrices to rank-1. Numerical case studies are performed in Section IV, and some conclusions are drawn in Section V.

5.2 Problem Formulation

5.2.1 General Notations

Let $\mathbb{R}$ and $\mathbb{C}$ respectively denote the sets of real and complex numbers. Calligraphic letters, e.g. $\mathcal{N}$, denote sets of indices. We use $|\cdot|$ to denote the absolute value or cardinality of a set. Also, superscripts $(^{\mathrm{T}})$, $(^{\mathrm{C}})$, and $(^{\mathrm{H}})$ denote the transpose, element-wise conjugate, and conjugate transpose (Hermitian) of matrices and vectors.

5.2.2 Power Distribution System Model

Let $\mathcal{N}_b$ and $\mathcal{E}$ denote the node and edge sets of a distribution system with a composite of single, two, and three transmission conductors. For a radially-fed system, each node $i \in \mathcal{N}_b$ has a distinct ancestor, such that number of ordered pairs, $(i,k) \in \mathcal{E}$, is $|\mathcal{E}| = |\mathcal{N}_b| - 1$. Let $\mathcal{T} = \{1, \ldots, t\}$ denote the set of SVRs. We use $\mathcal{E}_t \subset \mathcal{E}$ to distinguish line segments with SVRs. Additionally, we introduce $\mathcal{N}_t$ to denote the set of virtual nodes, $i' \in \mathcal{N}_t$, incident to the SVR's secondary side, where i' lies between i and k. Thus, the aggregate set of physical and virtual nodes is

$$\mathcal{N} = \mathcal{N}_b \cup \mathcal{N}_t$$

For notational simplicity, we assume $\mathcal{N}$ and $\mathcal{E}$ have three-phase connection in this section, while adapting the model to systems with missing phases is discussed later. We define the phase sets as $\Phi = \{a, b, c\}$, $\Phi' = \{b, c, a\}$, and $\Phi_\triangle = \{ab, bc, ca\}$. The root node, $i = 0$, has a fixed three-phase voltage given by $V^{\mathrm{ref}} = V_{\mathrm{nom}} \left[1, e^{-\mathrm{j}2\pi/3}, e^{\mathrm{j}2\pi/3}\right]^{\mathrm{T}}$. For all descendent nodes, the voltage vector is defined as $V_i \in \mathbb{C}^{|\Phi|}$, where $i > 0 \in \mathcal{N}$. Similarly, let $I_{ik} \in \mathbb{C}^{|\Phi|}$ define the three-phase currents flowing through the series impedance $z_{ik} \in \mathbb{C}^{|\Phi| \times |\Phi|}$, while $I_{k,\triangle} \in \mathbb{C}^{|\Phi_\triangle|}$ define those flowing through the delta-connected net injections as depicted in Fig. 5.2. For ease of exposition, we consider a joint wye- and delta-connected net injection

at every $i \in \mathcal{N}_b$, respectively defined as $\mathbf{s}_{i,\mathrm{Y}} = \left[s^a_{i,\mathrm{Y}}, s^b_{i,\mathrm{Y}}, s^c_{i,\mathrm{Y}}\right]^{\mathrm{T}}$ and $\mathbf{s}_{i,\triangle} = \left[s^{ab}_{i,\triangle}, s^{bc}_{i,\triangle}, s^{ca}_{i,\triangle}\right]^{\mathrm{T}}$. Each entry of the net-injection vectors is composed of $(s^{\phi}_{i,\mathrm{g}} - s^{\phi}_{i,\mathrm{d}})$, where g and d denote the DER and demand complex powers. $y_i \in \mathbb{C}^{|\Phi|}$ defines the shunt admittance connected at node i.

In what follows, we formulate a comprehensive multi-phase power system model. We then lift the system variables to formulate an extended branch flow model.

5.2.2.1 Ohm's Law

The difference between voltage vectors across the ends of each (i, k) connected through a series impedance is expressed as:

$$V_k = V_i - Z_{ik} I_{ik} \quad \forall (i,k) \in \mathcal{E} \tag{5.1}$$

5.2.2.2 Power Balance Equation

the KCL equation is first written for ith node, where $m \to i \to k$:

$$I_i = \sum_{(i,k)\in\mathcal{E}} I_{ik} - I_{mi} \quad \forall i \in \mathcal{N}_b \tag{5.2}$$

$I_i \in \mathbb{C}^{|\Phi|}$ is the net injection current. I_{mi} and I_{ik} are the currents flowing into and away from node i, respectively. Multiplying (5.2) by $\mathrm{diag}(V_i^{\mathrm{H}})$, and conjugating the resultant renders the power balance at node i, which can be written as:

$$\mathbf{s}_i = \sum_{(i,k)\in\mathcal{E}} \mathrm{diag}(V_i I_{ik}^{\mathrm{H}}) - \left(\mathrm{diag}(V_m I_{mi}^{\mathrm{H}}) - z_{mi} I_{mi} I_{mi}^{H}\right) \; \forall i \in \mathcal{N}_b \tag{5.3}$$

The net injection current, I_i, is also a function of currents flowing from DER-load ensembles and shunt elements, which can be expressed as follows:

$$I_i = I_{i,\mathrm{Y}} + \Gamma^{\mathrm{T}} I_{i,\triangle} - y_i V_i \qquad \forall i \in \mathcal{N}_b \tag{5.4}$$

where

$$\Gamma = \begin{bmatrix} 1 & -1 & 0 \\ 0 & 1 & -1 \\ -1 & 0 & 1 \end{bmatrix}$$

Again, multiplying (5.4) by $\mathrm{diag}(V_i^{\mathrm{H}})$ and taking conjugate yields

$$\mathbf{s}_i = \mathbf{s}_i^{\mathrm{Y}} + \mathrm{diag}(V_i I_{i,\triangle}^{\mathrm{H}} \Gamma) - \mathrm{diag}(V_i V_i^{\mathrm{H}} y_i^{\mathrm{H}}) \qquad \forall i \in \mathcal{N}_b \tag{5.5}$$

While the wye-connected net injection is readily formulated in (5.5), the net injections across the phase pairs are $\mathrm{diag}(\Gamma V_i I_{i,\triangle}^{\mathrm{H}})$.

Table 5.2: SVR ratio matrix and generalized constants

SVR Connection	Wye	Closed-Delta	Open-Delta
$\mathbf{A}_{i'}$	$\begin{bmatrix} r_t^a & 0 & 0 \\ 0 & r_t^b & 0 \\ 0 & 0 & r_t^c \end{bmatrix}$	$\begin{bmatrix} r_t^{ab} & 1-r_t^{ab} & 0 \\ 0 & r_t^{bc} & 1-r_t^{bc} \\ 1-r_t^{ca} & 0 & r_t^{ca} \end{bmatrix}$	$\begin{bmatrix} r_t^{ab} & 1-r_t^{ab} & 0 \\ 0 & 1 & 0 \\ 0 & 1-r_t^{cb} & r_t^{cb} \end{bmatrix}$
B	$\begin{bmatrix} 1 & 0 & 0 \\ 0 & 1 & 0 \\ 0 & 0 & 1 \end{bmatrix}$	$\begin{bmatrix} 1 & -1 & 0 \\ 0 & 1 & -1 \\ -1 & 0 & 1 \end{bmatrix}$	$\begin{bmatrix} 1 & -1 & 0 \\ 0 & 1 & 0 \\ 0 & -1 & 1 \end{bmatrix}$
C	$\mathbf{0}$	$\begin{bmatrix} 0 & 1 & 0 \\ 0 & 0 & -1 \\ 1 & 0 & 0 \end{bmatrix}$	$\begin{bmatrix} 0 & 1 & 0 \\ 0 & 0 & 0 \\ 0 & 1 & 0 \end{bmatrix}$

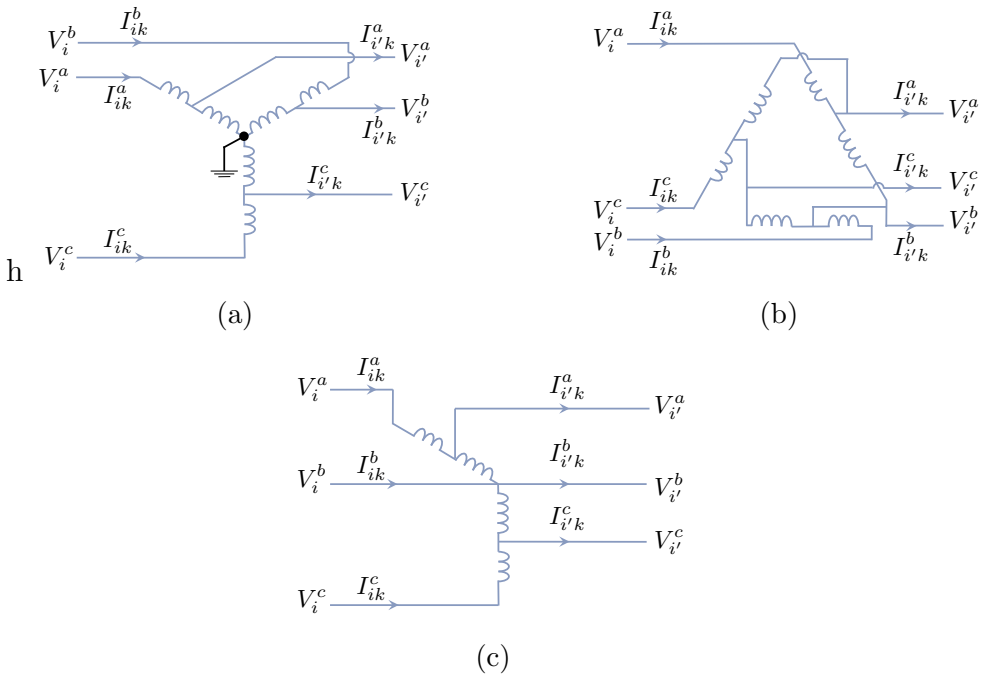

Figure 5.3: Type-B SVR: (a) wye connection, (b) closed-delta connection, and (c) open-delta connection.

5.2.2.3 Step-Voltage Regulator (SVR)

A set of autotransformers make up the three-phase SVR, which can be either wye, closed-delta, or open-delta connected. The latter requires two autotransformers across two pairs of phases. SVRs are either type-A or type-B, depending on where the series winding is located, and can typically take ± 8 or ± 16 tap positions.

To formulate a universal SVR model that suits all connections, we abuse the following assumptions:

- Autotransformers have separate tap changing circuits, enabling a non-uniform tap setting for each phase. Gang-operated SVRs are discussed in [22, 23].
- We rely on the generalized constants provided in Table 5.2 [21, 63].

- Only type-B SVRs are assumed for all connections, where the primary-side is connected via taps to the series winding.
- The series impedance of autotransformers is small compared to that of two-winding transformers [42]. It is therefore neglected.
- For open-delta connected SVRs, the two autotransformers are installed between phase *ab* and *cb*.

The three connections of SVRs are illustrated in Fig. 5.3. Let $\mathbf{r}_t \in \mathbb{R}^3$ be the ratio vector of SVR $t \in \mathcal{T}$, whose entries are consistent with the connection type. For example, $\mathbf{r}_t = [r_t^{ab}, 1, r_t^{cb}]^{\mathrm{T}}$ for open-delta connection. Equation (5.6) sets the SVR's tap changing limit.

$$\underline{r} \leq \mathbf{r}_t \leq \overline{r} \qquad \forall t \in \mathcal{T} \tag{5.6}$$

The tap position is retrieved using the following:

$$\mathrm{Tap}^{\phi} = \text{ round } \left(\frac{1 - r_t^{\phi}}{\hat{r}} \right) \qquad \forall \phi \in \Phi, \quad t \in \mathcal{T} \tag{5.7}$$

where $\hat{r} = (\overline{r} - \underline{r})/\text{No. of taps}$.

Let $(i,k) \in \mathcal{E}_t$, hence the voltage at and the current flowing away from $i' \in \mathcal{N}_t$ can be expressed as follows:

$$V_i = \mathbf{A}_{i'} V_{i'} \qquad \forall i' \in \mathcal{N}_t \tag{5.8a}$$

$$I_{ik} = (\mathbf{A}_{i'}^{\mathrm{T}})^{-1} I_{i'k} \qquad \forall (i,k) \in \mathcal{E}_t \tag{5.8b}$$

Utilizing the generalized constants, B and C, in Table 5.2, the ratio gain, $\mathbf{A}_{i'}$, composed as follows

$$\mathbf{A}_{i'} = \mathrm{diag}(\mathbf{r}_t)\mathrm{B} + \mathrm{C} \qquad \forall i' \in \mathcal{N}_t \tag{5.9}$$

From (5.8), we can infer the following power balance relationship:

$$\mathrm{diag}\left(V_{i'} I_{i'k}^{\mathrm{H}}\right) = \mathrm{diag}\left(\mathbf{A}_{i'}^{-1} V_i I_{ik}^{\mathrm{H}} \mathbf{A}_{i'}\right) \qquad \forall (i,k) \in \mathcal{E}_t \tag{5.10}$$

5.2.3 Rank-Constrained ACOPF

5.2.3.1 Matrix-based Variables

The previous constraints are reformulated to conform to the rank-constrained EBFM [24, 65], a higher-dimension problem with lower sources of non-convexity. To this end, the vector variable products are lifted to be matrix variables:

$$\mathbf{V}_i = V_i V_i^{\mathrm{H}}, \qquad \mathbf{I}_{ik} = I_{ik} I_{ik}^{\mathrm{H}}, \qquad \mathbf{I}_{i,\triangle} = I_{i\triangle} I_{i,\triangle}^{\mathrm{H}}$$
$$\mathbf{S}_{ik} = V_i I_{ik}^{\mathrm{H}}, \qquad \mathbf{S}_i = V_i I_{i,\triangle}^{\mathrm{H}}$$

The real and surrogate variables are interrelated through the following PSD matrices, defined as $\mathbf{X}_{ij}$ and $\mathbf{X}_i^{\triangle}$:

$$\mathbf{X}_{ik} = \begin{bmatrix} V_i \\ I_{ik} \end{bmatrix} \begin{bmatrix} V_i \\ I_{ik} \end{bmatrix}^{\mathrm{H}} = \begin{bmatrix} \mathbf{V}_i & \mathbf{S}_{ik} \\ \mathbf{S}_{ik}^H & \mathbf{I}_{ik} \end{bmatrix} \tag{5.11a}$$

$$\mathbf{X}_i^{\triangle} = \begin{bmatrix} V_i \\ I_{i,\triangle} \end{bmatrix} \begin{bmatrix} V_i \\ I_{i,\triangle} \end{bmatrix}^{\mathrm{H}} = \begin{bmatrix} \mathbf{V}_i & \mathbf{S}_i \\ \mathbf{S}_i^H & \mathbf{I}_{i,\triangle} \end{bmatrix} \tag{5.11b}$$

With the surrogate variables, constraints (5.1), (5.3), (5.5), (5.8a), and (5.10) can subsequently be re-written as:

$$\mathbf{V}_k = \mathbf{V}_i - Z_{ik}\mathbf{I}_{ik}Z_{ik}^{\mathrm{H}} \quad \forall (i,k) \in \mathcal{E} \tag{5.12a}$$

$$\mathbf{s}_i = \sum_{(i,k)\in\mathcal{E}} \mathrm{diag}(\mathbf{S}_{ik}) - (\mathrm{diag}(\mathbf{S}_{mi}) - z_{mi}\mathbf{I}_{mi}) \; \forall i \in \mathcal{N}_b \tag{5.12b}$$

$$\mathbf{s}_i = \mathbf{s}_i^{\mathrm{Y}} + \mathrm{diag}(\mathbf{S}_i\Gamma) - \mathrm{diag}(\mathbf{V}_i y_i^{\mathrm{H}}) \qquad \forall i \in \mathcal{N}_b \tag{5.12c}$$

$$\mathbf{s}_{i,\triangle} = \mathrm{diag}(\Gamma\mathbf{S}_i) \qquad \forall i \in \mathcal{N}_b \tag{5.12d}$$

$$\mathbf{V}_i = \mathbf{A}_{i'}\mathbf{V}_{i'}\mathbf{A}_{i'}^{\mathrm{T}} \qquad \forall i' \in \mathcal{N}_t \tag{5.12e}$$

$$\mathrm{diag}\left(\mathbf{S}_{i'k}\right) = \mathrm{diag}\left(\mathbf{A}_{i'}^{-1}\mathbf{S}_{ik}\mathbf{A}_{i'}\right) \qquad \forall (i,k) \in \mathcal{E}_t \tag{5.12f}$$

5.2.3.2 Objective Function

Minimizing the nodal voltage deviations from the desired range is set as an operational objective of the optimization routine. Let $\kappa_i \in \mathbb{R}^{|\Phi|}$ denote a non-negative vector variable, defined for every $i \in \mathcal{N}$ and constrained as:

$$\kappa_i \geq \mathrm{diag}(\mathbf{V}_i) - V^- \tag{5.13a}$$

$$\kappa_i \geq V^+ - \mathrm{diag}(\mathbf{V}_i) \tag{5.13b}$$

$$\kappa_i \geq 0 \tag{5.13c}$$

where V^- and V^+ are pre-defined minimum and maximum squared voltage threshold vectors. Thus, regulating the voltage is achieved by minimizing $f_{\mathrm{v}} = \sum_{i\in\mathcal{N}}\sum_{\phi\in\Phi}\kappa_i^{\phi}$.

5.2.3.3 Non-Convex EBFM Problem

$$\mathbf{P}_{\mathrm{NC}}: \quad \min \quad c_0 f_{\mathrm{v}} \tag{5.14a}$$

$$\text{s. t.} \quad (5.11), (5.12), (5.13) \tag{5.14b}$$

$$\mathbf{V}_0 = V^{\mathrm{ref}} V^{\mathrm{ref\,H}} \tag{5.14c}$$

$$\underline{V} \leq \mathrm{diag}(\mathbf{V}_i) \leq \overline{V} \qquad \forall i' \in \mathcal{N} \tag{5.14d}$$

$$\mathrm{diag}(\mathbf{I}_{i,\triangle}) \leq \overline{I} \qquad \forall (i,k) \in \mathcal{E} \tag{5.14e}$$

$$0 \leq \Re(s_{i,\mathrm{g}}) \leq \overline{P} \qquad \forall i \in \mathcal{N} \tag{5.14f}$$

$$|\Im(s_{i,\mathrm{g}})| \leq \xi \Re(s_{i,\mathrm{g}}) \quad \forall i \in \mathcal{N} \tag{5.14g}$$

$$\mathbf{X}_{ik} \succeq 0 \qquad \forall (i,k) \in \mathcal{E} \tag{5.14h}$$

$$\mathbf{X}_i^{\triangle} \succeq 0 \qquad \forall i \in \mathcal{N} \tag{5.14i}$$

$$\mathrm{rank}(\mathbf{X}_{ik}) = 1 \qquad \forall (i,k) \in \mathcal{E} \tag{5.14j}$$

$$\mathrm{rank}(\mathbf{X}_i^{\triangle}) = 1 \qquad \forall i \in \mathcal{N} \tag{5.14k}$$

(5.14d) constrains the squared voltages. (5.14e) sets an upper bound on the currents through the delta connection. (5.14f)-(5.14g) are the DER's active and reactive power constraints, respectively. The DERs are assumed to be constant power factor (PF), and thus $\xi = \sqrt{(1-\mathrm{PF}^2)}/\mathrm{PF}$. (5.14j)-(5.14k) are the rank 1 constraints related to the power flow and the delta-connected net injection.

The non-convexity of $\mathbf{P}_{\mathrm{NC}}$ originates from:

- The trilinear equality constraints in (5.12e)-(5.12f).
- The rank-1 constraints in (5.14j)-(5.14k).

5.3 Convex Relaxations and Iteration

In this section, we summarize the convexification techniques to render $\mathbf{P}_{\mathrm{NC}}$ a convex problem that solves to lower-bound solutions. Moreover, we propose the use of convex iteration to retrieve the exactness of the relaxed model (upper-bound solutions), thereby enabling the recovery of system original variables.

5.3.1 Convex Relaxations

5.3.1.1 Relaxing Rank-1 Constraints

The non-convex rank-1 constraints of the PSD matrices, (5.14j)-(5.14k), are dropped from the problem. The relaxation of the power-flow PSD matrix (5.14j) has been practiced for many applications, and the solutions hold exact for most IEEE feeders [24]. On the other hand, the relaxation of the power-injection PSD matrix (5.14k) is reported to result in inexact solutions [65].

5.3.1.2 Relaxing SVR Voltage Constraint

By defining the following new variables:

$$\tilde{\mathbf{V}}_i = \mathrm{B}\mathbf{V}_{i'}\mathrm{B}^{\mathrm{T}}, \qquad \hat{\mathbf{V}}_i = \mathrm{B}\mathbf{V}_{i'}\mathrm{C}^{\mathrm{T}}, \qquad \check{\mathbf{V}}_i = \mathrm{C}\mathbf{V}_{i'}\mathrm{B}^{\mathrm{T}} \tag{5.15a}$$

$$\bar{\mathbf{V}}_i = \mathrm{diag}(\mathbf{r}_t)\tilde{\mathbf{V}}_i\mathrm{diag}(\mathbf{r}_t) + \mathrm{diag}(\mathbf{r}_t)\hat{\mathbf{V}}_i + \check{\mathbf{V}}_i\mathrm{diag}(\mathbf{r}_t) \tag{5.15b}$$

the primary-side voltage constraint in (5.12e) can then be expanded as follows:

$$\mathbf{V}_i = \bar{\mathbf{V}}_i + \mathrm{C}\mathbf{V}_{i'}\mathrm{C}^{\mathrm{T}} \tag{5.16}$$

It is evident from (5.15b) that $\bar{\mathbf{V}}_i$ is a function of a trilinear term (first term) and bilinear terms (second and third), whereas $\mathbf{V}_i$ is linear in both $\mathbf{V}_{i'}$ and $\bar{\mathbf{V}}_i$. Therefore, we relax the diagonal and non-diagonal elements of (5.15b).

5.3.1.2.1 Digonal Elements

given that the tap ratios are confined within the inequality constraint in (5.6), the relaxation of the diagonal elements of (5.15b) is obtained by the set of constraints in (5.17):

$$\text{diag}(\bar{\mathbf{V}}_i) \geq \underline{r}^2 \text{diag}(\tilde{\mathbf{V}}_i) + \underline{r}\text{diag}(\hat{\mathbf{V}}_i) + \underline{r}\text{diag}(\check{\mathbf{V}}_i) \tag{5.17a}$$

$$\text{diag}(\bar{\mathbf{V}}_i) \leq \overline{r}^2 \text{diag}(\tilde{\mathbf{V}}_i) + \overline{r}\text{diag}(\hat{\mathbf{V}}_i) + \overline{r}\text{diag}(\check{\mathbf{V}}_i) \tag{5.17b}$$

Note that $\text{diag}(\hat{\mathbf{V}}_i) = \text{diag}(\check{\mathbf{V}}_i)$ because they are transpose of each other. Also, for wye-connected SVRs, only the first term to the RHS of (5.17) is non-zero.

5.3.1.2.2 Non-diagonal Elements

We make use of two facts to relax the non-diagonal elements:

- It is known that angle differences among any pair of phases, (ϕ, ϕ') do not radically deviate from their nominal in multi-phase radial distribution feeders [57, Assumption 3], such that the following inequality holds for any $\overline{\theta} > 0$:

$$90^\circ \leq 120^\circ - \overline{\theta} \leq \theta^\phi - \theta^{\phi'} \leq 120^\circ + \overline{\theta} \leq 180^\circ \quad \forall \phi \in \Phi, \phi' \in \Phi'$$

- Coupled with the fact that constraining elements with a pair combination of (a, b), (b, c), and (c, a) is sufficient given the Hermitian symmetry of a 3×3 PSD matrix [57,

Proof], the non-diagonal real and imaginary elements of (5.15b) are relaxed as

$$\forall \phi \in \Phi, \phi' \in \Phi' :$$

$$\Re(\bar{\mathbf{V}}_i^{\phi\phi'}) \leq \underline{r}^2 \Re(\tilde{\mathbf{V}}_i^{\phi\phi'}) + \underline{r} \Re(\hat{\mathbf{V}}_i^{\phi\phi'}) + \underline{r} \Re(\check{\mathbf{V}}_i^{\phi\phi'}) \tag{5.18a}$$

$$\Re(\bar{\mathbf{V}}_i^{\phi\phi'}) \geq \overline{r}^2 \Re(\tilde{\mathbf{V}}_i^{\phi\phi'}) + \overline{r} \Re(\hat{\mathbf{V}}_i^{\phi\phi'}) + \overline{r} \Re(\check{\mathbf{V}}_i^{\phi\phi'}) \tag{5.18b}$$

$$\Im(\bar{\mathbf{V}}_i^{\phi\phi'}) \geq \underline{r}^2 \Im(\tilde{\mathbf{V}}_i^{\phi\phi'}) + \underline{r} \Im(\hat{\mathbf{V}}_i^{\phi\phi'}) + \underline{r} \Im(\check{\mathbf{V}}_i^{\phi\phi'}) \tag{5.18c}$$

$$\Im(\bar{\mathbf{V}}_i^{\phi\phi'}) \leq \overline{r}^2 \Im(\tilde{\mathbf{V}}_i^{\phi\phi'}) + \overline{r} \Im(\hat{\mathbf{V}}_i^{\phi\phi'}) + \overline{r} \Im(\check{\mathbf{V}}_i^{\phi\phi'}) \tag{5.18d}$$

Remark 4 *the variable* $\bar{\mathbf{V}}_i$ *is Hermitian, but not rank-1. For the previous SVR voltage model, only* $\mathbf{V}_i$ *and* $\mathbf{V}_{i'}$ *should be rank-1.*

Remark 5 *The tap ratios are implicitly formed by the inequality constraints. Hence, retrieving the optimal tap ratios is possible upon solving the problem by treating* (5.15b) *as a quadratic equation with unknown* $\mathbf{r}_t$*.*

A rank-1 secondary-side voltage PSD matrix entails that its recovered voltage vector, $V_{i'}$, is a result of some $\mathbf{A}_{i'} V_i$. At this stage, enforcing the previous set of inequality constraints further widens the relaxation.

5.3.1.3 Relaxing SVR Power Constraint

Th constraint in (5.12f) is relaxed as (5.19) based on observation of ratio matrix for wye and delta SVR connections. The diagonal power elements through wye-connected SVRs are equivalent due the diagonal ratio matrix. For delta-connected SVRs, the constraint is relaxed based on the conservation of power.

$$\text{Wye-connected SVRs:} \qquad \text{diag}(\mathbf{S}_{i'k}) = \text{diag}(\mathbf{S}_{ik}) \tag{5.19a}$$

$$\text{Delta-connected SVRs:} \qquad \text{Tr}(\mathbf{S}_{i'k}) = \text{Tr}(\mathbf{S}_{ik}) \tag{5.19b}$$

For wye-connected SVRs, $\text{diag}(\mathbf{S}_{i'k}) = \text{diag}(\mathbf{S}_{ik})$ is satisfied. For open-delta connected SVRs:

$$\text{diag}(\mathbf{S}_{i'k}) = \begin{bmatrix} S_{ik}^{aa} \pm \eta^a S_{ik}^{ba} \\ S_{ik}^{bb} \mp (\eta^a S_{ik}^{ba} + \eta^c S_{ik}^{bc}) \\ S_{ik}^{cc} \pm \eta^c S_{ik}^{bc} \end{bmatrix} \tag{5.20}$$

where η^ϕ is a small number, $(\eta^\phi = r_t^\phi - 1)$. As per the conservation of power, the trace of the power flowing into the primary side equals that flowing away from the secondary side. If we enforce the trace as in (5.19b), the mutual elements cancel out each other and the resultant is:

$$\text{Tr}(\mathbf{S}_{i'k}) = S_{ik}^{aa} + S_{ik}^{bb} + S_{ik}^{cc} \tag{5.21}$$

Similar conclusions can be drawn for the closed-delta connected SVRs.

5.3.1.4 Overall Relaxed Problem

The convexified version of (5.14) is written as:

$$\begin{aligned} \mathbf{P}_{\text{LB}}: \quad & \min \quad c_0 f_{\text{v}} \\ & \text{s. t.} \quad (5.11), (5.12\text{a})\text{-}(5.12\text{d}), (5.13), (5.14\text{c})\text{-}(5.14\text{g}), (5.15\text{a}) \\ & (5.16), (5.17), (5.18), (5.19) \end{aligned} \tag{5.22}$$

The problem in (5.22) provides a lower bound to the original problem, (5.14), because of the introduced relaxations compounded with the voltage-related objective function.

5.3.2 Retrieving Exactness via Convex Iteration

The convex iteration is generally understood to refer to convex problems whose rank relaxation is strengthened iteratively [69]. The technique has shown potential, in the power system area, for the economic dispatch problem in the distribution [32] and transmission [57] systems. The former considers the case where DER offer prices differ per phase, which inflicts higher-rank solutions.

5.3.2.1 Convex Iteration Application

We can succinctly refer to all $N \times N$ PSD matrices in (5.22) as $\mathbf{X}$, where $N = 2|\Phi|$. By arranging the eigenvalues, $\lambda(\mathbf{X}^*) \in \mathbb{R}^N$, in a descending order, the rank-1 condition is attained if the trace of each $\mathbf{X}$ is equal to its first eigenvalue:

$$\mathrm{Tr}(\mathbf{X}) - \lambda_1 = \mathrm{Tr}(\mathbf{X}) - \sum_{n=1}^{N} \lambda_n = 0 \tag{5.23}$$

(5.23) establishes that eigenvalues of $n > 1$ are zeros. This can alternatively be expressed as

$$\sum_{n=2}^{N} \lambda_n = \mathrm{Tr}(\mathbf{XW}) = 0 \tag{5.24}$$

where $\mathbf{W}$ is a PSD matrix, referred to as the direction matrix, which corresponds to the zero eigenvalues with a trace equal to N. It is originally an optimal solution to an SDP problem with known $\mathbf{X}^*$ [69]. For computational efficiency, a closed-form solution to $\mathbf{W}$ can be computed upon solving (5.22) and utilizing the singular value decomposition (`svd` in Matlab) of $\mathbf{X}^*$ as

$$\mathbf{X}^* = U \Lambda U^{\mathrm{T}} \tag{5.25}$$

$$\mathbf{W} = U(:, 2:N) U(:, 2:N)^{\mathrm{T}} \tag{5.26}$$

The direction matrix is therefore exploited to re-formulate (5.22) as (5.27) with linear regularization terms $\text{Tr}(\mathbf{X}\mathbf{W}^*)$ appended to the objective function and updated iteratively to drive $\mathbf{X}$ to rank-1. The problem (5.22) can serve as an initialization. Fig. 5.4 shows the iteration process. The convergence of the problem has been proven by [69].

5.3.2.2 Overall Iterative Problem

$$\begin{aligned}
\mathbf{P}_{\text{UB}}: \quad \min \quad & c_0 f_{\text{v}} + c_1 \sum_{(i,k)\in\mathcal{E}} \text{Tr}(\mathbf{X}_{ik}\mathbf{W}_{ik}^*) \\
& + c_2 \sum_{i\in\mathcal{N}^{\triangle}} \text{Tr}(\mathbf{X}_i^{\triangle}\mathbf{W}_i^*) \\
\text{s. t.} \quad & (5.11), (5.12\text{a})\text{-}(5.12\text{d}), (5.13), (5.14\text{c})\text{-}(5.14\text{g}), (5.15\text{a}) \\
& (5.16), (5.17), (5.18), (5.19)
\end{aligned} \tag{5.27}$$

5.4 Numerical Experiments

The convex iteration problem is implemented in CVX [37,38], and solved by Mosek [50]. Simulations are performed on a laptop with Intel Core i7 2.7 GHz processor, 16 GB RAM, and MAC OS 10.14.

We conduct multiple case studies on IEEE 13-bus, 37-bus and 123-bus feeders to demonstrate:

- the effectiveness of the proposed method in driving inexact solutions to AC feasible and exact ones.
- the importance of internalizing the physical connection of loads, DERs and SVRs.
- the advantage of the proposed method over those proposed by the literature.

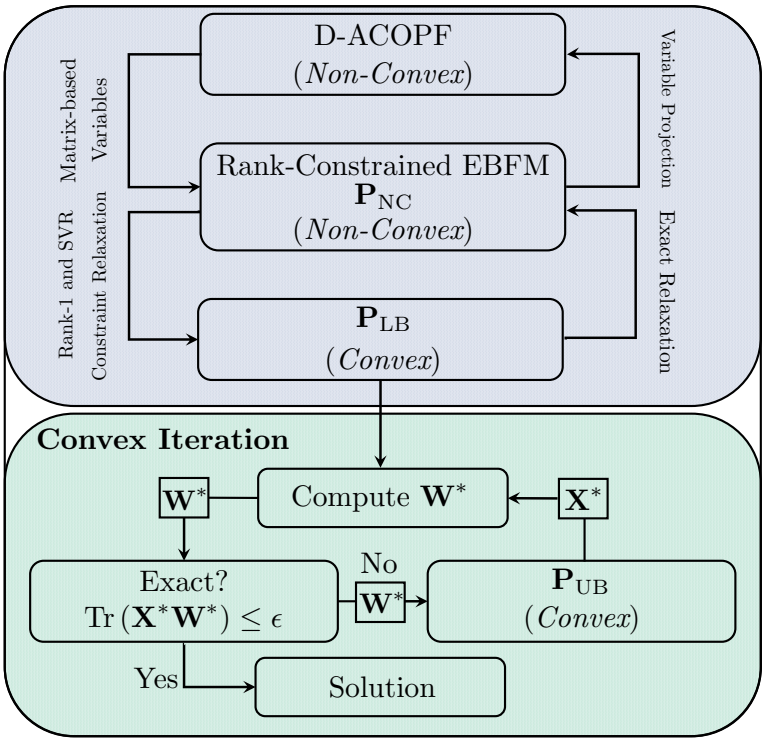

Figure 5.4: Flowchart of the proposed model; exactness recovery via convex iteration.

The 13-bus and 123-bus feeders have a composite of wye- and delta-connected loads, while the 37-bus feeder loads are all delta-connected. The distributed loads are halved and lumped to adjacent buses. Capacitors and transformers are modeled, and switches are replaced by short lines. The voltages are confined as per ANSI $\pm 5\%$ limits, i.e. $\overline{V} = 1.05^2$ and $\underline{V} = 0.95^2$. The turns ratio limits are $\overline{r} = 1.05$ and $\underline{r} = 0.95$.

Fig. 5.5 depicts the radial feeder typologies with detailed delta-connected bus and SVR line locations (plotted in Matlab using `digraph`). DERs are on node 5, 8, 13, and 14 of the 13-bus feeder, node 6, 10, 20, 23, 30, and 36 of the 37-bus feeder, and node 37, 53, 55, 63, 72, 110,and 113 for the 123-bus feeder. For the 13-bus and 123-bus feeders, we set DERs to share a 20% penetration of the total feeder real power consumption. For the 37-bus feeder, total penetration of 60% is assumed.

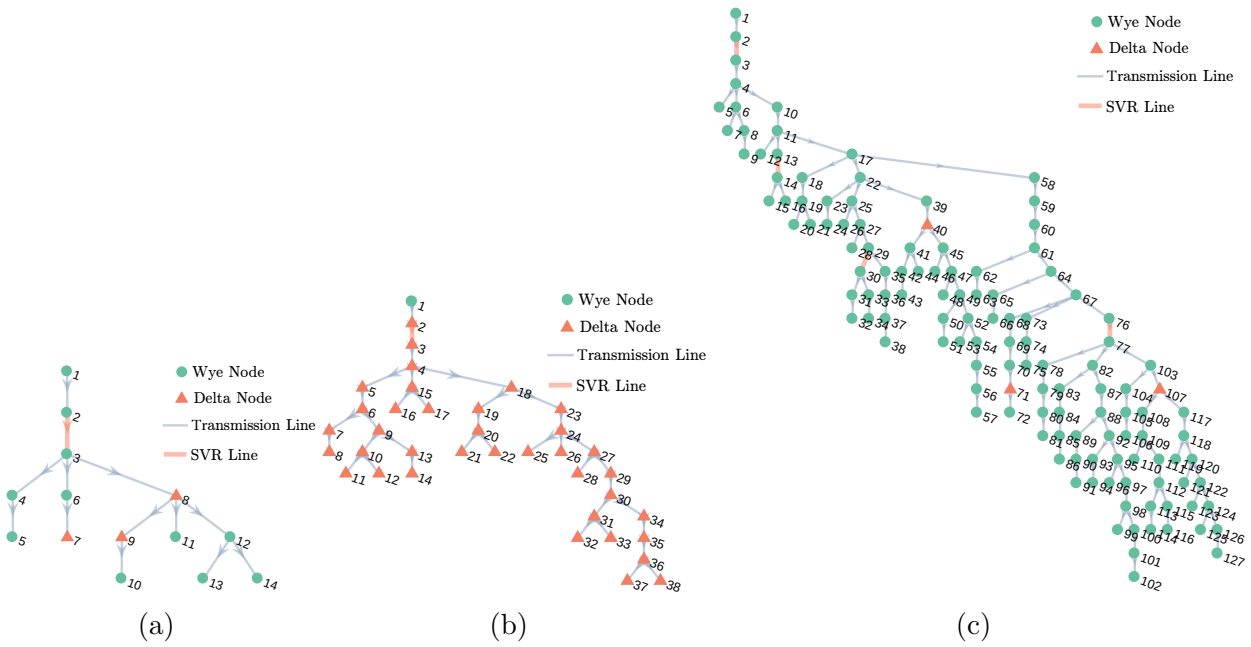

Figure 5.5: Locations of delta-connected buses and SVR lines in the (a) 13-bus, (b) 37-bus, and (c) 123-bus feeders.

5.4.1 Performance of the Convex Iteration Problem

We examine problem performance with the voltage positioning objective function considering different possible connections of loads, DERs and SVRs. The desired thresholds are set 3% from the nominal value, thus $V^+ = 1.03^2$ and $V^- = 0.97^2$. Y, $\triangle$, and O denote wye, closed-delta, and open delta SVR connections. For the 123-bus feeder, we assume mixed connections of the four SVRs, denoted as M, with SVR#1 (line 2-3) as closed-delta, SVR#2 and SVR#3 (lines 13-14 and 29-30) as wye, and SVR#4 (line 76-77) as open-delta.

Table 5.3 and 5.4 summarize the results. On each table, Fdr and Con. refer to the feeder, i.e. 13 bus, and connection of loads, respectively. In Table 5.3, columns 4 and 5 list the lower-bound objective values obtained at the first iteration, i.e. $\mathbf{P}_{\text{LB}}$, and those obtained at the convergence of the convex iteration.

The exactness of the solution is evaluated by computing the ratio of the second largest eigenvalue to the largest eigenvalue for each PSD matrix. In Table 5.3, Column 6 and 7

compute the eigenvalue ratios for $\mathbf{X}_{ik}$ averaged over all edges at the first and last iterations. Similarly, columns 8 and 9 compute the eigenvalue ratios for $\mathbf{X}_i$ averaged over all delta-connected nodes, at the first and last iterations. The small ratios at the convergence affirm the proposed method's success to drive the relaxed problem towards AC feasibility (single dominant eigenvalue). The deterioration of the trace regularization terms after each iteration is shown for two cases in Fig. 5.6.

In Table 5.4, ν measures the percentage of the maximum voltage deviation from the nominal value and computed as:

$$\nu = 100 \times \max_{i,\phi} |V_i^{\phi} - 1| \tag{5.28}$$

We also assess the impact of network and SVR connections on the aggregate DER powers and the retrieved tap positions. The results in Table 5.4 show discrepancies among the optimal dispatch, thereby confirming the significance of accounting for the actual connections.

The problem converges after two iterations, except for the 123-bus with open-delta SVRs. The star symbol of the 123-bus feeder with open-delta SVRs and mixed wye-delta loads is the only case in which higher coefficients of the regularization terms are required for convergence. For this case, c_1 and c_2 are respectively set as 10 and 5.

On average, the solve times of a single iteration are 0.9, 1.2 and 1.8 seconds for the 13-bus, 37-bus and 123-bus feeders.

5.4.2 Impact of DER Penetration on Convergence

In this section, we inspect the impact of DER penetration on the convergence. Since most of the connections converge within two iterations, we aim more attention at those with slower convergence. Specifically, we solve the 123-bus feeder with Y-$\triangle$ net loads and open-delta SVRs with increment penetration.

Table 5.3: Objective values, solution exactness, and problem performance

Fdr	Con.	SVR	Obj. Values $\mathbf{P}_{\text{LB}}$	Obj. Values $\mathbf{P}_{\text{UB}}$	λ_2/λ_1 $\mathbf{P}_{\text{LB}}$	λ_2/λ_1 $\mathbf{P}_{\text{UB}}$	$\lambda_2^{\triangle}/\lambda_1^{\triangle}$ $\mathbf{P}_{\text{LB}}$	$\lambda_2^{\triangle}/\lambda_1^{\triangle}$ $\mathbf{P}_{\text{UB}}$	Itr
13 bus	Y	Y	2.1136	2.3111	0.109	9e-13	-	-	2
		$\triangle$	2.1062	2.3101	0.127	2e-12	-	-	2
		$\perp$	2.1117	2.3480	0.124	1e-12	-	-	2
	Y-$\triangle$	Y	1.9201	2.2864	0.109	2e-12	0.374	1e-11	2
		$\triangle$	1.9201	2.2929	0.125	2e-12	0.370	9e-12	2
		$\perp$	1.9201	2.2963	0.119	2e-12	0.375	4e-12	2
37 bus	Y	Y	6.8318	7.1925	0.087	2e-12	-	-	2
		$\triangle$	6.8268	7.1286	0.103	3e-12	-	-	2
		$\perp$	6.8308	7.1567	0.100	3e-12	-	-	2
	$\triangle$	Y	6.8182	6.9902	0.075	2e-11	0.241	7e-11	2
		$\triangle$	6.8158	6.9756	0.099	7e-10	0.246	2e-10	2
		$\perp$	6.8197	6.9718	0.082	1e-10	0.243	5e-10	2
123 bus	Y	Y	15.9268	16.5212	0.112	3e-12	-	-	2
		$\triangle$	15.9196	16.5160	0.150	6e-9	-	-	2
		$\perp$	16.0268	17.6572	0.141	7e-9	-	-	3
		M	15.9208	16.5244	0.131	1e-10	-	-	2
	$\triangle$	Y	15.9246	16.5345	0.105	2e-11	0.259	3e-11	2
		$\triangle$	15.9177	16.5297	0.142	7e-9	0.27	1.8e-8	2
		$\perp$	15.9298	18.6393	0.127	2e-9	0.274	1e-7	4
		M	15.9190	16.5217	0.133	2e-12	0.271	3e-12	2

Table 5.4: Maximum voltage deviation, optimal DER dispatch, and optimal tap positions

Fdr	Con.	SVR	ν %	DER Power kW	DER Power kVAR	SVR Taps A	SVR Taps B	SVR Taps C
13 bus	Y	Y	2.1	635.43	307.75	-5	-6	-8
		△	2.1	635.43	307.75	-4	-3	-5
		⩘	2.4	635.43	307.75	-6	-	-7
	Y-△	Y	2	693.20	335.73	-8	-3	-7
		△	2.2	579.41	280.62	-5	-3	-5
		⩘	2.2	635.43	307.75	-6	-	-7
37 bus	Y	Y	0.5	1107.7	532.48	-6	-5	-8
		△	0.6	1080.1	494.59	-5	-4	-5
		⩘	0.6	1192.2	577.42	-6	-	-6
	△	Y	0.5	1214.2	581.26	-8	-4	-5
		△	0.5	1233.8	571.58	-4	-4	-4
		⩘	0.5	1310.5	607.84	-5	-	-5
123 bus	Y	Y	1.5	642.15	220.27	$-8^1, 1^2$ $0^3, 0^4$	$-3^1, 0^4$	$-5^1, 0^3$ 0^4
		△	1.5	631.29	235.21	$-5^1, 1^2$ $0^3, 0^4$	$-2^1, 0^4$	$-3^1, 0^3$ 0^4
		⩘	1.9	465.33	0.0016	$-6^1, 1^2$ $0^3, -1^4$	-	$-5^1, 0^3$ -1^4
		M	1.5	625.32	215.09	$-5^1, 1^2$ $0^3, 0^4$	-2^1	$-3^1, 0^3$ 0^4
	Y-△	Y	1.5	611.61	177.59	$-8^1, 1^2$ $0^3, 0^4$	$-4^1, 0^4$	$-5^1, 0^3$ 0^4
		△	1.5	609.68	191.73	$-5^1, 1^2$ $0^3, 0^4$	- $3^1, 0^4$	$-3^1, 0^3$ 0^4
		⩘*	1.6	473.97	- 4.184	$-6^1, 0^2$ $0^3, -1^4$	-	$-5^1, 0^3$ -1^4
		M	1.5	631.52	229.88	$-5^1, 1^2$ $0^3, 0^4$	-2^1	$-3^1, 0^3$ 0^4

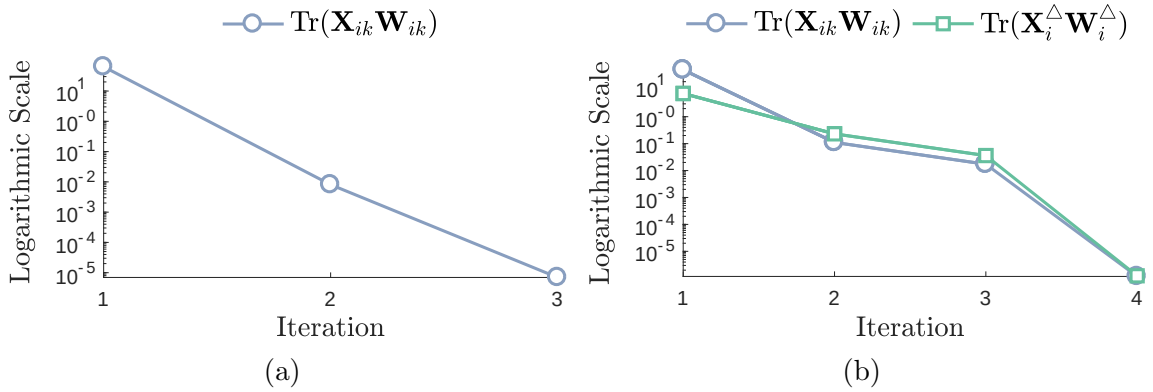

Figure 5.6: The decay of the regularization term(s) computed after each iteration for the 123-bus feeder with open-delta SVRs and (a) wye-connected net loads, or (b) mixed wye-delta connected loads. The D-ACOPF solution approaches exactness as $\sum$(XW) term(s) diminishes. Evidently, rank-1 solutions are retrieved upon convergence.

Fig. 5.7b, 5.7d, 5.7f, and 5.7h shows that the convergence rate decreases as the penetration level increases. In the 60% penetration level case, convergence is attained with unity coefficients, $c_1 = c_2 = 1$. Observing the voltage profile in Fig. 5.7a, 5.7c, 5.7e, and 5.7g, this may imply that the proposed problem may work better on distribution systems with high DER penetration and controllable assets that can effectively position the voltage within the desired limits.

5.4.3 Comparison with SVR Models in the Literature

We compare the proposed SVR model and those in [22,23] and [21] in terms of objective values and exactness (average eigenvalue ratios). Given that these references are limited to wye-connected networks, delta-connected net loads are not considered. Further, we also compute $\mathrm{P_{UB}}$ using the following objective function adopted by the literature, which is also used for local power markets [70–72]. In which case, the SVR constraints are the only source of inexactness, and so we choose smaller coefficients to penalize the regularization term, $c_1 = 0.001$.

Table 5.5: Comparison with SVR models in the literature for the 13-bus feeder

Method	SVR	f_{s}		f_{v}	
		Obj.	λ_2/λ_1	Obj.	λ_2/λ_1
Proposed	Y	0.7016	7e-12	2.3111	9e-13
	$\triangle$	0.7012	7e-12	2.3101	2e-12
	$\perp$	0.7015	1e-10	2.3480	1e-12
SDP [22, 23]	Y	0.7016	4e-10	2.2063	0.0843
McCormick Envelopes [21]	Y	0.7013	4e-11	2.1365	0.0510
	$\triangle$	0.7010	0.0014	2.1195	0.0548
	$\perp$	0.7012	0.0034	2.1107	0.0597

Table 5.6: Comparison with SVR models in the literature for the 37-bus feeder

Method	SVR	f_{s}		f_{v}	
		Obj.	λ_2/λ_1	Obj.	λ_2/λ_1
Proposed	Y	0.9911	1e-10	7.1925	2e-11
	$\triangle$	0.9893	2e-10	7.1286	3e-12
	$\perp$	0.9895	5e-11	7.1567	3e-12
McCormick Envelopes [21]	Y	0.9906	3e-04	6.7421	0.1126
	$\triangle$	0.9891	0.0037	6.7409	0.1296
	$\perp$	0.9892	0.0171	6.7345	0.1133

$$f_{\mathrm{s}} = \Re\left(\mathrm{Tr}\left(\mathbf{S}_{12}\right)\right) + \sum_{\phi\in\Phi} \Re(s_{i,\mathrm{g}}^{\phi}) \tag{5.29}$$

Contrary to the methods presented in the literature, the solutions in Table 5.5, 5.6, and 5.7 demonstrate the versatility of the proposed approach to SVR configurations, feeder scale and choice of the objective function. All the simulations with f_{s} converged after two iterations.

Table 5.7: Comparison with SVR models in the literature for the 123-bus feeder

Method	SVR	f_s		f_v	
		Obj.	λ_2/λ_1	Obj.	λ_2/λ_1
Proposed	Y	0.7059	3e-10	16.5212	3e-12
	$\triangle$	0.7058	8e-8	16.5158	7e-9
	$\perp$	0.7059	6e-8	17.6572	7e-9
SDP [22, 23]	Y	0.7060	2×10^{-7}	16.0169	0.0590
McCormick Envelopes [21]	Y	0.7059	$4e \times 10^{-4}$	16.2499	0.0188
	$\triangle$	0.7054	0.0067	16.1386	0.0300
	$\perp$	0.7056	0.0130	16.1212	0.0383

The proposed method is the only one that solves to exact solutions for all SVR connections using f_s. On the other hand, the SDP approach [22, 23] failed to solve the 37-bus feeder for the 60% penetration level, and therefore it is not included in 5.6. Moreover, the McCormick relaxation method does not yield tight relaxations for most cases. This is consistent with the findings in [21].

On the other hand, none of the literature methods produced exact solutions for the voltage-positioning objective function, f_v.

5.4.4 Comparison with Delta-Connection Model in the literature

The solutions to the proposed problem with delta-connected injections are compared with those provided by the non-iterative approach based on variable penalization [66, Algorithm 2]. Given that the variable penalization is only capable of solving delta-connected injections, the SVRs are removed, and f_s is set as the objective function. Hence, c_1 is set to zero for the proposed problem because the delta-connection PSD matrices are the only source of inexactness is this case. The following are the objective functions for the proposed

method (5.30) and the variable penalization approach (5.31):

$$f_{\text{con}} = \mathbf{1} f_{\text{s}} + \alpha \sum_{i \in \mathcal{N}^{\triangle}} \text{Tr}(\mathbf{X}_i^{\triangle} \mathbf{W}_i^{*}) \tag{5.30}$$

$$f_{\text{pen}} = \mathbf{1} f_{\text{s}} + \alpha \sum_{i \in \mathcal{N}^{\triangle}} \text{Tr}(\mathbf{I}_{i,\triangle}) \tag{5.31}$$

According to [66], the objective values are sensitive to the choice of penalty. We demonstrate that this is also the case with the convex iteration method. Also, we only show $(\lambda_2^{\triangle}/\lambda_1^{\triangle})$ because the exactness of the power-flow PSD matrices are not affected by the inexactness of the delta-connection power PSD matrices.

The simulations are performed on the 37-bus and 123-bus feeders with different choice of α. The penetration level is increased to 80% to compensate the absence of SVRs and keep the voltages within ANSI limits. The 13-bus feeder is omitted because it is not solvable even with this level of penetration.

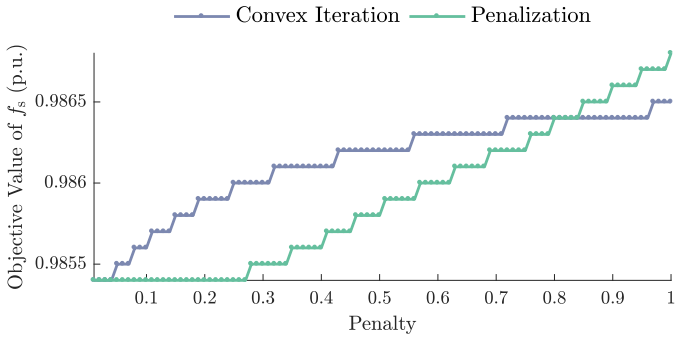

Figure 5.8: Comparison between the convex-iteration method and penalization method with different penalties for the 37-bus feeder.

Table 5.8 lists the results for the 37-bus feeder. While both methods yield the same objective values with small penalties, objective values enlarge as we increase the penalty. Fig. 5.8 shows the effect of increasing penalty weights by 0.01 for each step. It can be seen that the non-iterative penalization method generate lower objective values for the most

Table 5.8: Comparison with delta-connection model in the literature for the 37-bus feeder

α	Proposed			Penalization [66]	
	Obj.	λ_2/λ_1	Itr	Obj.	λ_2/λ_1
0.01	0.9854	2×10^{-12}	2	0.9854	5×10^{-12}
0.1	0.9856	2×10^{-13}	3	0.9854	3×10^{-12}
1	0.9862	4×10^{-13}	3	0.9868	8×10^{-13}

Table 5.9: Comparison with delta-connection model in the literature for the 123-bus feeder

α	Proposed			Penalization [66]	
	Obj.	λ_2/λ_1	Itr	Obj.	λ_2/λ_1
0.01	0.6994	1×10^{-11}	2	0.6994	5×10^{-12}
0.1	0.6994	5×10^{-12}	2	0.6994	3×10^{-12}
1	0.6994	1×10^{-11}	2	0.6994	8×10^{-11}

part. In [66], the objective values obtained with lowest penalty weights are declared as global optimum. Hence, the convex iteration is capable of solving to global optimality.

For the 123-bus in Table 5.9, the objective values are identical for all penalties. Perhaps the number of delta-connected loads adds to the sensitivity of the penalty to the objective value since the 37-bus feeder is all delta-connected.

5.5 Recovering Effective Tap Ratios, Voltage and Currents

If exact the problem converged, the rank-1 solution enables recovery of the system varaibles.

5.5.1 Effective Tap Ratios

The effective ratios are recovered upon convergence from the diagonal elements of voltage matrices.

Recovering the ratios of wye-connected SVRs is simple, since the ratio matrix, $\mathbf{A}_{i'}$ is diagonal and variables $\hat{V}_i^{\phi\phi}$ and $\check{V}_i^{\phi\phi}$ are zeros. Hence, only two variables are needed as in (5.33a). For delta-connected SVRs, all matrix variables are of some values. By observing (5.17), the following quadratic equation can be derived:

$$g(r_t^\phi) = \tilde{V}_i^{\phi\phi} r_t^\phi + 2\hat{V}_i^{\phi\phi} r_t^\phi - \bar{V}_i^{\phi\phi} = 0 \tag{5.32}$$

In this case, the effective ratios become the roots of (5.32), where $a = \tilde{V}_i^{\phi\phi}$, $b = 2\hat{V}_i^{\phi\phi}$, and $c = -\bar{V}_i^{\phi\phi}$. By invoking the intermediate value theorem, in which the solution should satisfy $r_t^\phi \in [\underline{r}, \overline{r}]$ [63], the effective per-phase tap ratio can be recovered as in (5.33b).

$$\text{Wye SVRs:} \qquad r_t^\phi = \sqrt{\frac{\bar{V}_i^{\phi\phi}}{\tilde{V}_i^{\phi\phi}}} = \sqrt{\frac{V_i^{\phi\phi}}{V_{i'}^{\phi\phi}}} \tag{5.33a}$$

$$\text{Dleta SVRs:} \qquad r_t^\phi = \frac{1}{\tilde{V}_i^{\phi\phi}} \left(-\hat{V}_i^{\phi\phi} + \sqrt{(\hat{V}_i^{\phi\phi})^2 + \tilde{V}_i^{\phi\phi} \bar{V}_i^{\phi\phi}} \right) \tag{5.33b}$$

Once the tap ratio vector, $\mathbf{r}_t$, the ratio matrix, $\mathbf{A}_t$ can be constructed.

5.5.2 Voltages and Currents Phasors

The voltages and currents can be retrieved as in [21, 24] using the following algorithm.

5.6 Conclusion

In this paper, we augment the convex D-ACOPF to solve applications of particular relevance to the distribution system optimization. Namely, we present an extended model that

accounts for the various connections of loads, DERs, and SVRs. Moreover, we set the objective function to minimize extreme voltage deviations. The relaxations of the introduced constraints inevitably position the solution outside the feasible region of the original non-convex problem. We then propose an iterative approach based on the convex iteration to steer the problem towards a physically-meaningful solution, in which variables are recoverable. The simulations and comparative studies with the existing literature demonstrate the superiority of the proposed problem with respect to exactness and speed of convergence for most connections.

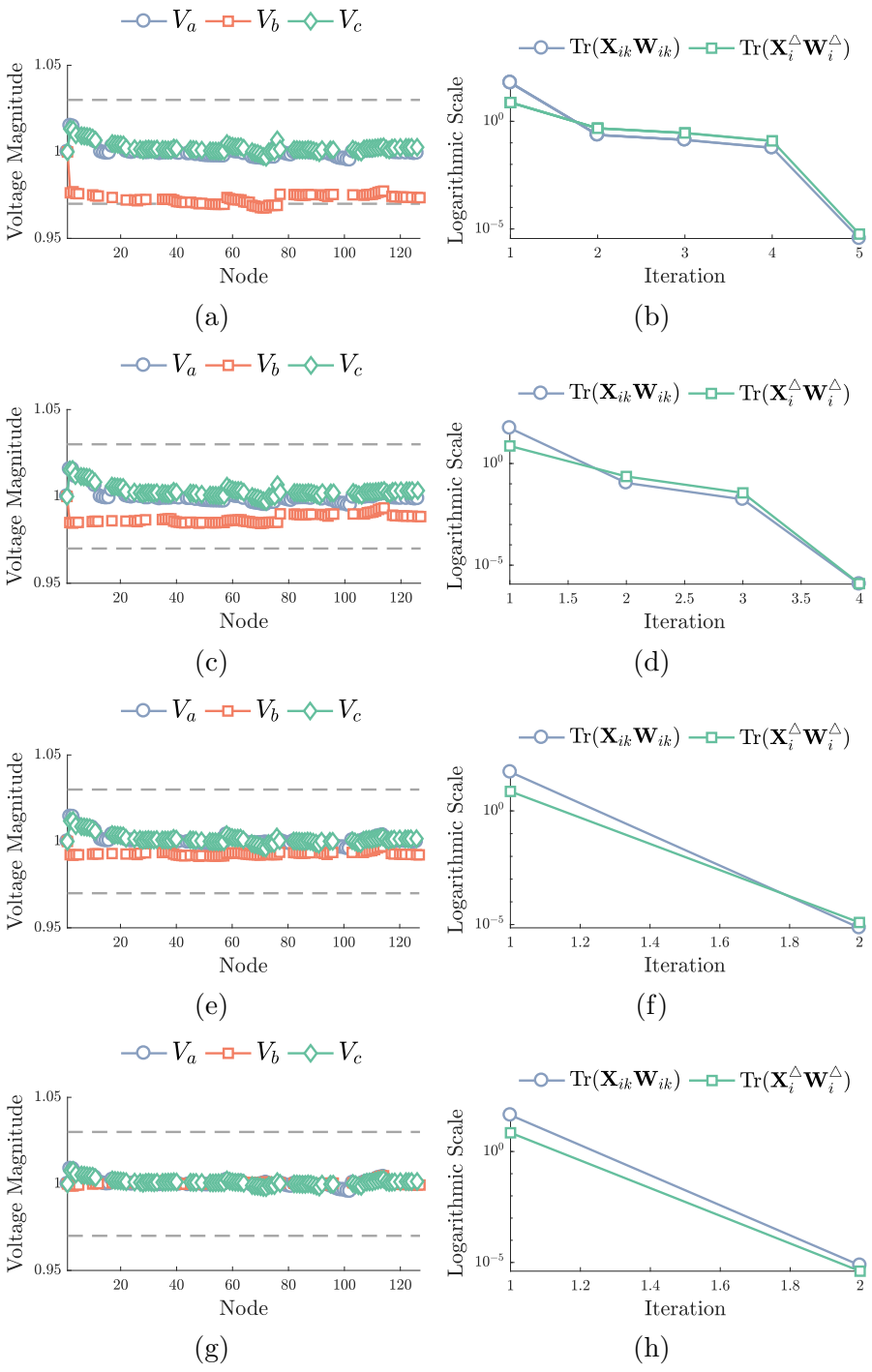

Figure 5.7: Examining the 123-bus feeder with f_{v}, open-delta SVR, and Y-$\triangle$ net loads. Penetration levels are 0% for (a) and (b), 20% for (c) and (d), 40% for (e) and (f), and 60% for (g) and (h).

Algorithm Retrieving $V_i, V_{i'}, I_{ik}, I_{i'k}$ and $I_{i,\triangle}$

Initialization: $\mathcal{N}_{\text{visit}} = 0$, $V_0 = V^{\text{ref}}$

while $\mathcal{N}_{\text{visit}} \neq \mathcal{N}$ **do**

Find $(i,k) \in \mathcal{E}$ such that $i \in \mathcal{N}_{\text{visit}}$ and $k \notin \mathcal{N}_{\text{visit}}$

Compute

$$I_{ik} = \frac{1}{\text{Tr}(\mathbf{V}_i)} \mathbf{S}_{ik}^{\text{H}} V_i$$

if $(i,k) \in \mathcal{E}_t$ **then**

Compute

$$V_{i'} = \text{A}_{i'}^{-1} V_i$$

$$I_{i'k} = \text{diag}(V_i^{\text{C}})^{-1} \text{diag}(\mathbf{S}_{i'k}^{\text{H}})$$

$$V_k = V_{i'} - Z_{i'k} I_{i'k}$$

else

Compute

$$V_k = V_i - Z_{ik} I_{ik}$$

end if

if $k \in \mathcal{N}_{\triangle}$ **then**

Compute

$$I_{k,\triangle} = \text{diag}(V_k^{\text{C}})^{-1} \mathbf{s}_{k,\triangle}^{\text{C}}$$

end if

end while

Chapter 6: Conclusion and Future Work

6.1 Conclusion

In this research, the convex distribution alternating-current optimal power flow (D-ACOPF) problems are augmented to enhance the solution accuracy and mitigate the trade-off between model precision and computational performance.

The first task is to model a generic D-ACOPF problem based on the mixed-integer second order conic programming that co-optimizes the operation of volt/var devices for balanced distribution systems with two scheduling timescales of predicted profiles of generation and load.

In the second part of this research, we design the co-optimization of step-voltage regulators (SVRs), known to be adaptable to system unbalances, with continuous photovoltaics (PVs) in multiphase distribution systems. The co-optimization is scheduled for the next day on an hourly basis, relying on the semidefinite programming multiphase D-ACOPF. A methodology based on the generalized Benders decomposition is proposed to address the difficulty of incorporating the discrete nature of SVRs into the rank-relaxed semidefinite program. Greater emphasis is also placed on solving the large-scale multi-time problem and alleviating the adverse impact of increased mechanical switching on the SVRs' maintenance costs and longevity.

In the third part of this research, we improve the convex multiphase D-ACOPF from the practical perspective. First, additional rank-relaxed SDP constraints, which describe the power injections between each pair of phases, are included. Second, we account for

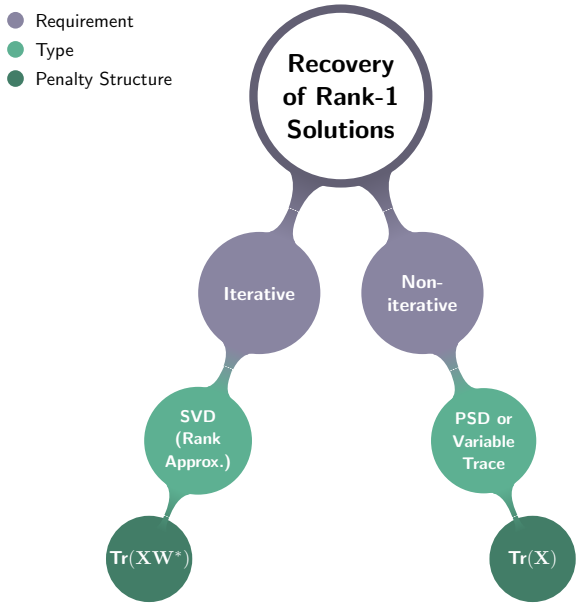

Figure 6.1: Types and structures of penalization methods to recover rank-1 solutions.

all connections of SVRs. Third, we set the objective function to reduce extreme voltage deviations from desired thresholds. As a result of the previous components, the SDP relaxation becomes inexact (infeasible). We propose to bypass the inexactness and retrieve the AC feasibility by strengthening the rank of positive semidefinite matrices iteratively. The simulations demonstrate that the efficacy of the convex iteration approach to recover the exactness. They also show that accounting for the actual connections is vital for a viable dispatch of SVRs and distributed energy resources.

6.2 Future Work

6.2.1 Investigating the Penalization Methods for D-ACOPF

Chapter 5 thoroughly discusses the convex iteration technique. In light of the extensive case studies carried out on multiple IEEE feeders with different connection assumptions, the ability of the convex iteration method to produce global optimal solutions needs to be investigated. Here are a few remarks:

- Despite the fast convergence rate, the optimal values are sensitive to the choice of penalties.

- Smaller penalties in general produce the lowest objective values, especially when a single source of inexactness is incorporated. However, the global optimality is unknown.

- The solutions of the ACOPF for transmission systems are benchmarked against the best known objective values provided by local solvers. Reference [73], as an example, found that approaching the global optimality is highly dependent on the choice of penalty coefficients.

- In [32], the convex iteration is applied on the D-ACOPF for minimizing the total power dispatch with disparate prices at each phase. The solutions are declared to be all global optimal. However, the choice of penalty coefficients has not been disclosed for any of the cases. It should be noted that the convergence of convex iteration method for the BFM is faster than the D-ACOPF developed in [32].

- Recently, reference [74] conducts a thorough empirical analysis to compare all non-iterative penalization, whose general structure is shown in Fig .6.1, on the transmission-system SDP and QC relaxations in terms of exactness, optimality and sensitivity to penalties. A similar study is urged for the SDP D-ACOPF. Some of the penalization methods presented in [74, 75] have not yet been explored on the SDP D-ACOPF.

6.2.2 Incorporating Energy-constrained Assets

The proposed convex-iteration problem in Chapter 5 have shown promising results and fast convergence for the single-time step operation. We explore to examine the possibility of extending the timescale to multi-time step operation, in which energy-constrained DERs can be incorporated. Energy-constrained DERs comprise, but are not limited to, deferrable

loads and distributed storage, which can only be dispatched based on their energy capability and constraints. In this section, we assume an hourly timescale for the multi-time scheduling problem, ($\mathcal{H} = 24$).

6.2.2.1 Deferrable Load (DL)

DLs are a branch of demand response (DR) applications. they are modeled as flexible loads whose power consumption can be dispatched within a pre-defined range, but must ultimately meet the energy consumption over the time horizon. There exists a plethora of models in the literature. We assume that the DSO wields direct control over the loads. Indirect control is out of the scope of this research.

The most simplistic form of DLs is to assume a continuous load flexibility to avoid the need for discrete variables. Let $i \in \mathcal{N}_{\mathrm{d}} \subset \mathcal{N}$ be the bus at which DL is connected:

$$\forall \phi \in \Phi :$$

$$\overline{P}_{\mathrm{d}} \leq \Re(s^{\phi}_{i,\mathrm{d},h}) \leq \underline{P}_{\mathrm{d}} \quad i \in \mathcal{N}_{\mathrm{d}}, h \in \mathcal{H} \tag{6.1a}$$

$$\overline{Q}_{\mathrm{d}} \leq \Im(s^{\phi}_{i,\mathrm{d},h}) \leq \underline{Q}_{\mathrm{d}} \quad i \in \mathcal{N}_{\mathrm{d}}, h \in \mathcal{H} \tag{6.1b}$$

$$\sum_{t \in \mathbb{H}} s^{\phi}_{i,\mathrm{d},h} = \mathrm{E}_{i,\mathrm{d}} \quad i \in \mathcal{N}_{\mathrm{d}} \tag{6.1c}$$

Constraints (6.1a) and (6.1b) model the real and reactive loads at $i \in \mathcal{N}_{\mathrm{d}}$ as variables enclosed by flexibility range. Constraint (6.1c) ensures that the diurnal consumption meets the required energy.

6.2.2.2 Energy Storage (ES)

Similar to the DLs, the time-related state-of-charge governs the ES model. Practically, the of charging and discharging energy conversion of ES devices are characterized with some shortage of efficiency. This inefficiency is usually modeled with wither NLP or MILP

complementary constraint. To maintain the computational advantage of the proposed model, the DS devices are assumed to be 100% efficient [51].

$$\forall \phi \in \Phi :$$

$$\overline{P}_{\mathrm{e}} \leq \Re(s^{\phi}_{i,\mathrm{e},h}) \leq \underline{P}_{\mathrm{e}} \quad i \in \mathcal{N}_{\mathrm{e}}, h \in \mathcal{H} \tag{6.2a}$$

$$\begin{bmatrix} \mathrm{S}_{i,\mathrm{e}} & s^{\phi}_{i,\mathrm{e},h} \\ (s^{\phi}_{i,\mathrm{e},h})^{\mathrm{C}} & \mathrm{S}_{i,\mathrm{e}} \end{bmatrix} \succeq 0 \quad i \in \mathcal{N}_{\mathrm{e}}, h \in \mathcal{H} \tag{6.2b}$$

$$E_{i,h} = E_{i,h-1} - \Delta h \Re(s^{\phi}_{i,\mathrm{e},h}) \quad i \in \mathcal{N}_{\mathrm{e}}, h \in \mathcal{H} \tag{6.2c}$$

$$\overline{E} \leq E_{i,h} \leq \underline{E} \quad i \in \mathcal{N}_{\mathrm{e}}, h \in \mathcal{H} \tag{6.2d}$$

$$E_{i,24} = E_{i,1} \quad i \in \mathcal{N}_{\mathrm{e}}, h \in \mathcal{H} \tag{6.2e}$$

Constraint (6.2a) sets the limit for the charging and discharging power. Constraint (6.2b) caps the real and reactive power. Constraint (6.2c) models the state of charge (SOC), while (6.2d) limits the amount of energy charge discharge for each time interval. Constraint (6.2e) ensures an adequate SOC at the end of the day.

6.2.2.3 Example

We carry out a numerical test on the 13-bus feeder. Besides the SVR and capacitor banks modeled as in Chapter 5, we assume two DLs and a single 3MWh ES. The DLs are placed on node 5 and 10, and the ES is also placed on node 10. The load, solar, and DL flexibility profiles are depicted in Fig. 6.2. The initial ES' SOC is 80%, whereas $\overline{E}$ and $\underline{E}$ are chosen as 40% and 90% to avoid cycling. The voltage-positioning objective presented in (5.13) is selected with $c_0 = 1$. Because the rank is minimized over the day-ahead horizon, c_1 and

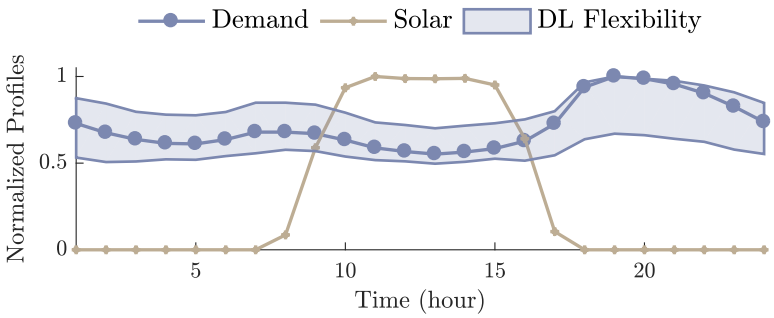

Figure 6.2: Hourly demand and solar profiles.

c_2 are set to 5. We conduct multiple case studies to see the effect of DLs and ESs on the voltage profile, and the effect of SVR connection on the SOC, taps, and Var dispatch.

6.2.2.3.1 DL and ES Impact on Voltage Profile

From 6.3, we notice that the largest voltage deviation occurs when DLs and ESs are not considered. On the other hand, the least voltage deviation is achieved by jointly enabling the loads to defer consumption and ES to use stored solar energy to mitigate the mitigate the high loading in the evening hours.

6.2.2.3.2 SVR Connection Impact on Optimal Dispatch

We demonstrate the impact of SVR connection on the dispatch of ESs, taps, and PV Vars.

The ES is delta-connected, and PVs are mixed wye-delta connected. Observing the temporal dispatch in 6.4, generation and consumption of the ES appears to be less significant on phase c, perhaps due to the large capacitance on phase c. Also, PVs do not compensate any Vars on phase b because it's the least loaded phase in the 13-feeder. On the other hand, we observe the obvious change of SOC profile with different SVRs. The change in SOC at phase a is hardly noticeable.

Fig. 6.4 serves as an example of the coordinated operation of various controllable devices within the system. It should be mentioned that there are other control variables that are not platted, e.g. DLs and ES Vars , but certainly played a role in achieving the voltage positioning objective.

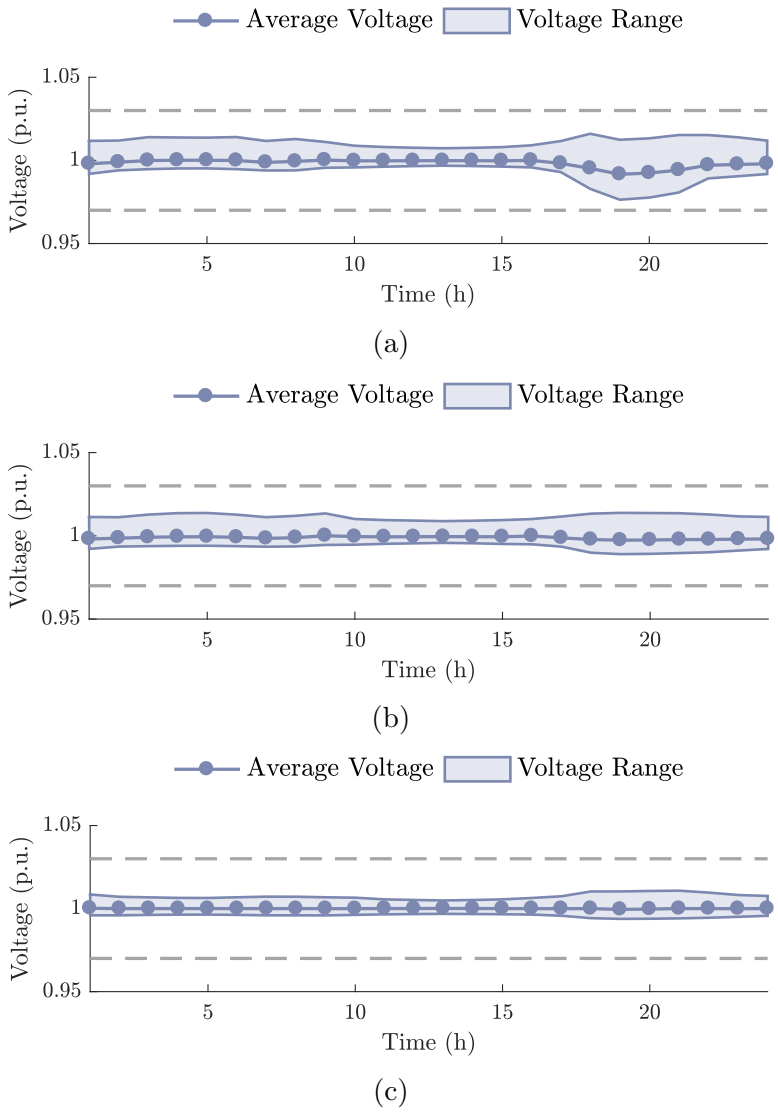

Figure 6.3: The voltage profile (a) without DLs or ESs, (b) with DLs, (c) with DLs and ESs.

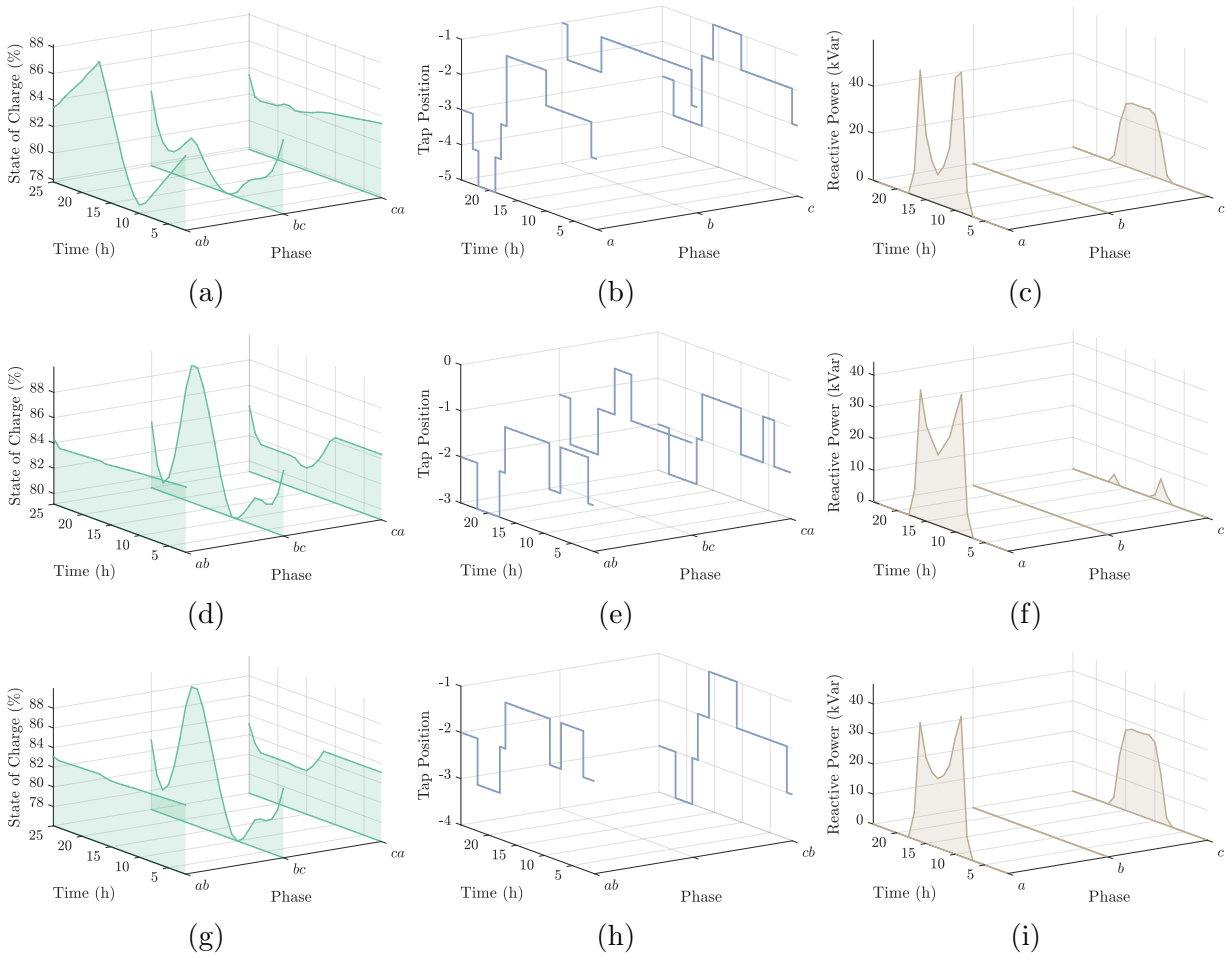

Figure 6.4: The temporal state of charge, tap position and PV Var dispatch for (a)-(c) wye SVRs, (d)-(f) closed-delta SVRs, (g)-(i) open-delta SVRs.

References

[1] J. Dong, Y. Xue, M. Olama, T. Kuruganti, J. Nutaro, and C. Winstead, "Distribution voltage control: Current status and future trends," in *2018 9th IEEE International Symposium on Power Electronics for Distributed Generation Systems (PEDG)*. IEEE, 2018, pp. 1–7.

[2] "Solar industry research data," 2019, (last accessed on August-2019). [Online]. Available: \url{https://www.seia.org/solar-industry-research-data}

[3] M. Madrigal, R. Uluski, and K. Mensan Gaba, *Practical Guidance for Defining a Smart Grid Modernization Strategy: The Case of Distribution (Revised Edition)*. The World Bank, 2017.

[4] E. Pourjafari and M. Reformat, "A support vector regression based model predictive control for volt-var optimization of distribution systems," *IEEE Access*, vol. 7, pp. 93 352–93 363, 2019.

[5] C. Li, V. R. Disfani, Z. K. Pecenak, S. Mohajeryami, and J. Kleissl, "Optimal oltc voltage control scheme to enable high solar penetrations," *Electric Power Systems Research*, vol. 160, pp. 318–326, 2018.

[6] "U.s. energy information administration," (last accessed on August 13th, 2019). [Online]. Available: https://www.eia.gov

[7] J. Stoustrup, A. Annaswamy, A. Chakrabortty, and Z. Qu, "Smart grid control."

[8] S. Boyd and L. Vandenberghe, *Convex optimization*. Cambridge university press, 2004.

[9] J. A. Taylor, *Convex optimization of power systems*. Cambridge University Press, 2015.

[10] W. Warwick, T. Hardy, M. Hoffman, and J. Homer, "Electricity distribution system baseline report," *Prepared by Pacific Northwest National Laboratory for the U.S. Department of Energy*, 2016.

[11] Y. P. Agalgaonkar, B. C. Pal, and R. A. Jabr, "Distribution voltage control considering the impact of pv generation on tap changers and autonomous regulators," *IEEE Transactions on Power Systems*, vol. 29, no. 1, pp. 182–192, 2014.

[12] S. Paudyal, C. A. Canizares, and K. Bhattacharya, "Optimal operation of distribution feeders in smart grids," *IEEE Transactions on Industrial Electronics*, vol. 58, no. 10, pp. 4495–4503, 2011.

[13] Q. Nguyen, H. V. Padullaparti, K.-W. Lao, S. Santoso, X. Ke, and N. Samaan, "Exact optimal power dispatch in unbalanced distribution systems with high pv penetration," *IEEE Transactions on Power Systems*, vol. 34, no. 1, pp. 718–728, 2018.

[14] N. Daratha, B. Das, and J. Sharma, "Coordination between oltc and svc for voltage regulation in unbalanced distribution system distributed generation," *IEEE Transactions on Power Systems*, vol. 29, no. 1, pp. 289–299, 2013.

[15] F. U. Nazir, B. C. Pal, and R. A. Jabr, "A two-stage chance constrained volt/var control scheme for active distribution networks with nodal power uncertainties," *IEEE Transactions on Power Systems*, vol. 34, no. 1, pp. 314–325, 2018.

[16] S. R. Shukla, S. Paudyal, and M. R. Almassalkhi, "Efficient distribution system optimal power flow with discrete control of load tap changers," *IEEE Transactions on Power Systems*, vol. 34, no. 4, pp. 2970–2979, 2019.

[17] R. Zafar, J. Ravishankar, J. E. Fletcher, and H. R. Pota, "Multi-timescale model predictive control of battery energy storage system using conic relaxation in smart distribution grids," *IEEE Transactions on Power Systems*, vol. 33, no. 6, pp. 7152–7161, 2018.

[18] X. Chen, W. Wu, and B. Zhang, "Robust capacity assessment of distributed generation in unbalanced distribution networks incorporating anm techniques," *IEEE Transactions on Sustainable Energy*, vol. 9, no. 2, pp. 651–663, 2017.

[19] R. R. Jha, A. Dubey, C.-C. Liu, and K. P. Schneider, "Bi-level volt-var optimization to coordinate smart inverters with voltage control devices," *IEEE Transactions on Power Systems*, vol. 34, no. 3, pp. 1801–1813, 2019.

[20] B. A. Robbins, H. Zhu, and A. D. Domínguez-García, "Optimal tap setting of voltage regulation transformers in unbalanced distribution systems," *IEEE Transactions on Power Systems*, vol. 31, no. 1, pp. 256–267, 2015.

[21] M. Bazrafshan, N. Gatsis, and H. Zhu, "Optimal power flow with step-voltage regulators in multi-phase distribution networks," *IEEE Transactions on Power Systems*, 2019.

[22] Y. Liu, J. Li, L. Wu, and T. Ortmeyer, "Chordal relaxation based acopf for unbalanced distribution systems with ders and voltage regulation devices," *IEEE Transactions on Power Systems*, vol. 33, no. 1, pp. 970–984, 2017.

[23] Y. Liu, J. Li, and L. Wu, "Coordinated optimal network reconfiguration and voltage regulator/der control for unbalanced distribution systems," *IEEE Transactions on Smart Grid*, vol. 10, no. 3, pp. 2912–2922, 2018.

[24] L. Gan and S. H. Low, "Convex relaxations and linear approximation for optimal power flow in multiphase radial networks," in *2014 Power Systems Computation Conference*. IEEE, 2014, pp. 1–9.

[25] R. Dobbe, O. Sondermeijer, D. Fridovich-Keil, D. Arnold, D. Callaway, and C. Tomlin, "Towards distributed energy services: Decentralizing optimal power flow with machine learning," *IEEE Transactions on Smart Grid*, 2019.

[26] R. A. Jabr, "Radial distribution load flow using conic programming," *IEEE transactions on power systems*, vol. 21, no. 3, pp. 1458–1459, 2006.

[27] M. Farivar and S. H. Low, "Branch flow model: Relaxations and convexification: Part i," *IEEE Transactions on Power Systems*, vol. 28, no. 3, pp. 2554–2564, 2013.

[28] M. Baran and F. F. Wu, "Optimal sizing of capacitors placed on a radial distribution system," *IEEE Transactions on power Delivery*, vol. 4, no. 1, pp. 735–743, 1989.

[29] N. Li, L. Chen, and S. H. Low, "Exact convex relaxation of opf for radial networks using branch flow model," in *2012 IEEE Third International Conference on Smart Grid Communications (SmartGridComm)*. IEEE, 2012, pp. 7–12.

[30] E. Dall'Anese, H. Zhu, and G. B. Giannakis, "Distributed optimal power flow for smart microgrids," *IEEE Transactions on Smart Grid*, vol. 4, no. 3, pp. 1464–1475, 2013.

[31] J. Lavaei and S. H. Low, "Zero duality gap in optimal power flow problem," *IEEE Transactions on Power Systems*, vol. 27, no. 1, pp. 92–107, 2011.

[32] W. Wang and N. Yu, "Chordal conversion based convex iteration algorithm for three-phase optimal power flow problems," *IEEE Transactions on Power Systems*, vol. 33, no. 2, pp. 1603–1613, 2017.

[33] I. Alsaleh, L. Fan, and H. G. Aghamolki, "Volt/var optimization with minimum equipment operation under high pv penetration," in *2018 North American Power Symposium (NAPS)*. IEEE, 2018, pp. 1–6.

[34] W. Wei, J. Wang, N. Li, and S. Mei, "Optimal power flow of radial networks and its variations: A sequential convex optimization approach," *IEEE Transactions on Smart Grid*, vol. 8, no. 6, pp. 2974–2987, 2017.

[35] L. Gan, N. Li, U. Topcu, and S. H. Low, "Exact convex relaxation of optimal power flow in radial networks," *IEEE Transactions on Automatic Control*, vol. 60, no. 1, pp. 72–87, 2014.

[36] W. Wu, Z. Tian, and B. Zhang, "An exact linearization method for oltc of transformer in branch flow model," *IEEE Transactions on Power Systems*, vol. 32, no. 3, pp. 2475–2476, 2016.

[37] M. Grant and S. Boyd, "CVX: Matlab software for disciplined convex programming, version 2.1," http://cvxr.com/cvx, Mar. 2014.

[38] M. Grant and S. Boyd, "Graph implementations for nonsmooth convex programs," in *Recent Advances in Learning and Control*, ser. Lecture Notes in Control and Information Sciences, V. Blondel, S. Boyd, and H. Kimura, Eds. Springer-Verlag Limited, 2008, pp. 95–110, http://stanford.edu/~boyd/graph_dcp.html.

[39] L. Gurobi Optimization, "Gurobi optimizer reference manual," 2020. [Online]. Available: http://www.gurobi.com

[40] Q. Li and V. Vittal, "Non-iterative enhanced sdp relaxations for optimal scheduling of distributed energy storage in distribution systems," *IEEE Transactions on Power Systems*, vol. 32, no. 3, pp. 1721–1732, 2016.

[41] I. Alsaleh and L. Fan, "Multi-time co-optimization of voltage regulators and photovoltaics in unbalanced distribution systems," *IEEE Transactions on Sustainable Energy*, 2020.

[42] W. H. Kersting, *Distribution system modeling and analysis*. CRC press, 2012.

[43] I. Alsaleh, L. Fan, and M. Ma, "Mixed-integer sdp relaxation-based volt/var optimization for unbalanced distribution systems," in *2019 IEEE Power Energy Society General Meeting (PESGM)*, 2019, pp. 1–5.

[44] A. M. Geoffrion, "Generalized benders decomposition," *Journal of optimization theory and applications*, vol. 10, no. 4, pp. 237–260, 1972.

[45] J. F. Benders, "Partitioning procedures for solving mixed-variables programming problems," *Numerische mathematik*, vol. 4, no. 1, pp. 238–252, 1962.

[46] A. Nasri, S. J. Kazempour, A. J. Conejo, and M. Ghandhari, "Network-constrained ac unit commitment under uncertainty: A benders decomposition approach," *IEEE transactions on power systems*, vol. 31, no. 1, pp. 412–422, 2015.

[47] A. Schwele, J. Kazempour, and P. Pinson, "Do unit commitment constraints affect generation expansion planning? a scalable stochastic model," *Energy Systems*, pp. 1–36, 2019.

[48] H. Chen, H. Ngan, and Y. Zhang, *Power System Optimization: Large-scale Complex Systems Approaches*. John Wiley & Sons, 2016.

[49] S. Ghosh, F. Ding, J. Simpson, T. Harris, M. Baggu, H. G. Aghamolki, and W. Ren, "Techno-economic analysis for grid edge intelligence: A preliminary study on smart voltage regulator controls," in *2019 IEEE Power & Energy Society Innovative Smart Grid Technologies Conference (ISGT)*. IEEE, 2019, pp. 1–5.

[50] M. ApS, "The mosek optimization toolbox for matlab manual." 2017. [Online]. Available: https://docs.mosek.com/8.0/toolbox/index.html

[51] X. Chen, E. Dall'Anese, C. Zhao, and N. Li, "Aggregate power flexibility in unbalanced distribution systems," *IEEE Transactions on Smart Grid*, vol. 11, no. 1, pp. 258–269, 2019.

[52] J. Löfberg, "Yalmip : A toolbox for modeling and optimization in matlab," in *In Proceedings of the CACSD Conference*, Taipei, Taiwan, 2004.

[53] K. Baker, "Solutions of dc opf are never ac feasible," *arXiv preprint arXiv:1912.00319*, 2019.

[54] X. Bai, H. Wei, K. Fujisawa, and Y. Wang, "Semidefinite programming for optimal power flow problems," *International Journal of Electrical Power & Energy Systems*, vol. 30, no. 6-7, pp. 383–392, 2008.

[55] R. A. Jabr, "Exploiting sparsity in sdp relaxations of the opf problem," *IEEE Transactions on Power Systems*, vol. 27, no. 2, pp. 1138–1139, 2011.

[56] D. K. Molzahn, J. T. Holzer, B. C. Lesieutre, and C. L. DeMarco, "Implementation of a large-scale optimal power flow solver based on semidefinite programming," *IEEE Transactions on Power Systems*, vol. 28, no. 4, pp. 3987–3998, 2013.

[57] M. Ma, L. Fan, Z. Miao, B. Zeng, and H. Ghassempour, "A sparse convex ac opf solver and convex iteration implementation based on 3-node cycles," *Electric Power Systems Research*, vol. 180, p. 106169, 2020.

[58] Z. Miao, L. Fan, H. G. Aghamolki, and B. Zeng, "Least squares estimation based sdp cuts for socp relaxation of ac opf," *IEEE Transactions on Automatic Control*, vol. 63, no. 1, pp. 241–248, 2017.

[59] D. K. Molzahn and I. A. Hiskens, "Sparsity-exploiting moment-based relaxations of the optimal power flow problem," *IEEE Transactions on Power Systems*, vol. 30, no. 6, pp. 3168–3180, 2014.

[60] C. Coffrin, H. L. Hijazi, and P. Van Hentenryck, "The qc relaxation: Theoretical and computational results on optimal power flow," *arXiv preprint arXiv:1502.07847*, 2015.

[61] C. Bingane, M. F. Anjos, and S. Le Digabel, "Tight-and-cheap conic relaxation for the ac optimal power flow problem," *IEEE Transactions on Power Systems*, vol. 33, no. 6, pp. 7181–7188, 2018.

[62] N. Nazir and M. Almassalkhi, "Voltage positioning using co-optimization of controllable grid assets," *arXiv preprint arXiv:1911.00338*, 2019.

[63] M. Bazrafshan, N. Gatsis, and H. Zhu, "Optimal tap selection of step-voltage regulators in multi-phase distribution networks," in *2018 Power Systems Computation Conference (PSCC)*. IEEE, 2018, pp. 1–7.

[64] M. Bazrafshan and N. Gatsis, "Convergence of the z-bus method for three-phase distribution load-flow with zip loads," *IEEE Transactions on Power Systems*, vol. 33, no. 1, pp. 153–165, 2017.

[65] C. Zhao, E. Dall-Anese, and S. H. Low, "Optimal power flow in multiphase radial networks with delta connections," National Renewable Energy Lab.(NREL), Golden, CO (United States), Tech. Rep., 2017.

[66] F. Zhou, A. S. Zamzam, S. H. Low, and N. D. Sidiropoulos, "Exactness of opf relaxation on three-phase radial networks with delta connections," *arXiv preprint arXiv:2005.07803*, 2020.

[67] R. Madani, M. Ashraphijuo, and J. Lavaei, "Promises of conic relaxation for contingency-constrained optimal power flow problem," *IEEE Transactions on Power Systems*, vol. 31, no. 2, pp. 1297–1307, 2015.

[68] R. Madani, S. Sojoudi, and J. Lavaei, "Convex relaxation for optimal power flow problem: Mesh networks," *IEEE Transactions on Power Systems*, vol. 30, no. 1, pp. 199–211, 2014.

[69] J. Dattorro, "Convex optimization & euclidean distance geometry," 2005.

[70] L. Bai, J. Wang, C. Wang, C. Chen, and F. Li, "Distribution locational marginal pricing (dlmp) for congestion management and voltage support," *IEEE Transactions on Power Systems*, vol. 33, no. 4, pp. 4061–4073, 2018.

[71] I. Alsaleh and L. Fan, "Distribution locational marginal pricing (dlmp) for multiphase systems," in *2018 North American Power Symposium (NAPS)*, 2018, pp. 1–6.

[72] A. Alassaf, L. Fan, and I. Alsaleh, "Day-ahead distribution market analysis via convex bilevel programming," in *2019 North American Power Symposium (NAPS)*, 2019, pp. 1–6.

[73] R. D. Zimmerman, C. E. Murillo-Sánchez, and R. J. Thomas, "Matpower: Steady-state operations, planning, and analysis tools for power systems research and education," *IEEE Transactions on power systems*, vol. 26, no. 1, pp. 12–19, 2010.

[74] A. Venzke, S. Chatzivasileiadis, and D. K. Molzahn, "Inexact convex relaxations for ac optimal power flow: Towards ac feasibility," *arXiv preprint arXiv:1902.04815*, 2019.

[75] M. Fazel, H. Hindi, and S. P. Boyd, "A rank minimization heuristic with application to minimum order system approximation," in *Proceedings of the 2001 American Control Conference.(Cat. No. 01CH37148)*, vol. 6. IEEE, 2001, pp. 4734–4739.

Appendix A: Copyright Permissions

- Reprint permission of a published paper for Chapter 3

no-reply@copyright.com <no-reply@copyright.com> Fri, Apr 17, 2020 at 11:34 AM
To: ialsaleh@mail.usf.edu

IEEE
Requesting permission to reuse content from an IEEE publication

Your order has been cancelled

Dear Mr. Ibrahim Alsaleh,

Your IEEE request has been cancelled for the following reason:
Dear Ibrahim Alsaleh,

The IEEE does not require individuals working on a dissertation/thesis to obtain a formal reuse license however, you must follow the requirements listed below:

Full-Text Article

If you are using the entire IEEE copyright owned article, the following IEEE copyright/credit notice should be placed prominently in the references: © [year of original publication] IEEE. Reprinted, with
permission, from [author names, paper title, IEEE publication title, and month/year of publication]

Kind regards, M.E. Brennan.

You will not be charged for this order.

Order Summary

Licensee:	University of South Florida
Order Date:	Apr 16, 2020
Order Number:	501561807
Publication:	IEEE Proceedings
Title:	Volt/Var Optimization with Minimum Equipment Operation under High PV Penetration
Type of Use:	Thesis/Dissertation
Order Total:	Not Available

Appendix B: Copyright Permissions

- Reprint permission of an accepted paper for Chapter 4

> - **Does IEEE require individuals working on a thesis or dissertation to obtain formal permission for reuse?**
>
> The IEEE does not require individuals working on a thesis to obtain a formal reuse license, however, you must follow the requirements listed below:
>
> **Full-Text Article**
>
> If you are using the entire IEEE copyright owned article, the following IEEE copyright/ credit notice should be placed prominently in the references: © [year of original publication] IEEE. Reprinted, with permission, from [author names, paper title, IEEE publication title, and month/year of publication]
>
> Only the accepted version of an IEEE copyrighted paper can be used when posting the paper or your thesis on-line.

About the Author

Ibrahim Alsaleh was born in 1989. He received BSc from the University of Hail, Hail, Saudi Arabia in 2012. In 2016, he also received MSc from the University of South Florida, Tampa, USA where he is currently working towards his PhD since 2016. Ibrahim has also been affiliated with the University of Hail since 2013, where he was granted a scholarship to pursue graduate degrees in USA. After graduation, Ibrahim is expected to join the University of Hail as an Assistant Professor. His research interests include distribution system modernization, volt/var optimization and convex programming.